

國立交通大學

機械工程學系

博士論文

平板式微型甲醇蒸汽重組器熱質傳特性
與流道設計之研究

Study on Heat and Mass Transfer Characteristics and Flow Channel
Design in a Plate Methanol Steam Micro-Reformer

研究生：薛清益

指導教授：陳俊勳 教授

曲新生 教授

中華民國九十九年五月

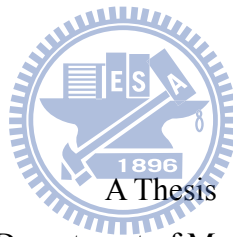
平板式微型甲醇蒸汽重組器熱質傳特性
與流道設計之研究

Study on Heat and Mass Transfer Characteristics and Flow Channel
Design in a Plate Methanol Steam Micro-Reformer

研究生：薛清益
指導教授：陳俊勳、曲新生

Student : Ching-Yi Hsueh
Advisor: Chiun-Hsun Chen
Hsin-Sen Chu

國立交通大學
機械工程學系
博士論文



Submitted to Department of Mechanical Engineering
National Chiao Tung University
in partial Fulfillment of the Requirements
for the Degree of
Doctor of Philosophy
in
Mechanical Engineering

May 2010

Hsinchu, Taiwan, Republic of China

中華民國九十九年五月

平板式微型甲醇重組器熱質傳特性與流道設計之研究

學生：薛清益

指導教授：陳俊勳、曲新生

摘要

本論文係以數值分析探討平板式微型甲醇蒸汽重組器（包含甲醇蒸汽重組器與甲醇觸媒燃燒器）之熱質傳現象，本研究首先針對微型甲醇蒸汽重組器，探討幾何效應與熱流效應對甲醇轉化率及氣體濃度分佈之影響，以俾獲得較佳的流道設計與操作條件，接著並加入甲醇觸媒燃燒器，其結果可以提供平板式微型甲醇蒸汽重組器一個完整的設計資訊。

本研究探討的議題主要分為二個部份：第一部份是以微型甲醇蒸汽重組器為主，並不考慮甲醇觸媒燃燒器。首先建立一甲醇蒸汽重組器之二維流道數學模型，並探討幾何參數與熱流參數對重組器性能與流道內熱質傳現象之影響。研究結果發現當壁面溫度由200度升高至260度時，甲醇轉換效率約提升49%，結果也顯示當入口甲醇與水之燃料比由1.0變為1.6時，流道出口之CO濃度會從1.72%降低至0.95%。而選用較長的流道長度、較低的流道高度、較大的觸媒高度、較大的觸媒孔隙度、較高的壁面溫度與較低的雷諾數等參數可以有效提升微型重組器之性能。接著建立甲醇蒸氣重組器之三維流道數學模型，並探討不同流道高寬比與流道幾何尺寸對氣體傳輸現象與微型甲醇蒸汽重組器性能之影響。結果顯示，壁面傳導效應對於模型之溫度分佈會有顯著的影響，因此在分析模型中，必須考慮壁面傳導效應之影響。結果亦顯示，較低的流道高寬比會有較好的微型甲醇蒸汽重組器性能，主要是由於較低的流道高寬比會有較大的化學反應面積，而流道尺寸較小時，則會有較佳的甲醇轉化率，此乃肇因於較小的流道尺寸會有較均勻的溫度分佈，因此能有效提升燃料使用率。最後將已經建立之三維流道模組進一步擴展至具蛇

型流道之微型甲醇蒸汽重組器，並利用數值方法探討壁面溫度、入口燃料比與雷諾數對具蛇型流道之微型甲醇蒸汽重組器性能與傳輸現象之影響。結果顯示，藉由降低雷諾數與提高入口燃料比可以有效提升甲醇轉換效率。而加熱壁面在蛇型流道之頂端($Y=1$)或底部($Y=0$)時，吾人發現加熱壁面在流道頂端時，會有較佳的甲醇轉換率，此乃肇因於加熱壁面在流道頂端時，會有較大的化學反應。

而本論文第二部份主要是利用數值方法針對微型甲醇蒸氣重組器並搭配觸媒燃燒器之熱質傳特性與性能進行研究，首先建立甲醇蒸氣重組器搭配觸媒燃燒器之三維流道數學模型，來探討不同流動形式與幾何參數對微型甲醇重組器性能之影響，結果顯示採用逆向流比起平行流可以有效改善重組器 10% 的效能，主要是由於逆向流有較佳的熱管理能力，因此能有效改善重組器之轉換效率，結果也顯示，適當的幾何參數會有較佳的熱管理能力與甲醇轉換率，而當燃燒器有較大的雷諾數時，會有較大的壁面溫度，因此能有效提升甲醇轉化率。接著建立具不同流道形狀(蛇型流道與直通流道)之三維甲醇蒸汽重組器搭配甲醇觸媒燃燒器模型，並探討不同流道對甲醇轉化率與傳輸現象之影響。結果顯示，具蛇型流道之微型甲醇蒸汽重組器與甲醇觸媒燃燒器會有最佳的甲醇轉換率，此乃肇因於採用蛇型流道作為微型甲醇蒸汽重組器與甲醇觸媒燃燒器之流道時，會有較佳的熱管理能力。本論文之數值模型可以有效的分析微型重組器內傳輸現象，其結果將有助於今後平板式微型重組器之設計。

Study on heat and mass transfer characteristics and channel design in a plate methanol steam micro-reformer

Student: Ching-Yi Hsueh

Advisor: Chiun-Hsun Chen

Hsin-Sen Chu

ABSTRACT

This dissertation aims to examine numerically heat and mass transport phenomena in the plate methanol steam micro-reformer (including methanol steam micro-reformer and methanol catalytic combustor). The first focus is to investigate the effects of geometric and thermo-fluid parameters on the methanol conversion and gas concentration distributions of the methanol steam micro-reformer in order to obtain better channel designs and operating conditions. Furthermore, a methanol steam micro-reformer with a methanol catalytic combustor is considered in the present work. The results can provide comprehensive information for designing the plate methanol steam micro-reformer.

This study can be divided into two parts. In the first part, the research only considered the plate methanol steam micro-reformer, namely the methanol catalytic combustor is not included in it. Firstly, a 2-dimensional channel model of the methanol steam micro-reformer is established to investigate effects of geometric and thermo-fluid parameters on performance and heat and mass transfer phenomena in micro-reformer channels. The results of the modeling suggest that the methanol conversion could be improved by 49 %-points by increasing the wall temperature from 200 °C to 260 °C. The results also show that the CO concentration would be reduced from 1.72% to 0.95% with the H₂O/CH₃OH molar ratio values ranging from 1.0 to 1.6. The values of parameters that enhance the performance of micro-reformer were identified, such as longer channel length, smaller channel height, thicker catalyst layer, larger catalyst porosity, lower Reynolds number and higher wall temperature.

Secondly, a 3-dimensional channel model of the methanol steam micro-reformer is developed to investigate the effects of various height and width ratios and channel geometric size on the reactant gas transport characteristics and micro-reformer performance. The predictions show that conduction through the wall plays a significant effect on the temperature distribution and must be considered in the modeling. The predicted results also demonstrated that better performance is noted for a micro-reformer with lower aspect-ratio channel. This is due to the larger the chemical reaction surface area for a lower aspect-ratio channel. The results indicate that the smaller channel size experiences a better methanol conversion. This is due to the fact that a smaller channel has a much more uniform temperature distribution, which in turn, fuel utilization efficiency is improved for a smaller channel reformer. Finally, the established 3-dimensional channel model of a plate methanol steam micro-reformer extends to be a plate methanol steam micro-reformer with serpentine flow field. A numerical investigation of the transport phenomena and performance of a plate methanol steam micro-reformer with serpentine flow field as a function of wall temperature, fuel ratio and Reynolds number are presented. The methanol conversion is improved by decreasing the Reynolds number or increasing the S/C molar ratio. When the serpentine flow field of the channel is heated either through top plate ($Y=1$) or the bottom plate ($Y=0$), we observe a higher degree of methanol conversion for the case with top plate heating. This is due to the stronger chemical reaction for the case with top plate heating.

In the second part, a numerical study is performed to examine the characteristics of heat and mass transfer and the performance of a plate methanol steam micro-reformer with a methanol catalytic combustor. Firstly, a three-dimensional channel numerical model of a micro-reformer with combustor is developed to examine the effects of various flow configurations and geometric parameters on micro-reformer performance. Comparing the co- and counter-current flows via numerical simulation, the results show that the methanol

conversion for counter-current flow could be improved by 10%. This is due to the fact that counter-current flow leads to a better thermal management, which in turn improves fuel conversion efficiency. The results also reveal that the appropriate geometric parameters exist for a micro-reformer with a combustor to obtain better thermal management and methanol conversion. With a higher Reynolds number on the combustor side, the wall temperature is increased and the methanol conversion can thus be enhanced. In addition, the three-dimensional models of a plate methanol steam micro-reformer and a methanol catalytic combustor with the parallel flow field and the serpentine flow field have been established to investigate the performance and transport phenomena in the micro-reformer. The methanol conversion of the micro-reformer with the serpentine flow field and the combustor with the serpentine flow field is the best due to a better thermal management in the micro-reformer. The numerical model provides an efficient way to characterize the transport phenomena within the micro-reformer, and the results will benefit the future design for the plate methanol steam micro-reformer.



ACKNOWLEDGEMENTS

首先感謝恩師 曲新生及陳俊勳教授，恩師除了在學術上悉心的指導我之外，在待人處世方面更是值得我學習的典範。其次，感謝 顏維謀教授在交大求學過程中給予我莫大的幫助，使我的博士論文能進行的十分順利。也很感謝口試委員翁政義、陳朝光、林清發及陳慶耀諸位教授對於論文的建議及指導，使得本論文更加的嚴謹及完整。

此外，特別感謝交大曲新生師門與陳俊勳師門的學長、學姐、同學及學弟妹們在學業及生活上的關心與照顧，幫助我在研究過程中解決許多困難。也感謝華梵大學熱流實驗室的學長、學姐及學弟妹們為我的生活帶來了許多歡樂的回憶。

最後特別感謝我的家人，在這漫長的求學過程中，不斷給予我許多的支持及鼓勵，陪伴我經歷了許多挫折及挑戰，僅以此論文獻給所有幫助、關心及照顧我的人。

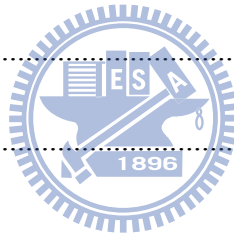


TABLE OF CONTENTS

CHINESE ABSTRACT	i
ENGLISH ABSTRACT	iii
ACKNOWLEDGEMENTS	vi
TABLE OF CONTENTS	vii
LIST OF TABLES.....	x
LIST OF FIGURES.....	xi
NOMENCLATURE	xvii
CHAPTER 1 INTRODUCTION.....	1
1.1 Background.....	1
1.2 Literature Survey	5
1.3 Objectives	13
CHAPTER 2 MATHEMATICAL MODEL AND ANALYSIS	25
2.1 The Model of the Methanol Steam Micro-Reformer.....	25
2.1.1 Model Description	25
2.1.2 Assumption	26
2.1.3 Governing Equations	26
2.1.4 Boundary Conditions.....	30
2.2 The Model of a Plate Methanol Steam Micro-Reformer with Methanol Catalytic Combustor	31

2.2.1 Model Description	31
2.3.2 Assumption	33
2.3.3 Governing Equations	33
2.3.4 Boundary Conditions	37
CHAPTER 3 METHOD OF SOLUTION	44
3.1 Flow Chart	44
3.2 Numerical Method	45
CHAPTER 4 RESULTS AND DISCUSSION	48
4.1 Two-Dimensional Channel Model of a Plate Methanol Steam Micro-Reformer	48
4.1.1 Effects of the Geometric Parameters on the Heat and Mass Transfer and Methanol Conversion in a Micro-Reformer Channel	49
4.1.2 Effects of Thermo-Fluid Parameters on the Heat and Mass transfer and Methanol Conversion in a Micro-Reformer Channel	53
4.2 Three-Dimensional Channel Model of a Plate Methanol Steam Micro-Reformer ...	55
4.2.1 Effects of Channel with Various Height and Width Ratios on Micro-Reformer Performance and Local Transport Phenomena	56
4.2.2 Effects of Geometric Size on the Transport Phenomena and Performance of Micro-Reformer	61
4.3 Three-Dimensional Model of a Plate Methanol Steam Micro-Reformer with Serpentine Flow Field Design	62
4.3.1 Effects of Thermo-Fluid Parameters on the Plate Methanol Steam Micro-Reformer with Serpentine Flow Field Performance	63

4.3.2 Effects of Various Heated Plates on Micro-Reformer Performance.....	66
4.4 Three-Dimensional Channel Model of a Plate Methanol Steam Micro-Reformer with Methanol Catalytic Combustor.....	67
4.4.1 Effects of Various Flow Configurations and Geometric Parameters on Micro-Reformer Performance	68
4.4.2 Effects of the Reynolds Number (Re) on Heat and Mass Transfer Phenomena and Micro-Reformer Performance.....	71
4.5 Three-Dimensional Model of a Plate Methanol Steam Micro-Reformer with Methanol Catalytic Combustor for Parallel Flow Field and Serpentine Flow Field	73
CHAPTER 5 CONCLUSIONS AND RECOMMENDATION.....	136
5-1 Conclusions.....	136
5-2 Recommendations.....	139
REFERENCE.....	141



LIST OF TABLES

Table 1-1 Energy density of various batteries and fuels [1]	16
Table 1-2 Comparison of reforming technologies[4]	17
Table 4-1 Parameters used in the two-dimensional channel model of a plate methanol steam micro-reformer	77
Table 4-2 Methanol mole fractions for the various grids	78
Table 4-3 The cases with various aspect-ratio channels used in this work	79
Table 4-4 Parameters used in the three-dimensional channel model of a plate methanol steam micro-reformer	80
Table 4-5 Mole fractions of methanol for the various grid tests at different axial locations....	81
Table 4-6 Parameters used in the three-dimensional model of the plate methanol steam micro-reformer with serpentine flow field design.....	82
Table 4-7 Temperature distributions (°C) for the various grid tests at different axial locations	83
Table 4-8 Parameters used in the three-dimensional channel model of a plate methanol steam micro-reformer with methanol catalytic combustor	84
Table 4-9 Temperature distributions (°C) for the various grid tests at different axial locations	85
Table 4-10 Parameters used in the three-dimensional model of a plate methanol steam micro-reformer with methanol catalytic combustor	86

LIST OF FIGURES

Fig. 1-1 Applications of the fuel cell (ERL/ITRI).....	18
Fig. 1-2 Photograph of the (a) small PEMFC and (b) micro-reformer [6].....	19
Fig. 1-3 Schematic of fuel reforming process [7].....	20
Fig. 1-4 Photograph of the plate methanol steam micro-reformer [7].....	21
Fig. 1-5 Structure of micro-reformer [6]	22
Fig. 1-6 Schematic of methanol reforming system [6].....	23
Fig. 1-7 Schematic of PhD thesis structure	24
Fig. 2-1 Schematic diagram of the two-dimensional channel model of a plate methanol steam micro-reformer	39
Fig. 2-2 Schematic diagram of the three-dimensional channel model of a plate methanol steam micro-reformer	40
Fig. 2-3 Schematic diagram of the three-dimensional model of a plate methanol steam micro-reformer with serpentine flow field design.....	41
Fig. 2-4 Schematic diagram of the three-dimensional channel model of a plate methanol steam micro-reformer with methanol catalytic combustor	42
Fig. 2-5 (a) Schematic diagram of a plate methanol steam micro-reformer with methanol catalytic combustor, (b) Parallel Flow Field and (c) Serpentine Flow Field.....	43
Fig. 3-1 Numerical flow diagram of the solution procedure	46
Fig. 3-2 The scalar control volume used for the discretisation of the governing equation	47
Fig. 4-1 Comparison of predicted methanol conversion with the experimental data of Park et al. [16].....	87

Fig. 4-2 Effects of geometric parameters and wall temperature on (a) the methanol conversion and (b) the CO concentration (ppm) at the outlet.....	88
Fig. 4-3 Effects of geometric parameters and H ₂ O/CH ₃ OH molar ratio on the CO concentration at (a) T _w =200 °C and (b) T _w =260 °C.....	89
Fig. 4-4 Effects of the channel heights on temperature distributions along the centerline of the channel at T _w =200 °C and T _w =260 °C.....	90
Fig. 4-5 Effects of wall temperature on the cross-sectioned temperature at different axial locations for H=1.0mm. (a) T _w =200 °C and (b) T _w =260 °C.....	91
Fig. 4-6 Effects of wall temperature on the cross-sectioned velocity at different axial locations for H=0.2mm. (a) T _w =200 °C and (b) T _w =260 °C.....	92
Fig. 4-7 Variations of the mole fraction of the various species along the channel (a) T _w =200 °C and (b) T _w =260 °C.....	93
Fig. 4-8 Effects of geometric parameters on the local CH ₃ OH mole fraction along the channel (a) T _w =200 °C and (b) T _w =260 °C.....	94
Fig. 4-9 Effects of geometric parameters on the local H ₂ mole fraction along the channel at T _w =200 °C and (b) T _w =260 °C.....	95
Fig. 4-10 Effects of geometric parameters on the local CO mole fraction along the channel at (a) T _w =200 °C and (b) T _w =260 °C.....	96
Fig. 4-11 Effects of thermo-fluid parameters on the local CH ₃ OH mole fraction along the channel at (a) T _w =200 °C and (b) T _w =260 °C.....	97
Fig. 4-12 Effects of thermo-fluid parameters on the local H ₂ mole fraction along the channel at (a) T _w =200 °C and (b) T _w =260 °C.....	98
Fig. 4-13 Effects of thermo-fluid parameters on the local CO mole fraction along the channel	

at (a) $T_w=200\text{ }^\circ\text{C}$ and (b) $T_w=260\text{ }^\circ\text{C}$	99
Fig. 4-14 Comparisons of the predicted results with and without wall conduction effects for the temperature and CH_3OH mole fraction distributions along the centerline of the channel ($Y=0.5$).....	100
Fig. 4-15 Comparison of predicted methanol conversion with previous experimental data of Park et al. [16]	101
Fig. 4-16 Variations of the mole fractions of the various species along the channel center line ($\gamma=0.5$)	102
Fig. 4-17 Effects of aspect ratios of channel and wall temperature on methanol conversion and CO concentration (ppm) at outlet of channel	103
Fig. 4-18 Effects of aspect ratios of channel on local methanol conversion along center line of channel at $T_w=200\text{ }^\circ\text{C}$ and $T_w=260\text{ }^\circ\text{C}$	104
Fig. 4-19 Effects of aspect ratios of channel at $T_w=200\text{ }^\circ\text{C}$ and $T_w=260\text{ }^\circ\text{C}$ on (a) local H_2 mole fraction and (b) local CO mole fraction along center line of channel	105
Fig. 4-20 Effects of aspect ratios of channel at $T_w=200\text{ }^\circ\text{C}$ and $T_w=260\text{ }^\circ\text{C}$ on (a) local velocity and (b) local pressure along center line of channel	106
Fig. 4-21 Effects of aspect ratios of channel at $T_w=200\text{ }^\circ\text{C}$ and $T_w=260\text{ }^\circ\text{C}$ on (a) local temperature along center line of channel and (b) local reaction rates of methanol steam reforming along interface between flow channel and catalyst layer	107
Fig. 4-22 Effects of aspect ratios of channel and Reynolds number on methanol conversion and H_2 production rate at $T_w=260\text{ }^\circ\text{C}$	108
Fig. 4-23 Effects of geometric size of channel on local temperature along center line of channel at $T_w=200\text{ }^\circ\text{C}$ and $T_w=260\text{ }^\circ\text{C}$	109

Fig. 4-24 Effects of geometric size of channel and Reynolds number on local CH ₃ OH mole fraction along center line of channel at (a) T _w =200 °C and (b) T _w =260 °C.....	110
Fig. 4-25 Effects of various wall temperatures on (a) the temperature distributions and (b) the CH ₃ OH mole fraction and H ₂ mole fraction distributions along the centerline of the serpentine flow field (Y=0.5).	111
Fig. 4-26 Effects of various wall temperatures on (a) the local velocity and (b) the local pressure along the centerline of the serpentine flow field (Y=0.5).	112
Fig. 4-27 Effects of Reynolds numbers at T _w =230°C on (a) the temperature distributions and (b) the CH ₃ OH mole fraction and H ₂ mole fraction distributions along the center line of the serpentine flow field (Y=0.5).....	113
Fig. 4-28 Effects of H ₂ O/CH ₃ OH molar ratio (S/C) at T _w =230°C on (a) the temperature distributions and (b) the CH ₃ OH mole fraction and CO mole fraction distributions along the center line of the serpentine flow field (Y=0.5)	114
Fig. 4-29 Local distributions of (a) CH ₃ OH mole fraction, (b) H ₂ mole fraction and (c) CO mole fraction along the cross-section of Y=0.5 at T _w =230°C.....	115
Fig. 4-30 Local distributions of (a) CH ₃ OH mole fraction, (b) H ₂ mole fraction and (c) CO mole fraction along the interface between the flow channel and catalyst layer (Y=0.95) at T _w =230°	116
Fig. 4-31 Effects of wall temperature and inlet fuel Reynolds number on the methanol conversion and H ₂ production rate	117
Fig. 4-32 Effects of heating different channel plates on the temperature and CH ₃ OH mole fraction distributions along the center line of the serpentine flow field (Y=0.5) ...	118
Fig. 4-33 Comparison of theoretical simulation of present results with previous experimental	

data by Won et al. [24].....	119
Fig. 4-34 Comparisons of the simulation results with and without wall conduction effects for the temperature distributions and CH ₃ OH mole fraction distributions along the centerline of the channel.....	120
Fig. 4-35 Effects of co- and counter-current flow configurations on (a) the temperature distributions along different axial location lines and (b) the local distributions of the mole fractions of the various species along the center line of the reforming channel (Y=0.167)	121
Fig. 4-36 Effects of the channel height of the combustor on (a) the temperature distributions along the top centerline of the reforming channel and (b) the CH ₃ OH mole fraction distributions along the center line of the reforming channel.....	122
Fig. 4-37 Effects of the channel height of the reformer on (a) the temperature distributions along the top centerline of the reforming channel and (b) the CH ₃ OH mole fraction distributions along the center line of the reforming channel.....	123
Fig. 4-38 Effects of the channel width on (a) the temperature distributions along the top centerline of the reforming channel (Y=0.333) and (b) the CH ₃ OH mole fraction distributions along the center line of the reforming channel (Y=0.167)	124
Fig. 4-39 Effects of the steel widths on (a) the temperature distributions along the top centerline of the reforming channel (Y=0.333) and (b) the CH ₃ OH mole fraction distributions along the center line of the reforming channel (Y=0.167)	125
Fig. 4-40 Effects of the Reynolds number (Re) for the combustor on (a) the temperature distributions along the top centerline of the reforming channel (Y=0.333) and (b) the CH ₃ OH mole fraction distributions along the centerline of the reforming channel (Y=0.167)	126

Fig. 4-41 Effects of the Reynolds number (Re) for the reformer on (a) the temperature distributions along the top centerline of the reforming channel (Y=0.333) and (b) the CH ₃ OH mole fraction distributions along the center line of the reforming channel (Y=0.167).....	127
Fig. 4-42 Effects of the Reynolds number (Re) of the combustor on wall temperature and methanol conversion.....	128
Fig. 4-43 Effects of the inlet flow rate (Q _{0,R}) of the reformer and various flow field designs on (a) wall temperature and (b) methanol conversion.....	129
Fig. 4-44 Effects of inlet flow rate (Q _{0,C}) of the combustor and various flow field designs on (a) wall temperature and (b) methanol conversion.....	130
Fig. 4-45 The temperature distributions on the top cross-section of the reforming channel for reformer and combustor with various flow field designs.....	131
Fig. 4-46 The CH ₃ OH mole fraction distributions on the middle cross-section of the reforming channel for reformer and combustor with various flow field designs.....	132
Fig. 4-47 The H ₂ mole fraction distributions on the middle cross-section of the reforming channel for reformer and combustor with various flow field designs.....	133
Fig. 4-48 The CO mole fraction distributions on the middle cross-section of the reforming channel for reformer and combustor with various flow field designs.....	134
Fig. 4-49 Effects of the inlet flow rate (Q _{0,R}) of the reformer and various flow field designs on the H ₂ production rate.....	135

NOMENCLATURE

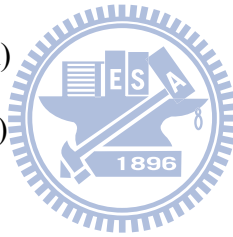
C_i	concentration of species i (mol m^{-3})
c_p	specific heat at constant pressure ($\text{kJ kg}^{-1} \text{K}^{-1}$)
D	hydraulic diameter (m)
D_{eff}	effective mass diffusivity ($\text{m}^2 \text{s}^{-1}$)
D_k	mass diffusion coefficient ($\text{m}^2 \text{s}^{-1}$)
D_p	catalyst particle diameter (m)
E_a	activation energy (kJ mol^{-1})
H	channel height (m)
H_C	combustion flow channel (m)
H_R	reforming flow channel (m)
H_W	solid wall thickness (m)
ΔH_{SR}	Enthalpy of reaction for steam reforming (kJ mol^{-1})
ΔH_{rWGS}	Enthalpy of reaction for the reverse water gas shift (kJ mol^{-1})
ΔH_{MD}	Enthalpy of reaction for decomposition reaction (kJ mol^{-1})
I, J, K	grid points in the x, y and z directions, respectively
k_{eff}	effective thermal conductivity ($\text{W m}^{-1}\text{K}^{-1}$)
k_f	fluid phase thermal conductivity ($\text{W m}^{-1}\text{K}^{-1}$)
k_p	permeability (m^2)
k_s	solid medium thermal conductivity ($\text{W m}^{-1}\text{K}^{-1}$)
k_1	pre-exponential factor for steam reforming
k_2	pre-exponential factor for the reverse water gas shift
k_3	pre-exponential factor for decomposition reaction
k_4	pre-exponential factor for combustion reaction

k_{-2}	pre-exponential factor for the water gas shift
L	flow channel length (m)
L_s	the total length from the serpentine flow channel inlet to outlet (m)
M_i	mole fraction of species i
$M_{w,i}$	molecular weight of species i (kg mol^{-1})
m_i	mass fraction of species i
p	pressure (Pa)
Q_{H_2}	hydrogen production rate at outlet ($\text{cm}^3 \text{ min}^{-1}$)
Q_C	inlet flow rate of the combustor
Q_R	inlet flow rate of the micro-reformer
R	universal gas constant ($\text{kJ kg}^{-1} \text{ K}^{-1}$)
R_{SR}	Arrhenius reaction rate coefficient for steam reforming ($\text{mol m}^{-3} \text{ s}^{-1}$)
R_{rWSG}	Arrhenius reaction rate coefficient for the reverse water gas shift ($\text{mol m}^{-3} \text{ s}^{-1}$)
R_{MD}	Arrhenius reaction rate coefficient for decomposition reaction ($\text{mol m}^{-3} \text{ s}^{-1}$)
$R_{\text{Combustion}}$	Arrhenius reaction rate coefficient for combustion reaction ($\text{mol m}^{-3} \text{ s}^{-1}$)
Re	Reynolds number, $Re = \rho u D / \mu$
Re_C	Reynolds number (Re) of the combustor
Re_R	Reynolds number (Re) of the micro-reformer
S/C	molar ratio of $\text{H}_2\text{O}/\text{CH}_3\text{OH}$
T	temperature ($^{\circ}\text{C}$)
T_w	wall temperature ($^{\circ}\text{C}$)
u, v, w	velocity components in the x, y and z directions, respectively, (m s^{-1})
$u_{0,C}$	inlet flow velocity on the combustion channel side (m s^{-1})
X	dimensionless distance from the flow channel inlet to outlet, $X = x/L$, $X = x_s/L_s$

x_s	the length from the serpentine flow channel inlet to outlet (m)
Y	dimensionless coordinate, $Y=y/H$, $Y= y/H_C+\delta_C+H_W+H_R+\delta_R$
x, y, z	coordinates (m)
W_R	channel width (m)
W_L	steel width (m)

Greek symbols

β	inertial loss coefficient
γ	aspect ratio (height and width ratio, $\delta_1+\delta_2/W_R$)
δ_C	combustion catalyst layer thickness (m)
δ_R	Reforming catalyst layer thickness (m)
δ_1	catalyst layer height (m)
δ_2	flow channel height (m)
ε	porosity
θ	dimensionless temperature, $\theta=(T-T_0)/(T_w-T_0)$
η	methanol conversion
λ'_i	the stoichiometric coefficient for reactant i in reaction
λ''_i	the stoichiometric coefficient for product i in reaction
τ	tortuosity of the porous medium
μ	viscosity ($\text{kg m}^{-1} \text{s}^{-1}$)
μ_{mix}	viscosity of the gas mixture ($\text{kg m}^{-1} \text{s}^{-1}$)
ϕ_{ij}	an auxiliary term in calculating viscosity of gas mixture
ρ	density (kg m^{-3})
ρ_s	catalyst density (kg m^{-3})



Subscripts

eff	effective
u	x-direction
v	y-direction
w	z-direction
0	inlet



CHAPTER 1

INTRODUCTION

1.1 Background

The demand for power sources with superior performance has increased due to the rapid growth of the portable electronics market. Moreover, technology progresses over time have enabled developments in electronics to move us into a microelectronics age. When devices make smaller, new functionalities are added. However, power consumption rises alarmingly. Therefore, the power sources must produce adequate power output while at the same time maintaining criteria such as a very small volume and lightweight packaging. Primary and secondary batteries have been the energy storage solution for these devices. However, batteries are a chemical process, but they do not last long enough. Until recently, one innovative way is to utilize the hydrogen and feed it to a fuel cell, producing electricity. Kundu et al. [1] presented fuel cells promise to provide higher power density and longer durability than batteries (Table 1-1). In fuel cell, electricity and water are produced from hydrogen and oxygen in an electrochemical reaction. Besides, fuel cells are quiet, efficient and convert energy electrochemically rather than mechanically. Therefore, fuel cells are widely regarded as the most promising energy storage devices for mobiles, laptops, and personal digital assistants (PDA) in the 21st century due to their properties of high energy density, low noise, and low pollution.

The fuel cells often have a maximum power of 1-50W that will be referred as micro fuel cell. In recent years, the proton exchange membrane fuel cell (PEMFC) and the direct methanol fuel cell (DMFC) have become widely used as micro fuel cells. Direct conversion may involve fuels such as methanol, ethanol, formic acid, and ethylene glycol are converted

into electrons through a direct fuel cell system. In direct fuel cell system, the main studies focused on DMFC, but DMFC has still issues due to a low rate of oxidation and a high crossover rate. The PEMFC is highly attractive for both portable and stationary application due to its high operating efficiency and environmental friendliness. This gives the PEMFCs great flexibility of a wide range of applications, Fig 1-1. PEMFCs have been proposed as battery replacements. Ball and Wietschl [2] presented applications of PEMFC in portable power sources need to carry enough hydrogen fuel. However, the hydrogen storage problem is still difficult to overcome. To solve this technical difficulty, one possible solution is to employ a reformer. Indirect energy conversion systems is to first reform methanol, ethanol, gasoline followed by feeding the reformat gas into miniature PEM fuel cell. The reformers often have characteristic dimensions, such as channel gaps, which are on the micro-scale (typically $1000\mu\text{m}$) or meso-scale (1000 μm to a few centimeters) and will be referred to in this article as micro-reformers. These features are significantly smaller than many conventional reformers, and they can significantly enhance mass and heat transfer rates. Therefore, micro-reformers are being developed for using with the miniature PEMFCs, to overcome the high risk of carrying a large quantity of hydrogen.

In reforming systems, the electronic energy system is generated using concentrated hydrogen produced by reforming from a fuel such as methanol. Holladay et al. [3] showed methanol is an attractive fuel because of its low reforming temperatures, good miscibility with water and low content of sulfur compounds. From the technological point of view, methanol clearly has distinct advantages as a fuel for fuel cell applications. First, methanol is liquid at atmospheric conditions and has a high hydrogen-to-carbon ratio relative to gasoline. Secondly, it can be reformed to hydrogen at much lower temperatures (200-300 $^{\circ}\text{C}$), and is more efficient as compared to gasoline and methane (700-800 $^{\circ}\text{C}$). Finally, methanol is an environmentally friendly fuel, as it is readily biodegradable in air, soil and water. Therefore, methanol clearly

has distinct advantages as a fuel for fuel cell applications due to its higher hydrogen-to-carbon ratio, low reforming temperature and greater environmental friendliness.

Holladay et al. [4] presented the majority of reformers currently being developed are designed to produce hydrogen from methanol. Three basic reforming technologies are steam reforming, partial oxidation, and autothermal reforming. Table 1-2 summarizes the advantages and challenges of each of these processes. Endothermic methanol steam reforming requires an external heat source. Partial oxidation is an alternative to steam reforming, where the reaction heat is provided by the partial combustion of the methanol with oxygen. The autothermal reforming process is a thermally neutral hybrid of steam reforming and partial oxidation. The partial oxidation and autothermal processes do not require an external heat source, but an expensive and complex oxygen separation unit is needed. Because of the steam reforming produces higher yields of hydrogen than autothermal reforming and partial oxidation of hydrocarbon fuels. The requirement of an external heat source can be addressed through the advanced heat and mass transfer provided by combustors. Hence, steam reforming is generally the preferred process for hydrogen production. A portable hydrogen production unit based on methanol steam reforming would be simpler and less costly than other alternatives.

The plate reformers have better performance than cylindrical reformers due to better heat and mass transfer is presented by Kolb et al. [5]. The plate methanol steam reformers are regarded as being micro-structured coated wall reformers, when patterning channels or similar fluid paths with a size below 1 mm. The advantages of micro-structured reformers enhanced heat and mass transfer are observed. Micro-structured reformers are much more suitable for the distributed production of hydrogen compared to conventional systems. One of the main features of micro-structured reformers is their high surface to volume ratio which is several orders of magnitude higher compared to traditional packed bed reactors. Micro-structured

multi-channel reformers work under laminar flow conditions demonstrating low pressure drop compared to randomly packed beds, and allow easy thermal integration of the processes involved. From the stated above, the plate methanol steam micro-reformer with small PEMFC has become a potential candidate for portable electronic products in the near future.

Fig. 1-2 shows a photograph of the micro-reformer and micro fuel cell, while Fig 1-3 shows the schematic of a system that consists of a methanol steam reformer and a fuel cell. First, methanol is fed with water and is heated by the vaporizer. The methanol is reformed by the reforming catalyst to generate hydrogen in the steam reformer. To supply heat to the steam reformer, part of methanol be fed to the combustor that generates sufficient amount of heat to sustain the steam reforming of methanol. For PEM fuel cells, the carbon monoxide levels need to be below 10 ppm. Therefore, a final polishing step (preferential oxidizer (PrOx) reactor) is used. Fig. 1-4 shows the photograph of the plate methanol steam micro-reformer including the etched glass wafers, the cross-section of the reformer, and the complete micro-reformer. Fig. 1-5 presents a simplified cross-sectional diagram of the plate methanol steam micro-reformer. The micro-reformer is composed of four units with vaporizers, catalytic combustor, and a CO remover. The functions are separated into two reaction systems. One reaction system is the hydrogen production system in which the methanol aqueous solution is fed and then vaporized at vaporizer 1, it is reformed to H_2 with CO_2 and a trace of CO at the methanol reformer; and finally the CO is preferentially oxidized at the CO remover. The other reaction system, the catalytic combustion system, is used to supply heat to the hydrogen production system. In this system, the methanol is vaporized at vaporizer 2 and then burned at the catalytic combustor. Fig. 1-6 shows a schematic of these two reaction systems.

Consequently, safety issues, storage problems, and size or portability considerations make pure hydrogen feeding relatively difficult for electronic equipment applications. The combination of a methanol reformer with a PEMFC overcomes the high risk involved in

carrying a large quantity of hydrogen, and is thus a promising choice for miniaturized portable electronic systems, and could soon become the new choice for portable fuel cell applications.

1.2 Literature Survey

The methanol steam micro-reformers have received much attention due to their compact sizes and great potential to be used in portable fuel cell systems as a hydrogen generation unit. Several experiments for methanol steam reformers are currently in progress. Various reformer types have been used as the foundation for methanol steam reformer designs, including packed-bed reformers and plate reformers. Several successfully fabricated packed bed reformers for hydrogen production have been reported [8-10]. Kolb and Hessel [11] presented that the plate reformers have better performance than the packed bed reformers due to better heat and mass transfers. Therefore, the channels were patterned on the plate methanol steam reformers by several investigators [12-18]. As a result of the steam reforming being an endothermic reaction, the researchers have used electrical heat sources to supply heat flux to steam micro-reformers. Seo et al. [12] used stainless steel as a substrate to fabricate a unit of reformer and vaporizer. The heat for the endothermic reaction is from the electric heater and the developed fuel processor can generate sufficient hydrogen for a fuel cell with power output of 10W. Kwon et al. [13] made a micro-reformer by using silicon wafer substrate and a 'fill-and-dry' method for catalyst coating. The stack of micro-reformer occupies 15 cm³ only and the maximum hydrogen production rate occurs about at 320°C in their experiments. Ha et al. [14] fabricated a PDMS (poly dimethylsiloxane) micro-reformer, and used a heater to supply heat flux. Their experimental results showed that methanol conversion was about 30-40% in the operating temperatures of 180-240 °C. The methanol conversion and hydrogen production of a plate-type micro-reformer with micro channels patterned on the micro-reformer was examined experimentally by Lim et al.[15]. The results showed

approximately 78% conversion of methanol, with a hydrogen production rate of 3 L/h. Park et al. [16] fabricated a steam reformer and vaporizer, and then assembled a miniature reforming device. The micro-channels were patterned on the steam reformer and the vaporizer. Their experimental results showed about 90% conversion of the methanol, with a hydrogen production rate of 0.498 mol/h, enough to supply a 15 W fuel cell. Jeong et al. [17] studied the steam reforming of methanol over a series of Cu/Zn-based catalysts by a micro-reformer. They found that a micro-reformer coated with Cu/ZnO/ZrO₂/Al₂O₃ catalyst with an undercoated Al₂O₃ buffer layer exhibits higher methanol conversion rate and lower CO concentration in the outlet gas. Kundu et al. [18] studied the stability and performance of microchannel reactor for methanol steam reforming with different sols as a binder in the coating of catalyst. They found the mixed sol of alumina and zirconia comparatively produced better performance.

The plate integrated fuel processor, consisting of the various micro structured modules, was developed to produce hydrogen for fuel cell systems. The fuel processor includes a fuel vaporizer, a catalytic combustor and a steam reformer. The catalytic combustor supplied heat to the steam reforming reaction, and the hydrogen was produced by the micro methanol steam reformer. Therefore, several studies have used catalytic burners to supply thermal energy to the entire micro-reformer [19-25]. Kwon et al. [19] utilized silicon fabrication technology to set up the reformer and the catalytic burner. Their results indicated that the methanol combustion reaction with the catalytic burner successfully generated heat to maintain reformer temperature. The methanol steam reformer combined with the catalytic burner produced 73% hydrogen with 65% conversion of the methanol. A micro methanol steam reformer which included a vaporizer, heat exchanger, catalytic combustor and steam reformer to produce hydrogen for a PEMFC was conducted experimentally by Park et al. [20, 21]. Their results showed that at a temperature of 250°C, the reformer could produce a gas flow

rate of 450 ml/min, with a gas composition of 73.3% H₂ at the micro channel outlet. Yoshida et al. [22] fabricated a micro channel methanol reformer integrated with a combustor and a micro channel vaporizer. An appropriate depth of the micro channel vaporizer could generate high yields of hydrogen was found in their work. Park et al. [23] fabricated a micro-structure reforming system including a methanol steam reformer, combustor and vaporizer. Catalytic combustion produced thermal energy which was used to supply the entire system. Their experimental results showed that enough hydrogen was produced by the reforming system for a 0.1 W PEMFC. Won et al. [24] fabricated a micro channel reactor including a vaporizer, methanol steam reformer and combustor, to produce hydrogen for a PEMFC. Their results indicated that at a temperature of 270°C, the reformer could produce a hydrogen flow rate of 3.9 l/h for 5.5 W fuel cell. A plate fuel processor was developed by Sohn et al. [25] for a 150W PEM fuel cell system. The fuel processor includes reformer, combustor, heat exchanger, and evaporator and could be operated without any external heat supply.

For the PEM fuel cell, the CO concentration must be less than 10 ppm, so a cleanup step is required after methanol steam reforming. The integration of the PrOx or water-gas-shift reaction equipment to reduce the CO concentration in the gas from the methanol steam reformer has been used by several researchers [26, 27]. Kwon et al. [26] used silicon to fabricate a reformer and preferential oxidizer (PrOx) reactor. The reactor produced hydrogen to supply the fuel cell. The experimental results showed that the reformer generated 27 cm³/min of hydrogen and that the CO was totally removed from the gas by the PrOx device. When the fuel cell was operated at 0.6 V, the power density was 230 mW/cm².

In order to reduce the research cost and design duration, modeling and simulation are often being used to obtain a better understanding of the processes in a channel. There have been various numerical studies of the fluid flow and heat transfer in channels since the early work [28-31]. Hishida [28] investigated forced and free convection in a channel with radiation.

The characteristics of fluid flow and heat transfer in micro channel cooling passages have been examined numerically by Liu [29]. Chiu et al. [30] and Chiu and Yan [31] developed numerical model to study mixed convection heat transfer in horizontal ducts and inclined ducts, respectively, with radiation effects. Massive amount of works on heat and mass transfer have focused mainly on parallel plate channel [32,33] and rectangular ducts [34]. Recently, the investigation of forced convection heat and mass transfer in vertical rectangular duct with film evaporation has been numerically examined by Boukadida and Nasrallah [35]. Analysis of chemical reaction coupled mass and heat transport phenomena in a reactor duct has been performed in the past decade [36-37]. The effects of catalyst loading and reformer geometry on the circular methane micro-reformer were studied numerically by Stutz et al. [36]. Yuan et al. [37] developed a model of the plate methane reformer, including the momentum equation, energy equation and chemical reaction equations to explore the temperature and gas distributions in the reformer ducts.

There are many research works about the developed catalysts used in the reforming reaction using different kinetics of the methanol steam reforming reactions [38-43]. Methanol can be reformed by two overall reactions in a reformer filled with the catalyst $\text{CuO}/\text{ZnO}/\text{Al}_2\text{O}_3$ as described by Amphlett et al.[38]. Peppley et al. [39, 40] studied the reaction network for methanol steam reforming over a $\text{Cu}/\text{ZnO}/\text{Al}_2\text{O}_3$ catalyst from BASF. The steam reforming of methanol over a $\text{Cu}/\text{ZrO}_2/\text{CeO}_3$ catalyst was investigated by Mastalir et al. [41]. The kinetic model suggested for the transformation involved the reverse water-gas shift and methanol decomposition, in addition to the steam reforming methanol reaction. Lee et al. [42] carried out a kinetic study of methanol steam reforming over a commercial catalyst $\text{CuO}/\text{ZnO}/\text{Al}_2\text{O}_3$.

Computational simulation and modeling are used extensively in research and industrial applications to obtain a better understanding of the fundamental processes and to optimize

designs before building prototypes for engineering applications. Therefore, more theoretical modeling for study of the methanol reformer is in progress. Known from the literature survey, several numerical models have been presented, with the simplest methods using a one-dimensional model to describe the methanol reformer conversion and the heat and mass transport phenomena [43-47]. Kawamura et al. [43] proposed a mathematical heat and mass model to analyze the transport phenomena in the plane methanol steam reformer channels. They successfully simulated methanol conversion and gas concentration distributions along the channel. Kim and Kwon [44] have numerically investigated the inner transport phenomena in the plate methanol steam reformer ducts. The results indicated that a lower inlet feed rate has a better methanol conversion. Their results also showed that smaller reformer volumes required a higher heat flux. Pattekar and Kothare et al. [45] developed one-dimensional models for radial and micro channel methanol reformers. The results demonstrated that a radial flow reformer had better hydrogen production rates and lower pressure drops than the micro channels of a plate reformer. Stamps and Gatzke [46] developed a reformer with a model PEMFC to study various design and operating parameters on system performance. They found that agreement of the theoretical and experimental results for the temperature, flow rate and CO concentration data. The simplest model to describe the methanol reformer conversion and the heat and mass transport phenomena was presented by Yoon et al.[47]. The results showed that appropriate reactor geometry can improve the reactant gas transport and the efficiency of thermal management.

As for the two-dimensional simulation about the methanol reformers, the literature survey has existed in the past decade [48-51]. Suh et al. [48, 49] employed a cylindrical mathematical model of a packed bed reformer to investigate heat and mass transport phenomena in a methanol reformer. The results showed good agreement between theoretical and experimental results, and also found that the internally heated reformer could improve the

methanol conversion. The effects of the methanol steam reforming rate in both a packed bed reformer and a wall coated reformer were examined by Karim et al. [50, 51]. The results showed that a wall coated reformer had better heat and mass transfer limitations and higher catalyst activity than a packed bed reformer. Their results also showed that the minimum reformer diameter yielded the highest catalyst activity and smallest temperature gradient.

There are many three-dimensional simulations of methanol reformers in the literature [7, 19, 27, 52-57]. Kwon et al. [19] investigated the pressure and velocity distributions in the micro-reformer channels by using computational fluid dynamics (CFD). The results show the reformer of 17 parallel micro-channels has a much more uniform velocity distribution than that of 36 parallel micro-channels. A uniform velocity distribution may have a better chemical reaction. A three-dimensional model of a micro-scale reactor to investigate velocity and pressure distributions was developed by Pattekar and Kothare [52]. Kim and Kown [27] developed a novel reforming channel to study the pressure, velocity, temperature and hydrogen mole fraction distributions in the reformer. The results show that the novel flow field had better performance than the serpentine flow field. A cylindrical model of the reformer which comprised of a methanol steam reformer and a CO methanator to simulate the conversion and temperature distributions in the reformer was investigated by Cao et al. [53]. Their results showed that the appropriate insulation thickness could reduce the heat losses and achieve a small volume and a high power density. Park et al. [54] developed 3-D, quasi-3-D and 1D models to study reformer performance. There was good agreement between the experimental and analytical results. Cao et al. [55] presented kinetic rate expressions and developed a homogenous model of a micro channel reformer to simulate the temperature distributions in a micro channel. Hsueh et al. [56] employed a numerical channel model to analyze various height and width ratios on the plate micro-reformer performance and reactant gas transport characteristics. The results indicated that a reduction in aspect ratio would

improve H₂ production rate and methanol conversion. Chen et al. [57] used a mathematical model of the plate-type reformer to investigate the heat and mass transfer in a reformer. The results showed that the CO concentration could reduce with lower temperature, larger H₂O/CH₃OH molar ratio and aspect ratio. Kim [7] developed a micro-reformer model to simulate the conversion and temperature distributions in the reformer. The results revealed that the methanol conversion increased with increasing the reformer temperature and decreasing the feed rate.

More theoretical modeling of steam reforming coupled with catalytic combustion for the plate reactors is currently in progress. A reactor model that combines a steam reformer and catalytic combustor was recently examined by several researchers [58-67]. The systems are fed by hydrocarbons which convert the hydrogen and generate heat, and studies have developed numerical models of a micro-reformer with a combustor to explore the heat and mass transport phenomena and fuel conversion efficiency. A two-dimensional model of a plate methane reformer with methane combustor to investigate thermo-fluid parameters and geometric parameters was developed by Zanfir and Gavriilidis [58]. Their results showed that the micro-reformers have better performance than traditional reformers due to their better heat and mass transfer. The results also showed that a higher channel height produces a lower conversion and much more uniform temperature distribution. More theoretical modeling of steam reforming couples with catalytic combustion for the plate reactors are currently in progress. Lattner and Harold [59] have numerically and experimentally investigated a bench-scale fixed-bed methanol reformer for autothermal reforming. This system was also used by Pepply et al. [40] and Reitz [60] who presented kinetic rate expressions for the simulations. Their results showed agreement between the theoretical and experimental results. Deshmukh and Vlachos [61, 62] presented a two-dimensional model of propane (C₃H₈) combustion with ammonia (NH₃) decomposition to investigate micro reactors for hydrogen

production. The results show that the H_2 production rate and the temperatures generated via the C_3H_8 combustion both increase as the flow rate of ammonia increases. The results also show that the co-current flow configuration has a lower reactor temperature and allows a wider spectrum of materials to be used than the counter-current flow configuration. A micro-channel model of the thermal integration of a steam reformer and a catalytic combustor was established by Arzamendi and collaborators [63-64]. Using the hydrogen produced by the reforming reaction from methanol and methane, the results showed the short diffusion distance and higher area to volume ratio required for using the micro reactor. The results also indicated that complete combustion of methane takes place over a very short distance. The reforming fuel is rapidly heated and then the methane reactor has a more uniform temperature distribution. Pan and collaborators [65, 66] developed the numerical models for a plate-fin methanol steam reformer and a bench-scale methanol autothermal reformer. A plate-fin reformer integrated endothermic and exothermic reactions into one unit. The combustor supplied the heat for the methanol steam reformer. Their numerical model accurately predicted the methanol conversion rate and the gas distributions. Varesano et al. [67] used an one-dimensional transient mathematical model to study the transport behavior in a steam reforming reactor with a burner that supplies heat. The transient characteristics of the reformer were examined in detail.

The flow field design in a fuel cell is one of the most important issues for PEMFC. An appropriate flow field design in the fuel cell can improve the reactant transport, the thermal and water management. To this end, different flow field configurations, including parallel, serpentine and interdigitated have been developed. Many efforts have been devoted to optimize the flow field design to improve cell performance [68-71]. In recent years, several studies based on the flow field designs theory are applied to the plate methanol reformer design. Different types of flow field designs for plate methanol micro-reformers have been

used to achieve more efficient methanol conversion. Kundu et al. [72] used different flow configurations, including serpentine and parallel flow fields, to improve plate methanol reformer performance.

1.3 Objectives

In the present study, the objective of this work is to investigate the transport phenomena and performance of the plate methanol steam micro-reformer (only including methanol steam micro-reformer and methanol catalytic combustor). Fig. 1-7 shows the structure of PhD thesis. The study is divided into five parts. Firstly, there have been various numerical studies of the fluid flow in plate methanol steam reformer channels [19, 52]. In order to simplify the analysis, many studies have considered the numerical model of methanol steam reformers, only including energy equation and concentration equations with chemical reaction [43-44, 46, 48-51, 53, 55]. Furthermore, the continuity equation, momentum equation, energy equation and species equations with chemical reaction were employed to explore the temperature and gas concentration distributions in the reformer by several researchers [7, 27, 54]. In this work, an attempt is made to examine the detailed fluid flow, heat and mass transfer coupled with chemical reactions in the plate methanol steam micro-reformer channels. Therefore, we develop a two-dimensional channel model of the plate methanol steam reformer to study the methanol conversion and local heat and mass transfer in the channel of a plate micro-reformer. The effects of geometric and thermo-fluid parameters on the plate methanol steam micro-reformer performance and the heat and mass transfer are numerically investigated in detailed.

Secondly, we extended our previous study to three a three-dimensional channel model of the plate methanol steam micro-reformer to analyze the local transport phenomena and micro-reformer performance. The geometric design of a reactor is one of the most important

issues. Appropriate reactor geometry can improve the reactant gas transport and the efficiency of thermal management [36-37, 47, 50-51, 73-75]. As stated above literature survey, while many studies have investigated the effects of reactor radius on cylindrical reactor performance [36, 47, 50-51, 73-75], few studies have reported on the flow channel designs of plate methanol steam micro-reformers. Therefore, based on flow channel designs, various aspect ratios of channels on plate methanol steam micro-reformers can potentially enhance fuel utilization. In this work, flow channels with various aspect ratios (height and width ratios) and geometric size are numerically examined the transport phenomena in a channel reformer. In addition, the thermo-fluid parameters (Reynolds number and wall temperature) are also investigated to examine their effects on the methanol conversion and efficiency of channel reformers.

Thirdly, the literature cited above has shown that micro-reformer performance can be enhanced by suitable thermo-fluid parameters. However, several researchers have studied plate steam reformers with a parallel flow field which is attractive due to its simplicity [44, 56-57]. There has been a limited amount of work investigating the effects of the different flow field designs on thermo-fluid parameters, especially for the serpentine flow field. Therefore, the objective of this section is to establish a three-dimensional serpentine flow field model of the plate methanol steam micro-reformer to investigate its transport phenomena and methanol conversion efficiency.

Fourthly, from the literature survey presented above, it was found that some literature is available on mathematical models of the methanol steam micro-reformer, but little information is available on mathematical models of a micro-reformer with a catalytic combustor. Therefore, the objective of the present study is to investigate the transport phenomena and the fuel conversion efficiency in a methanol steam micro-reformer with methanol catalytic combustor. A three-dimensional numerical model of a micro-reformer with

combustor is developed to examine the effects of various flow configurations and geometric parameters on micro-reformer performance.

Finally, from the literatures cited above, it is shown that the methanol conversion can be enhanced by a suitable flow channel design. However, there is only a limited amount of work to investigate the effect of different flow field designs on the performance especially for the serpentine flow field. Therefore, the objective of this section is to establish a three-dimensional computational model of the plate methanol micro-reformer with methanol catalytic combustor to investigate the performance and transport phenomena of the micro-reformer with various flow fields (parallel flow field and serpentine flow field). In this study, micro-reformer performance and gas transport phenomena can be accurately predicted from our simulation. Therefore, this model is useful and can be reduce the design time of a new plate methanol steam micro-reformer. Thus this can provide sufficient information for designing micro-reformer system.

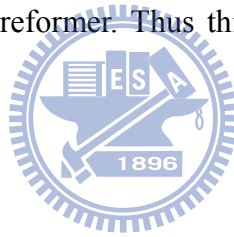


Table 1-1 Energy density of various batteries and fuels [1]

Fuel	Energy density (Wh kg ⁻¹)	Comments
BB-2590	81	Secondary
BA-5590	150	Primary
BA-5390	235	Primary
BA-8180	345	Primary Zn–Air battery, large unit
Compressed hydrogen	500~1000	5000 psig, value includes container weight
Sodium borohydride	3600	[NaBH ₄ + 2H ₂ O] weight only
Methanol	5500	Based on lower heating value of fuel
Most liquid hydrocarbons	~12,400	Based on lower heating value of fuel
Hydrogen gas	33,200	Unpacked
Nuclear material	2,800,000	Raw power

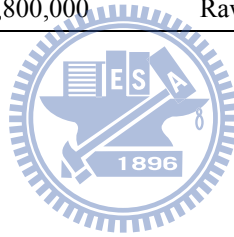
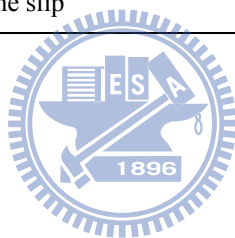


Table 1-2 Comparison of reforming technologies [4]

Technology	Advantages	Disadvantages
Steam reforming	<ol style="list-style-type: none"> 1. Most extensive industrial experience 2. Oxygen not required 3. Lowest process temperature 4. Best H₂/CO ratio for H₂ production 	<ol style="list-style-type: none"> 1. Highest air emissions
Autothermal reforming	<ol style="list-style-type: none"> 1. Lower process temperature than POX 2. Low methane slip 	<ol style="list-style-type: none"> 1. Limited commercial experience 2. Requires air or oxygen
Partial oxidaiton	<ol style="list-style-type: none"> 1. Decreased desulfurization requirement 2. No catalyst required 3. Low methane slip 	<ol style="list-style-type: none"> 1. Low H₂/CO ratio 2. Very high processing temperatures 3. Soot formation/handling adds process complexity



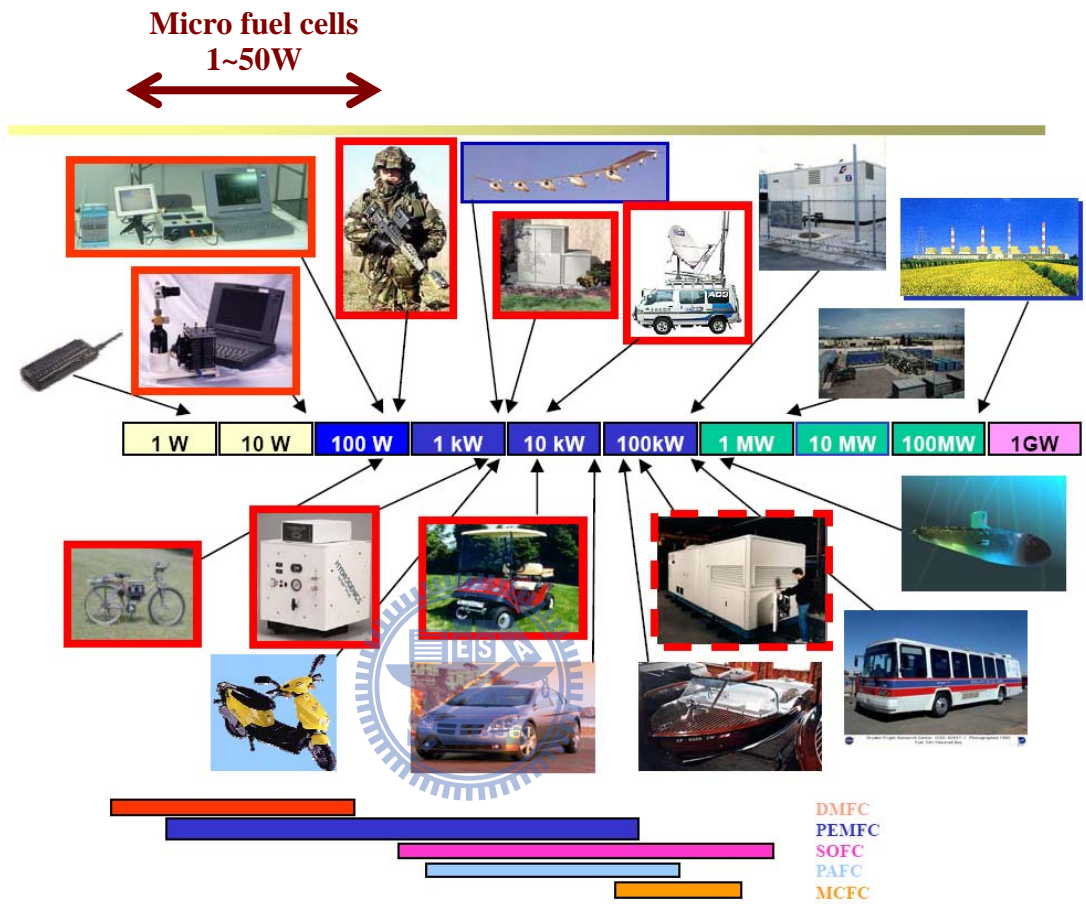


Fig. 1-1 Applications of the fuel cell (ERL/ITRI)

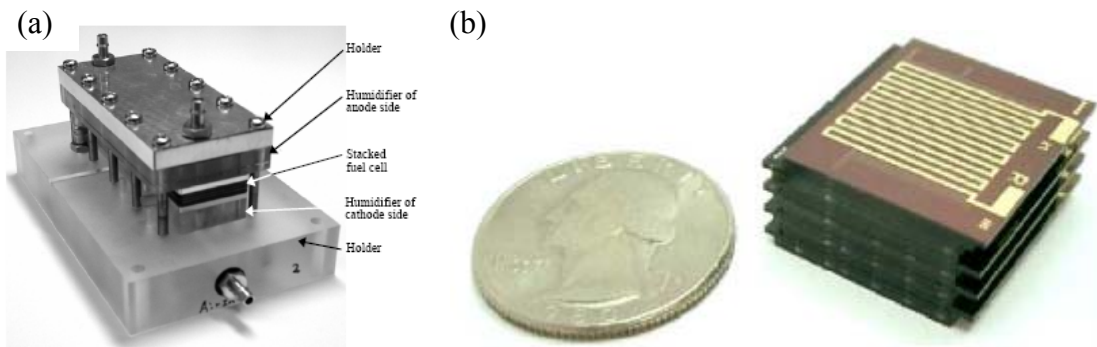


Fig. 1-2 Photograph of the (a) small PEMFC and (b) micro-reformer [6]



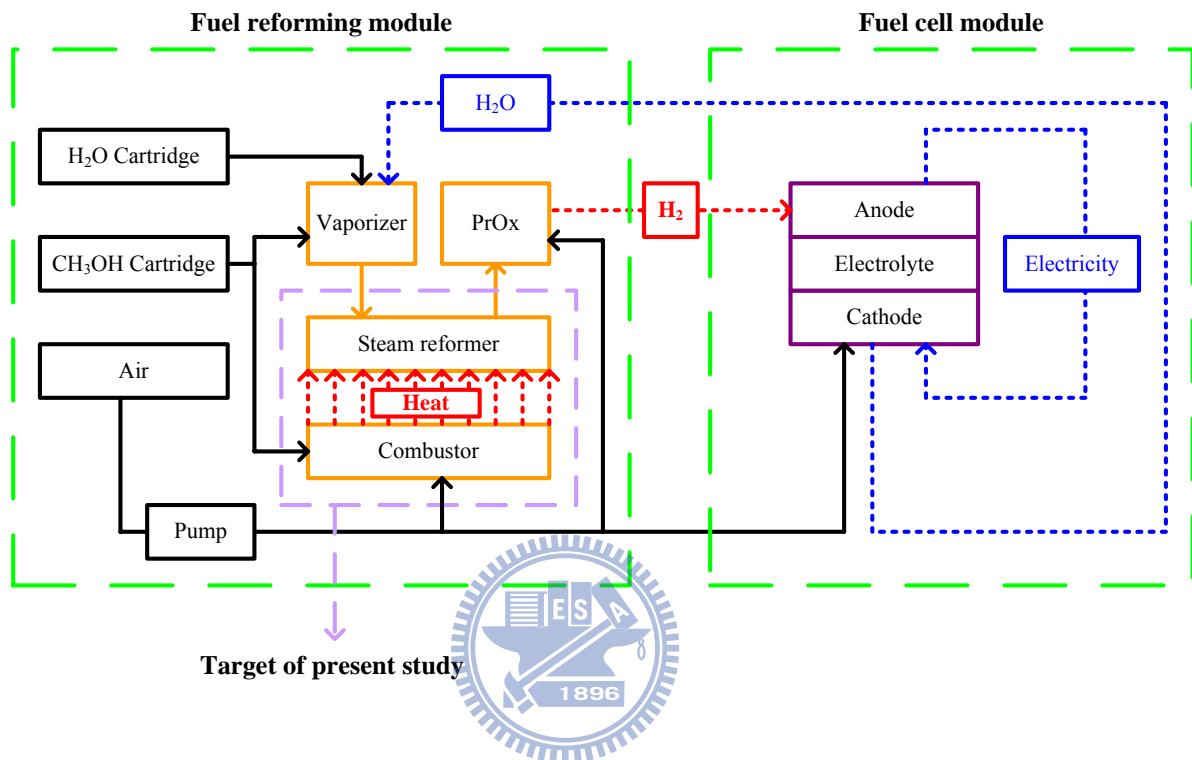


Fig. 1-3 Schematic of fuel reforming process [7]

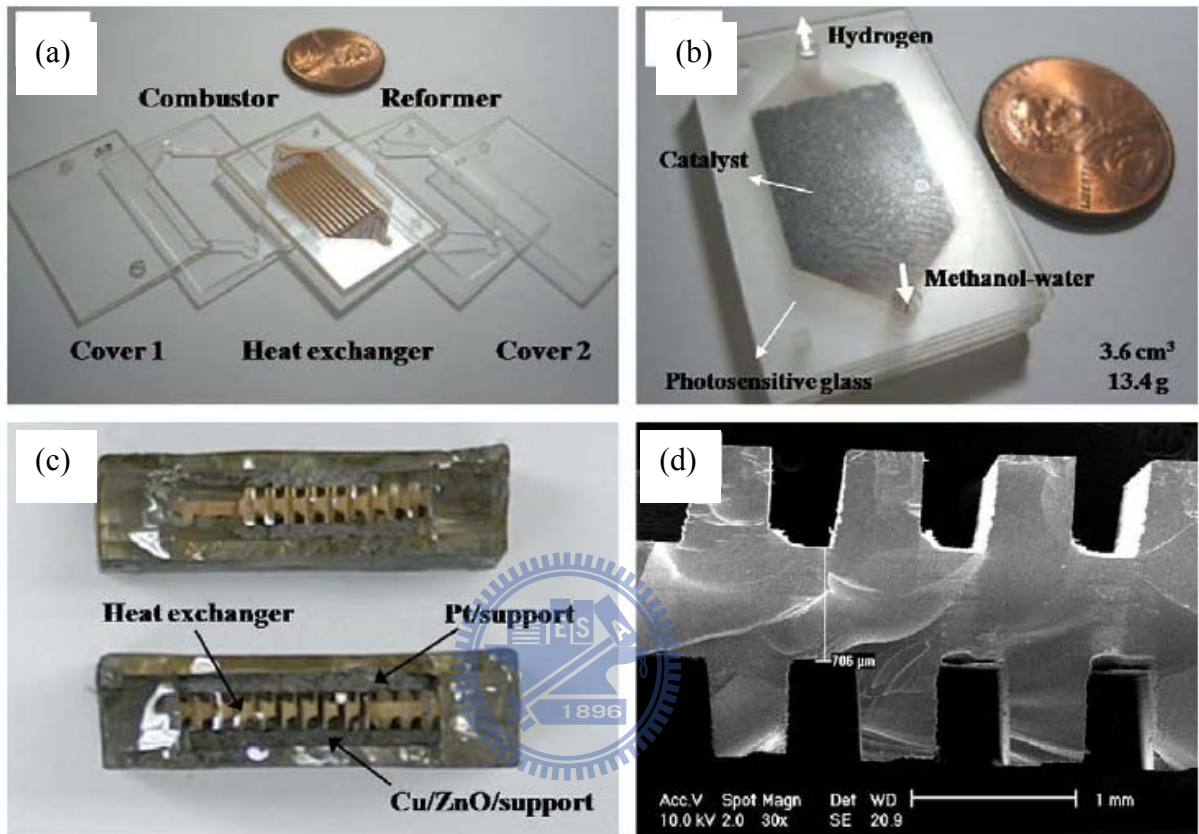


Fig. 1-4 Photograph of the plate methanol steam micro-reformer [7]

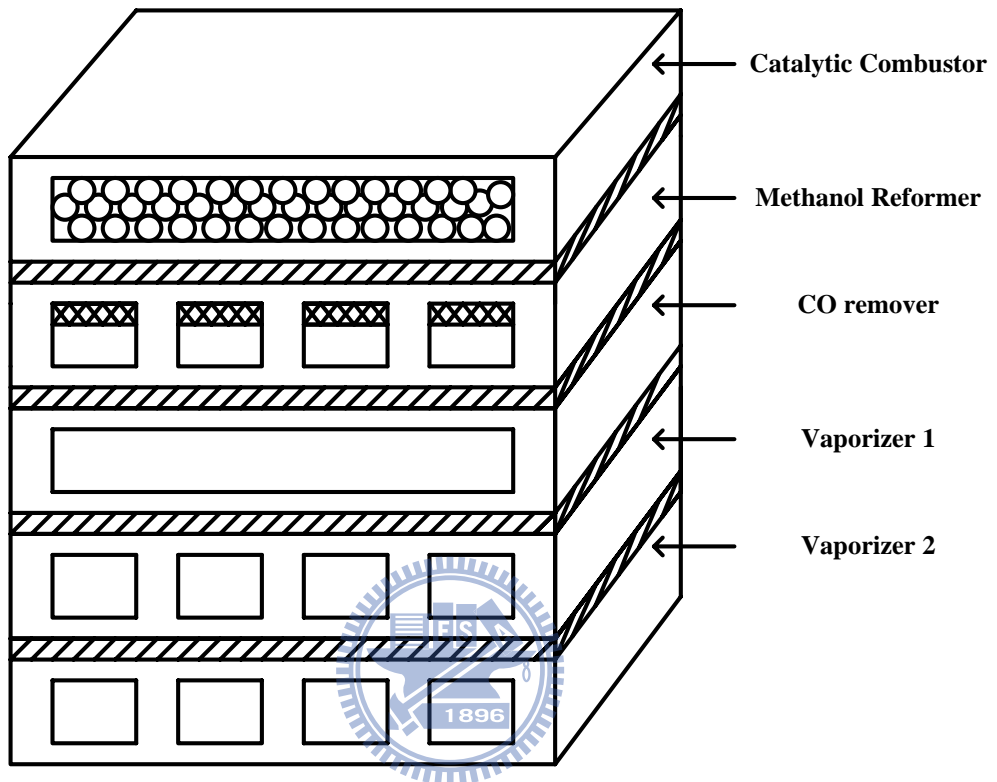


Fig. 1-5 Structure of micro-reformer [6]

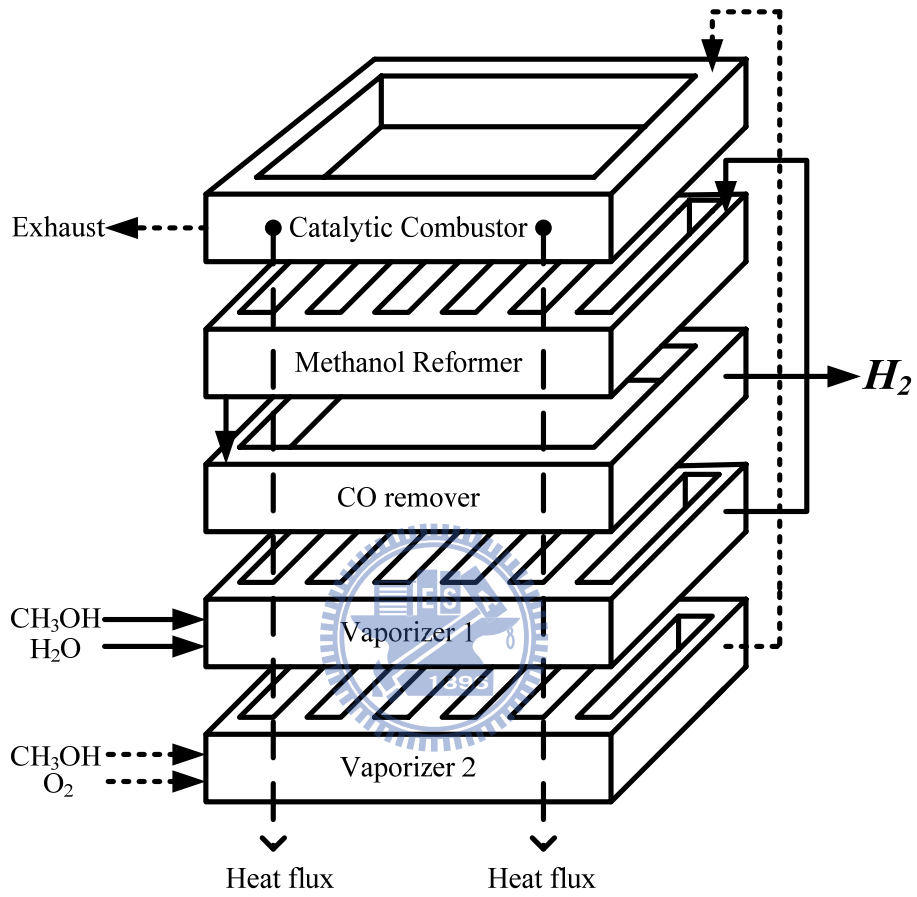


Fig. 1-6 Schematic of methanol reforming system [6]

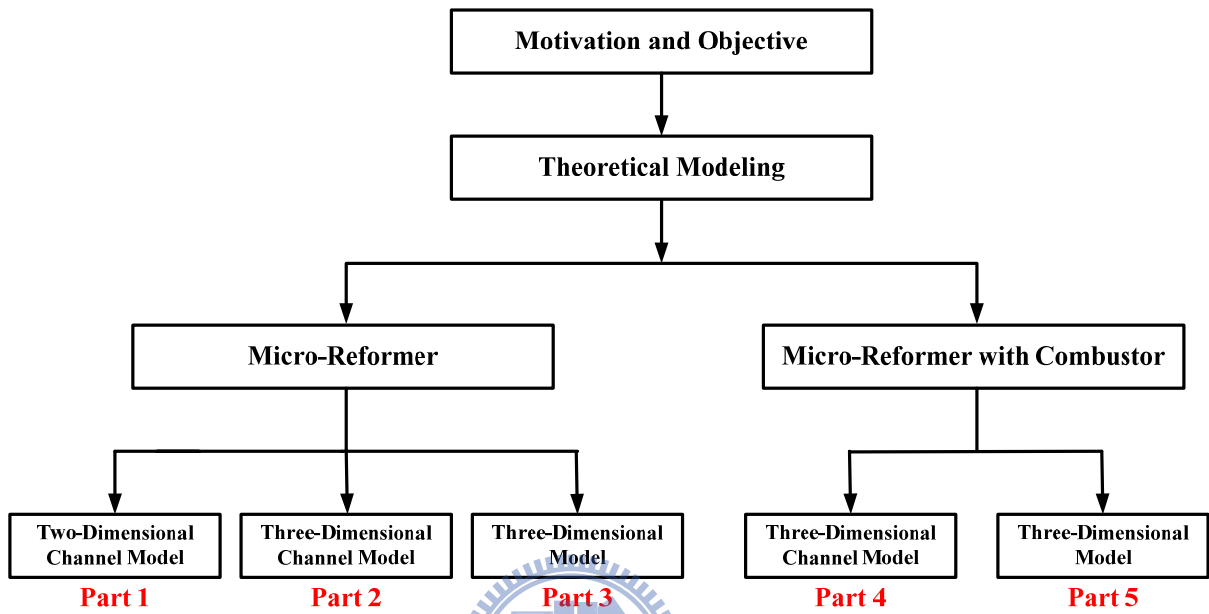


Fig. 1-7 Schematic of PhD thesis structure

CHAPTER 2

MATHEMATICAL MODEL AND ANALYSIS

2.1 The Model of the Methanol Steam Micro-Reformer

2.1.1 Model Description

In this section, the research only considered the plate methanol steam micro-reformer, namely the methanol catalytic combustor is not included in it. Firstly, a 2-dimensional channel model of the plate methanol steam micro-reformer would be established to study the methanol conversion and local heat and mass transfer in the channel of a plate methanol steam micro-reformer. Figure 2-1 presents a schematic of the two-dimensional channel geometry of the plate methanol steam micro-reformer used in the present work.

Then, the research extended my previous study to be a three-dimensional channel model of the plate methanol steam micro-reformer to analyze the local transport phenomena and micro-reformer performance. The channel is comprised of the flow channel, catalyst layer and solid wall. The governing equations include mass, momentum, energy and species equations. To reduce the computing time, the symmetric channel is considered only in this work. The schematic diagram of this work is shown in Fig. 2-2.

Finally, a three-dimensional computational model of heat and mass transfer in a micro-reformer with a serpentine flow field is proposed. The serpentine flow field has eight turns. A schematic illustration of the coordinate system is shown in Fig. 2-3. The channel of the serpentine flow field consists of a flow channel and a catalyst layer.

2.1.2 Assumption

To simplify the analysis, the following assumptions are made:

- (1) The flow is steady state;
- (2) The inlet fuel is an ideal gas;
- (3) The flow is laminar and incompressible;
- (4) The catalyst layer is isotropic;
- (5) The chemical reaction occurs only in the catalyst layer;
- (6) Thermal radiation and conduction in the gas phase are negligible compared to convection.

2.1.3 Governing Equations

According to the descriptions and assumptions above, the basic transport equations for the two-dimensional and three-dimensional plate methanol steam micro-reformer are as follows:

Continuity equation:

$$\frac{\partial u}{\partial x} + \frac{\partial v}{\partial y} + \frac{\partial w}{\partial z} = 0 \quad (2-1)$$

X-momentum equation:

$$\varepsilon\rho \left(u \frac{\partial u}{\partial x} + v \frac{\partial u}{\partial y} + w \frac{\partial u}{\partial z} \right) = -\varepsilon \frac{\partial p}{\partial x} + \varepsilon\mu \left(\frac{\partial^2 u}{\partial x^2} + \frac{\partial^2 u}{\partial y^2} + \frac{\partial^2 u}{\partial z^2} \right) + S_u \quad (2-2)$$

Y-momentum equation:

$$\varepsilon\rho \left(u \frac{\partial v}{\partial x} + v \frac{\partial v}{\partial y} + w \frac{\partial v}{\partial z} \right) = -\varepsilon \frac{\partial p}{\partial y} + \varepsilon\mu \left(\frac{\partial^2 v}{\partial x^2} + \frac{\partial^2 v}{\partial y^2} + \frac{\partial^2 v}{\partial z^2} \right) + S_v \quad (2-3)$$

Z-momentum equation:

$$\varepsilon\rho\left(u\frac{\partial w}{\partial x}+v\frac{\partial w}{\partial y}+w\frac{\partial w}{\partial z}\right)=-\varepsilon\frac{\partial p}{\partial z}+\varepsilon\mu\left(\frac{\partial^2 w}{\partial x^2}+\frac{\partial^2 w}{\partial y^2}+\frac{\partial^2 w}{\partial z^2}\right)+S_w \quad (2-4)$$

In the momentum equations, ε is the porosity of the medium. S_u , S_v and S_w are corrected terms for the reactant gas flow in the porous material of the catalyst layer of the micro-reformer. The S_u , S_v and S_w are zero in the flow channel region. While in the catalyst layer, S_u , S_v and S_w are different in each computation domain due to the difference in pressure when fluids pass through a porous medium. So, S_u , S_v and S_w in the catalyst layer are [76]:

$$S_u = -\frac{\mu u}{k_p} - \frac{\beta u \rho}{2} \sqrt{u^2 + v^2 + w^2} \quad (2-5)$$

$$S_v = -\frac{\mu v}{k_p} - \frac{\beta v \rho}{2} \sqrt{u^2 + v^2 + w^2} \quad (2-6)$$

$$S_w = -\frac{\mu w}{k_p} - \frac{\beta w \rho}{2} \sqrt{u^2 + v^2 + w^2} \quad (2-7)$$

where k_p is the permeability and β is the inertial loss coefficient in each component direction [76].

$$k_p = \frac{D_p^2 \varepsilon^3}{150(1-\varepsilon)^2} \quad (2-8)$$

$$\beta = \frac{3.5(1-\varepsilon)}{D_p \varepsilon^3} \quad (2-9)$$

and where D_p is the catalyst particle diameter.

The viscosity of the gas mixture can be calculated from Wilke's mixture rule [77] as follows:

$$\mu_{\text{mix}} = \frac{\sum_{i=1}^5 \frac{M_i \mu_i}{\sum_{j=1}^5 M_j \phi_{ij}}}{\sum_{j=1}^5 M_j \phi_{ij}} \quad (2-10)$$

where

$$\phi_{ij} = \sum_i \frac{\left[1 + \left(\frac{\mu_i}{\mu_j} \right)^{\frac{1}{2}} \left(\frac{M_{w,j}}{M_{w,i}} \right)^{\frac{1}{4}} \right]^2}{\left[8 \left(1 + \frac{M_{w,i}}{M_{w,j}} \right) \right]^{\frac{1}{2}}} \quad (2-11)$$

Species equation:

$$\left(u \frac{\partial m_i}{\partial x} + v \frac{\partial m_i}{\partial y} + w \frac{\partial m_i}{\partial z} \right) = D_{\text{eff}} \left(\frac{\partial^2 m_i}{\partial x^2} + \frac{\partial^2 m_i}{\partial y^2} + \frac{\partial^2 m_i}{\partial z^2} \right) + (1 - \varepsilon) \rho_s S_c \quad (2-12)$$

In the species equation, m_i denotes the mass fraction of the i^{th} species; the calculations have included CH_3OH , H_2O , H_2 , CO_2 and CO . In this work, the porosity ε is expressed as 0.38 and 1.00, in the catalyst layer and the flow channel, respectively. In Eq(2-12), D_{eff} is the effective diffusion coefficient based on the Stefan-Maxwell equations [51]. Eq(2-13) is employed to describe the influence of the porosity on the diffusion coefficient

$$D_{\text{eff}} = D_k \varepsilon^\tau \quad (2-13)$$

The diffusion coefficient D_k for the methanol steam micro-reformer was derived from the Stefan-Maxwell equations which were used to calculate the mean effective binary diffusivity [51].

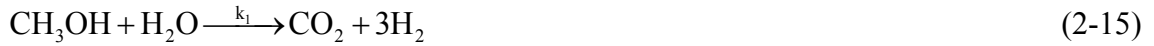
S_c represents the source terms due to the chemical reaction in the catalyst layer. Therefore, S_c is zero in the flow channel. Furthermore, S_c differs according to the reactant gases in the catalyst layer.

$$S_c = M_{w,i} (R_{\text{SR}} + R_{\text{rWGS}}) (\lambda_i'' - \lambda_i') \quad (2-14)$$

where λ_i' and λ_i'' are the stoichiometric coefficient for reactant i and product i , respectively, in the reaction.

According to the chemical kinetics of Hotz et al. [78], the steam reforming reaction is much faster than the decomposition and water-gas shift reaction. Purnama et al. [79] and

Agrell et al. [80] proposed that using a Cu/ZnO/AlO₃ catalyst for methanol steam reforming gives rise to two main chemical reactions, the steam reforming and the reverse water gas shift reactions. They also indicated that CO was generated by the reverse water gas shift reaction. Therefore, only the steam reforming reaction, Eq. (2-15), and the reverse water-gas shift reaction, Eq. (2-16), are considered in this study.



In this study, the model for methanol steam reforming is that used by Hsueh and collaborators [56, 57], and the Arrhenius equation is used to calculate the concentration of reactant gases generated by the chemical reaction.

$$R_{\text{SR}} = k_1 C_{\text{CH}_3\text{OH}}^{0.6} C_{\text{H}_2\text{O}}^{0.4} \exp\left(-\frac{E_a}{RT}\right) \quad (2-17)$$

$$R_{\text{rWGS}} = k_2 C_{\text{CO}_2} C_{\text{H}_2} \exp\left(-\frac{E_a}{RT}\right) - k_{-2} C_{\text{CO}} C_{\text{H}_2\text{O}} \exp\left(-\frac{E_a}{RT}\right) \quad (2-18)$$

where the steam reforming reaction is a non-reversible reaction and the reverse water-gas shift reaction is reversible. The constants k_1 and k_2 are the forward rate constants for the steam reforming reaction and the reverse water-gas shift reaction, respectively. The constant k_{-2} is the backward rate constant for the water-gas shift reaction.

To calculate the local temperature, the energy equations must be solved.

Energy equation:

$$\rho c_p \left(u \frac{\partial T}{\partial x} + v \frac{\partial T}{\partial y} + w \frac{\partial T}{\partial z} \right) = k_{\text{eff}} \left(\frac{\partial^2 T}{\partial x^2} + \frac{\partial^2 T}{\partial y^2} + \frac{\partial^2 T}{\partial z^2} \right) + \varepsilon S_t \quad (2-19)$$

In the energy equation, the effective thermal conductivity in the porous medium, k_{eff} , is the volume average of the fluid conductivity and solid conductivity. The effective thermal conductivity is given by

$$k_{\text{eff}} = \varepsilon k_f + (1 - \varepsilon)k_s \quad (2-20)$$

where k_f is the fluid phase thermal conductivity, k_s the solid medium thermal conductivity and ε the porosity of the medium.

In the energy equation, S_t is the source term due to the chemical reactions, which in the channel is zero. The catalyst layer experiences exothermic and endothermic chemical reactions, so S_t can be described as:

$$S_t = -(\Delta H_{\text{SR}} R_{\text{SR}} + \Delta H_{\text{rWGS}} R_{\text{rWGS}}) \quad (2-21)$$

where ΔH_{SR} is the enthalpy of reaction of the steam reforming reaction, and ΔH_{rWGS} is the enthalpy of reaction of the reverse water-gas shift reaction.

In the solid regions, the energy transport equation can be written as

$$\frac{\partial^2 T}{\partial x^2} + \frac{\partial^2 T}{\partial y^2} + \frac{\partial^2 T}{\partial z^2} = 0 \quad (2-22)$$



2.1.4 Boundary Conditions

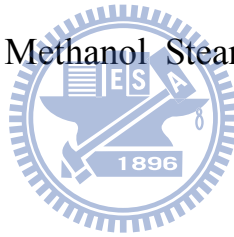
The boundary conditions of the present computation include those at the inlet, outlet, wall, and the interfaces between the flow channel and the catalyst layer.

- (1) The boundary conditions for inlets at the flow channel and the catalyst layer: The inlet flow velocity is constant, the inlet gas composition is constant, and the inlet temperature is constant.
- (2) The boundary conditions for outlets at the flow channel and the catalyst layer: The gauge pressure is zero.
- (3) The boundary conditions for the interface between the solid wall and the insulated walls: The temperature gradients are zero.
- (4) The boundary conditions for the interface between the flow channel and the insulated

walls: The velocities, temperature, temperature gradient, species concentration and species flux are zero.

- (5) The boundary conditions for the interface between the flow channel and solid wall. No slip and zero fluxes hold the velocities and the concentration gradients at zero.
- (6) The boundary conditions for the interface between the flow channel and the catalyst layer: The velocities, temperature, species concentration and species flux are continuous.
- (7) The boundary conditions for the interface between the heated wall and the catalyst layers: The velocities and the concentration gradient are assumed to be zero, and the temperature is assumed to be equal to the constant wall temperature.

2.2 The Model of a Plate Methanol Steam Micro-Reformer with Methanol Catalytic Combustor



2.2.1 Model Description

In order to simplify the multifarious changes due to the wall temperature variation, the model above did not consider the wall thermal boundary condition to be a non-uniform temperature. To keep everything isothermal there must be a continual input of heat because the reaction is endothermic. However, in actual experimental operations, a key design consideration for the reformer is how to supply the heat for the reaction. The supply of heat will result in a non-uniform temperature along the length of the flow channel. The heat consumed by the reaction will cause the temperature to decrease near the inlet of the channel where the rate is highest. This will cause the length of the reaction zone to increase. The energy balance must be couple with a heat source to design the proper heating device to match the load required by the reaction. Therefore, the study will give thought to this issue,

which is probably the most important results we could obtain from the reactor analysis. Consequently, a methanol steam micro-reformer with a methanol catalytic combustor would be considered in order to simulate the characteristics of the non-uniform temperature along the channel. Now, a reactor model with consideration of the methanol steam micro-reformer and methanol catalytic combustor has been developing.

This study extends the established 3-dimensional channel model of methanol steam micro-reformer to a reactor channel model with consideration of the methanol steam micro-reformer and methanol catalytic combustor in 3-dimensional model. The reactor consists of a methanol steam micro-reformer and a methanol catalytic combustion chamber. A schematic diagram of the physical system under consideration is shown in Fig. 2-4. The system consists of the solid wall, two catalyst layers and two flow channels each at the catalytic combustion/steam reforming side. It is seen that the methanol catalytic combustion chamber and the methanol steam reforming chamber are separated by a solid wall. Both sides of each channel are coated with a combustion catalyst layer and a steam reforming catalyst layer. The heat from the combustion reaction is used to drive the steam reforming reaction.

Next, the three-dimensional computational models with various flow fields have been established for methanol steam micro-reformer with methanol catalytic combustor. The flow fields in the methanol steam micro-reformer and methanol catalytic combustor include the parallel flow field and the serpentine flow field. The parallel flow field has five parallel channels and the serpentine flow field has one channel with four turns. A schematic illustration of these flow fields and associated coordinate system are shown in Fig. 2-5. The parallel flow field has five flow channels and each channel is 40mm in length. The serpentine flow field has one flow channel, the total flow channel length is five times the length of a channel in the parallel flow field, and there are four turning points. In this study, constant flow rate approach is utilized to investigate the effect of flow field on the performance of

micro-reformer. The u , v , and w are the velocity components in the x -, y -, and z -directions, respectively. The reactor consists of the solid wall, a steam reforming flow channel, a steam reforming catalyst layer, a catalytic combustion catalyst layer and a catalytic combustion flow channel.

2.3.2 Assumption

To simplify the analysis for the present study, the flowing assumptions are made:

- (1) The flow is steady state;
- (2) The inlet fuel is an ideal gas;
- (3) The flow is laminar and incompressible;
- (4) The catalyst layer is isotropic;
- (5) The chemical reaction occurs only in the catalyst layer;
- (6) Thermal radiation and conduction in the gas phase are negligible compared to convection.

2.3.3 Governing Equations

With the above assumptions, the gas transport equations for the three-dimensional reactor can be described as follows.

Continuity equation:

$$\frac{\partial u}{\partial x} + \frac{\partial v}{\partial y} + \frac{\partial w}{\partial z} = 0 \quad (2-23)$$

X-momentum equation:

$$\varepsilon \rho \left(u \frac{\partial u}{\partial x} + v \frac{\partial u}{\partial y} + w \frac{\partial u}{\partial z} \right) = -\varepsilon \frac{\partial p}{\partial x} + \varepsilon \mu \left(\frac{\partial^2 u}{\partial x^2} + \frac{\partial^2 u}{\partial y^2} + \frac{\partial^2 u}{\partial z^2} \right) + S_u \quad (2-24)$$

Y-momentum equation:

$$\varepsilon\rho\left(u\frac{\partial v}{\partial x}+v\frac{\partial v}{\partial y}+w\frac{\partial v}{\partial z}\right)=-\varepsilon\frac{\partial p}{\partial y}+\varepsilon\mu\left(\frac{\partial^2 v}{\partial x^2}+\frac{\partial^2 v}{\partial y^2}+\frac{\partial^2 v}{\partial z^2}\right)+S_v \quad (2-25)$$

Z-momentum equation:

$$\varepsilon\rho\left(u\frac{\partial w}{\partial x}+v\frac{\partial w}{\partial y}+w\frac{\partial w}{\partial z}\right)=-\varepsilon\frac{\partial p}{\partial z}+\varepsilon\mu\left(\frac{\partial^2 w}{\partial x^2}+\frac{\partial^2 w}{\partial y^2}+\frac{\partial^2 w}{\partial z^2}\right)+S_w \quad (2-26)$$

In the above equations, ε stands for the porosity of the medium. S_u , S_v and S_w are corrected terms of the reactant gas flow in a porous material in the catalyst layer. The source terms, S_u , S_v and S_w in the momentum equations are listed in Eqs. (2-24)-(2-26), respectively. Among them, the source terms, S_u , S_v and S_w account for the Ergun equations [76] in the x-, y- and z-directions, respectively. The parameter k_p stands for the permeability and β is the inertial loss coefficient in each component direction.

$$S_u = -\frac{\mu u}{k_p} - \frac{\beta u \rho}{2} \sqrt{u^2 + v^2 + w^2} \quad (2-27)$$

$$S_v = -\frac{\mu v}{k_p} - \frac{\beta v \rho}{2} \sqrt{u^2 + v^2 + w^2} \quad (2-28)$$

$$S_w = -\frac{\mu w}{k_p} - \frac{\beta w \rho}{2} \sqrt{u^2 + v^2 + w^2} \quad (2-29)$$

where

$$k_p = \frac{D_p^2 \varepsilon^3}{150(1-\varepsilon)^2} \quad (2-30)$$

$$\beta = \frac{3.5(1-\varepsilon)}{D_p \varepsilon^3} \quad (2-31)$$

Species equation:

$$\left(u\frac{\partial m_i}{\partial x}+v\frac{\partial m_i}{\partial y}+w\frac{\partial m_i}{\partial z}\right)=D_{\text{eff}}\left(\frac{\partial^2 m_i}{\partial x^2}+\frac{\partial^2 m_i}{\partial y^2}+\frac{\partial^2 m_i}{\partial z^2}\right)+(1-\varepsilon)\rho_s S_c \quad (2-32)$$

In the species equation, m_i denotes the mass fraction of the i^{th} species, where the various species are CH_3OH , H_2O , H_2 , CO_2 , CO and O_2 . In these expressions, the concentrations of CH_3OH , H_2O , H_2 , CO_2 , CO are calculated on the steam reforming side and CH_3OH , H_2O , CO_2 , O_2 are calculated on the combustion side. The effective diffusion coefficient, D_{eff} determined by the Stefan-Maxwell equations [77]. Eq. (2-33) is employed to describe the influence of the porosity on the diffusion coefficient

$$D_{\text{eff}} = D_k \varepsilon^\tau \quad (2-33)$$

The diffusion coefficient D_k for the methanol steam micro-reformer was derived from the Stefan-Maxwell equations which were used to calculate the mean effective binary diffusivity [51]. S_c is the source term of chemical reaction in the species equation, and differs according to the reactant gases in the catalyst layer. In the present study, there is no chemical reaction in the flow channel. Therefore, S_c is zero in the flow channel. In the catalyst layer, the source term of the species equation, S_c , can be described by the following modified concentration term:

$$S_c = \begin{cases} M_{w,i} (R_{\text{SR}} + R_{\text{rWGS}} + R_{\text{MD}}) (\lambda_i'' - \lambda_i') & \text{for steam reforming} \\ M_{w,i} (R_{\text{Combustion}}) (\lambda_i'' - \lambda_i') & \text{for combustion reaction} \end{cases} \quad (2-34)$$

where $M_{w,i}$ is the molecular weight of species i , and $R_{i,r}$ is the Arrhenius molar rate of creation and destruction of species i in the reaction. λ_i'' and λ_i' are the stoichiometric coefficient for reaction i and product i , respectively, in the reaction.

According to the chemical kinetics of Pepply et al. [40], the methanol steam reforming reaction consists of three overall reactions: one is a primary process in the methanol steam reforming and the others are the decomposition reaction and water-gas shift reaction. Therefore, the steam reforming reaction, Eq. (2-35), the reverse water-gas shift reaction, Eq.

(2-36), and the decomposition reaction, Eq. (2-37), are considered in this study.

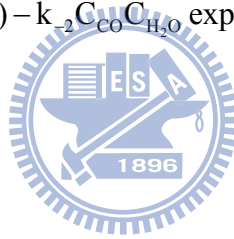


In this work, to simplify the analysis, the model of Mastalir et al. [41] for methanol steam reforming is used, and the Arrhenius equation is employed to calculate the reactant gases generated by the chemical reaction.

$$R_{\text{SR}} = k_1 C_{\text{CH}_3\text{OH}}^{0.6} C_{\text{H}_2\text{O}}^{0.4} \exp\left(-\frac{E_a}{RT}\right) - k_{-1} C_{\text{CO}_2} C_{\text{H}_2} \exp\left(-\frac{E_a}{RT}\right) \quad (2-38)$$

$$R_{\text{rWGS}} = k_2 C_{\text{CO}_2} C_{\text{H}_2} \exp\left(-\frac{E_a}{RT}\right) - k_{-2} C_{\text{CO}} C_{\text{H}_2\text{O}} \exp\left(-\frac{E_a}{RT}\right) \quad (2-39)$$

$$R_{\text{MD}} = k_3 C_{\text{CH}_3\text{OH}}^{1.3} \exp\left(-\frac{E_a}{RT}\right) \quad (2-40)$$



where the steam reforming reaction and reverse water-gas shift reaction are reversible reactions and the decomposition reaction is a non-reversible reaction. The constants k_1 , k_2 and k_3 are forward rate constants, and the constant k_{-1} and k_{-2} are the backward rate constants.

The reaction of the combustion catalyst layer can be represented by the following reaction Eq.(2-41). The reaction rate of methanol over the Pt/Al₂O₃ catalyst was calculated with Eq.(2-42), as proposed by Pasel et al.[81]



$$R_{\text{Combustion}} = k_4 C_{\text{CH}_3\text{OH}}^{1.3} \exp\left(-\frac{E_a}{RT}\right) \quad (2-42)$$

In order to evaluate the distributions of the local temperature, the energy equations must be solved.

Energy equation:

$$\rho c_p \left(u \frac{\partial T}{\partial x} + v \frac{\partial T}{\partial y} + w \frac{\partial T}{\partial z} \right) = k_{\text{eff}} \left(\frac{\partial^2 T}{\partial x^2} + \frac{\partial^2 T}{\partial y^2} + \frac{\partial^2 T}{\partial z^2} \right) + (1 - \varepsilon) \rho_s S_t \quad (2-43)$$

The effective thermal conductivity is modified to account for the porous medium effect:

$$k_{\text{eff}} = \varepsilon k_f + (1 - \varepsilon) k_s \quad (2-44)$$

where k_f is the fluid phase thermal conductivity, k_s is the solid medium thermal conductivity and ε is the porosity of the medium.

The source term S_t in the energy equation due to the chemical reactions is determined by

$$S_t = \begin{cases} -(\Delta H_{\text{SR}} R_{\text{SR}} + \Delta H_{\text{rWGS}} R_{\text{rWGS}} + \Delta H_{\text{MD}} R_{\text{MD}}) & \text{for steam reforming} \\ -(\Delta H_{\text{Combustion}} R_{\text{Combustion}}) & \text{for combustion reaction} \end{cases} \quad (2-45)$$

As for the energy equation of the solid wall, one has

$$\frac{\partial^2 T}{\partial x^2} + \frac{\partial^2 T}{\partial y^2} + \frac{\partial^2 T}{\partial z^2} = 0 \quad (2-46)$$

2.3.4 Boundary Conditions

The boundary conditions of the present computation include those at the inlet, the outlet, the wall, and the interface between the flow channel and the catalyst layer.

- (1) The boundary conditions for inlets at the flow channel and the catalyst layer: the inlet flow velocity is constant, the inlet gas composition is constant, and the inlet temperature is constant.
- (2) The boundary conditions for outlets at the flow channel and the catalyst layer: the gauge pressure is zero.

- (3) The boundary conditions for the interface between the solid wall and the insulated walls: the temperature gradients are zero.
- (4) The boundary conditions for the interface between the flow channel and solid wall: no slip and zero fluxes hold the velocities and the concentration gradients are zero.
- (5) The boundary conditions for the interface between the flow channel and the catalyst layer: the velocities, temperatures, species concentrations and species fluxes are continuous.



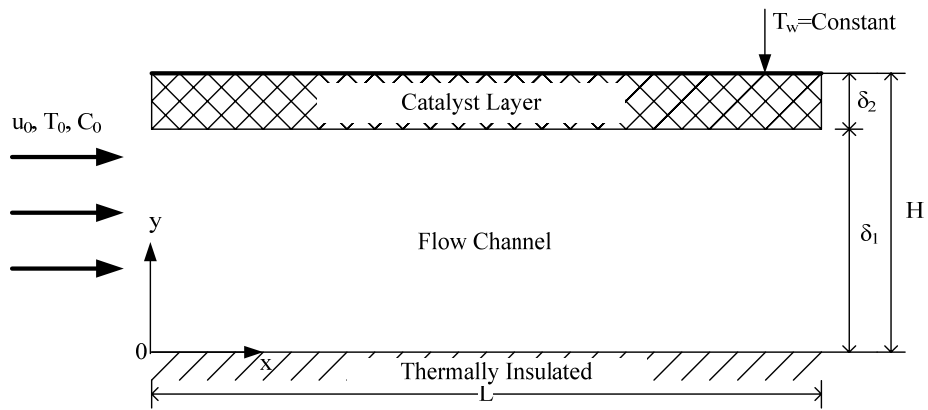
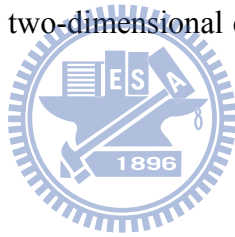


Fig. 2-1 Schematic diagram of the two-dimensional channel model of a plate methanol steam micro-reformer



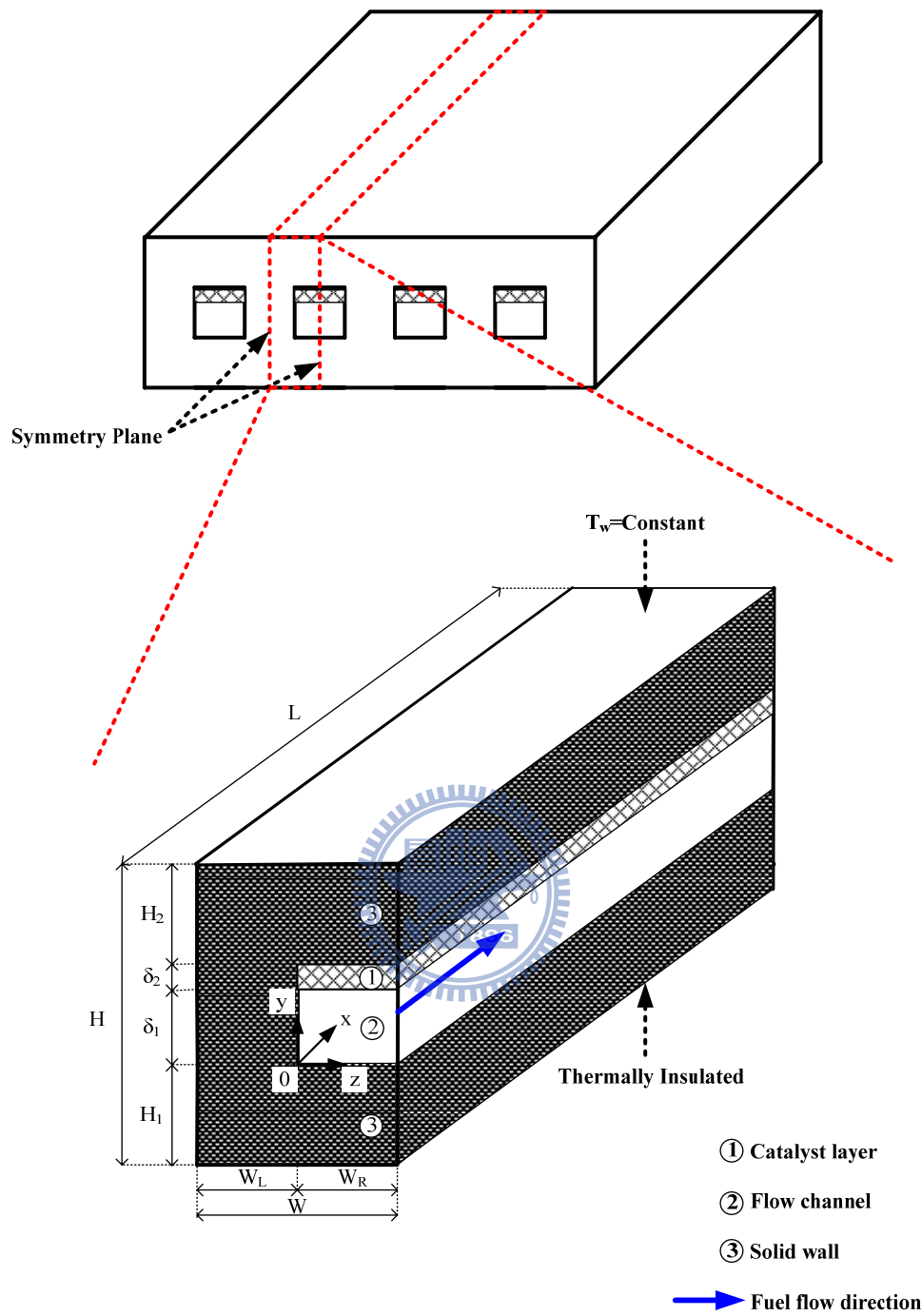


Fig. 2-2 Schematic diagram of the three-dimensional channel model of a plate methanol steam micro-reformer

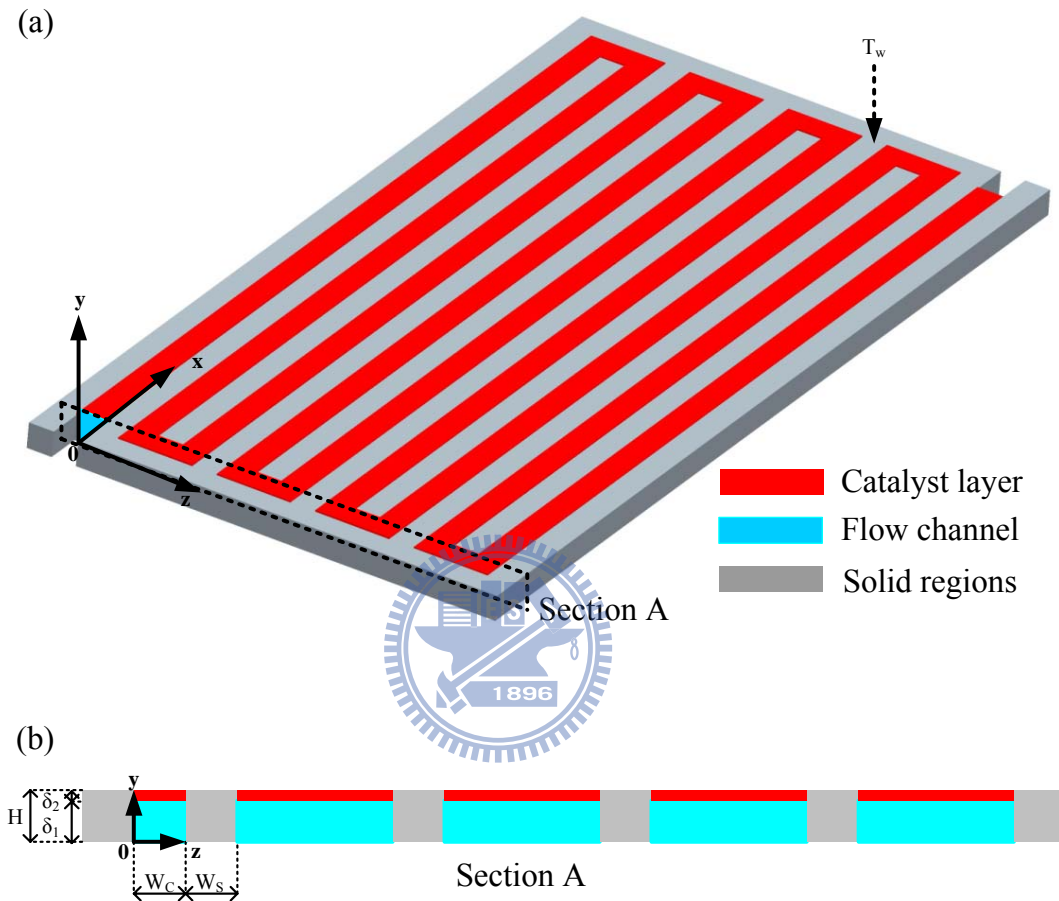


Fig. 2-3 Schematic diagram of the three-dimensional model of a plate methanol steam micro-reformer with serpentine flow field design

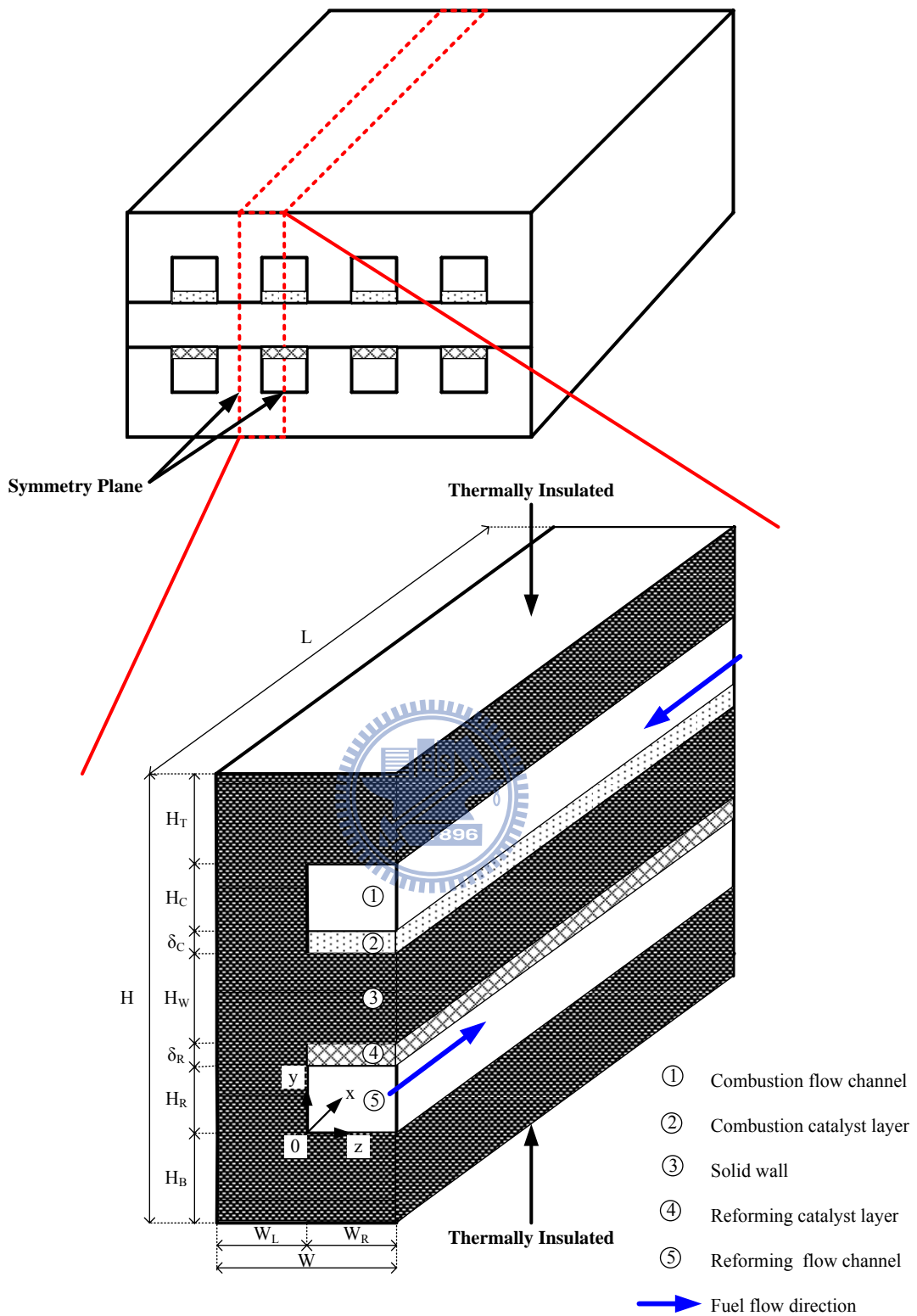


Fig. 2-4 Schematic diagram of the three-dimensional channel model of a plate methanol steam micro-reformer with methanol catalytic combustor

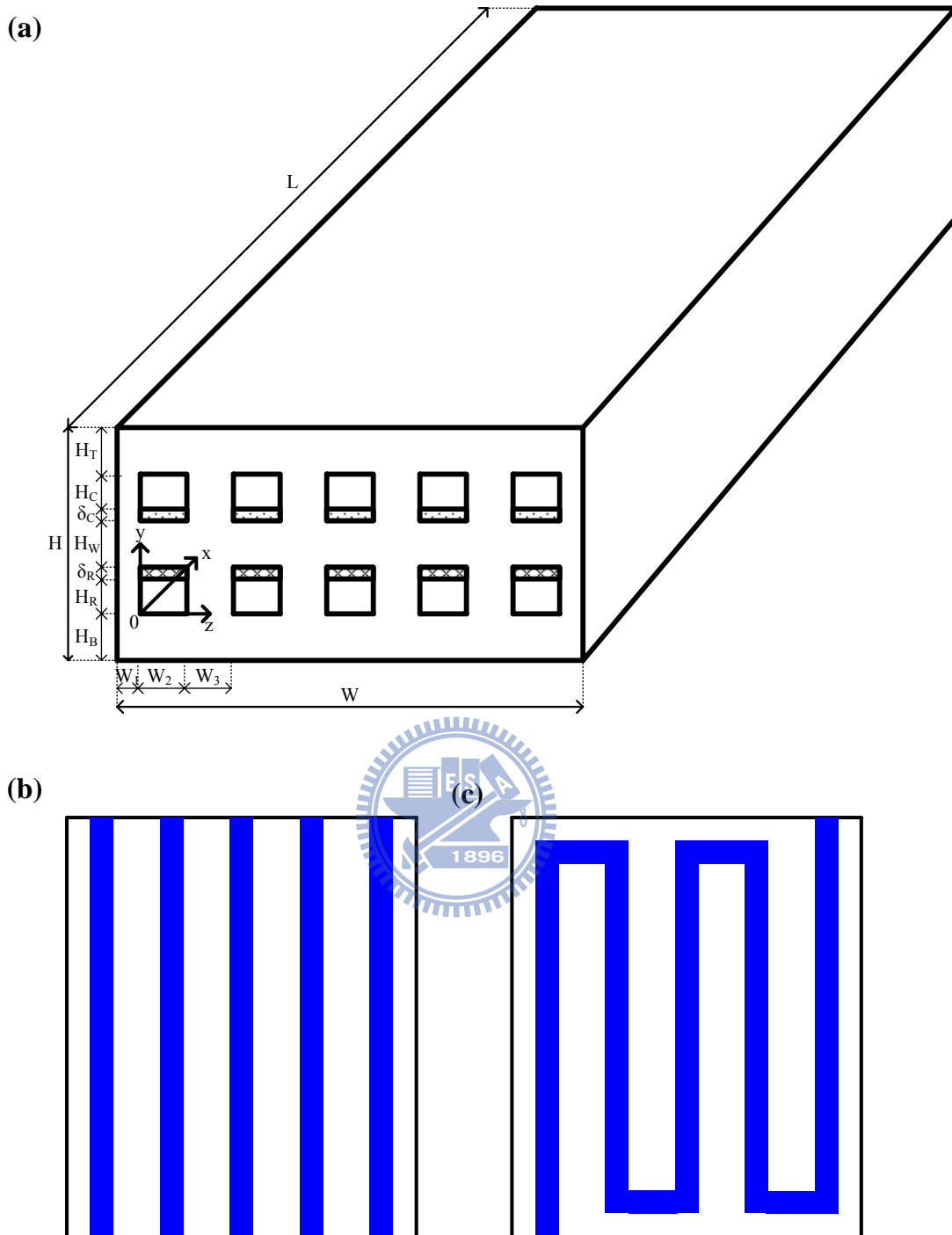


Fig. 2-5 (a) Schematic diagram of a plate methanol steam micro-reformer with methanol catalytic combustor, (b) Parallel Flow Field and (c) Serpentine Flow Field

CHAPTER 3

METHOD OF SOLUTION

3.1 Flow Chart

Using the segregated solver, the governing equations are solved sequentially. Because the governing equations are non-linear, several iterations of the solution loop must be performed before a converged solution is obtained. Each iteration consists of the steps illustrated in Figure 3-1 and outlined below:

1. Fluid properties are updated, based on the current solution.
2. The u , v , and w momentum equations are solved by using current values for pressure and face mass fluxes in order to update the velocity field.
3. Since the velocities obtained in Step 2 may not satisfy the continuity equation locally, an equation for the pressure correction is derived from the continuity equation and the linearized momentum equations. The pressure correction equation is then solved to obtain the necessary corrections for the pressure and velocity fields and the face mass fluxes such that continuity is satisfied.
4. The above steps are continued until the convergence criteria are met.
5. Where appropriate, equations for scalars such as energy and species are solved using the previously updated values of the other variables.
6. A check for convergence of the equation set is made.

3.2 Numerical Method

The solution to the governing equations is obtained by employing a finite volume method with the model domain divided into a number of cells and used as control volumes. The governing equations are numerically integrated over each of these computational cells or control volumes. The method exploits a collocated cell-centered variable arrangement with the local or cell-averaged values of the physical quantities evaluated and stored at each cell center.

A generalized form of the transport equation for mass, momentum, energy can be expressed in a conservative form as follows:

$$\nabla \cdot (\rho \phi \vec{v}) = \nabla \cdot (\Gamma \nabla \phi) + S_\phi \quad (3-1)$$

where ϕ is a general dependent variable, \vec{v} is velocity vector, S_ϕ is the source per unit volume and ρ is the density. With the discretization of the governing equations, the coupled finite-difference equations become

$$a_p \phi_p = a_E \phi_E + a_W \phi_W + a_N \phi_N + a_S \phi_S + S_\phi \quad (3-2)$$

where ϕ_p is the value of ϕ at the current point P, $\phi_E \dots \phi_S$ stand for the values of the grid points adjacent to the point P, and $a_p \dots a_s$ are known as the link coefficients. The discretised form for the scalar control volume shows in Fig. 3-2. All equations were numerically solved using the commercial CFD program, FLUENT[®] 6.1. The SIMPLE algorithm was employed to solve the convection-diffusion equations. The convergence criteria for the normalized residuals for each variable were restricted to be less than 10^{-6} .

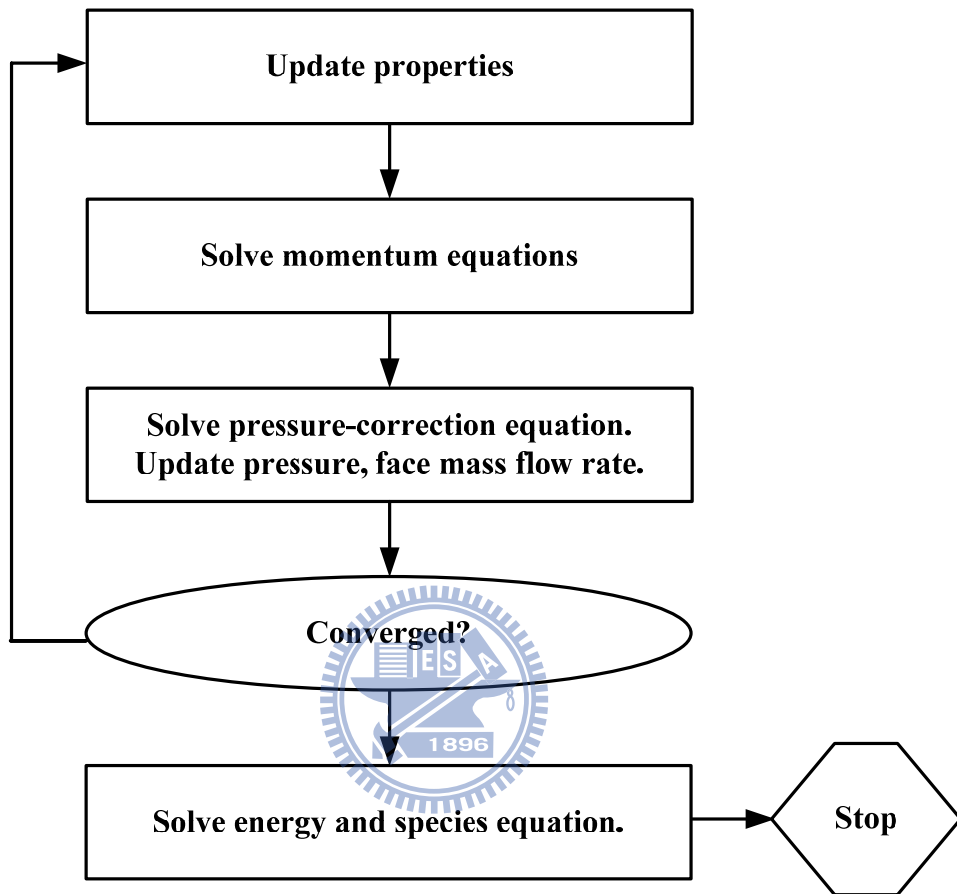


Fig. 3-1 Numerical flow diagram of the solution procedure

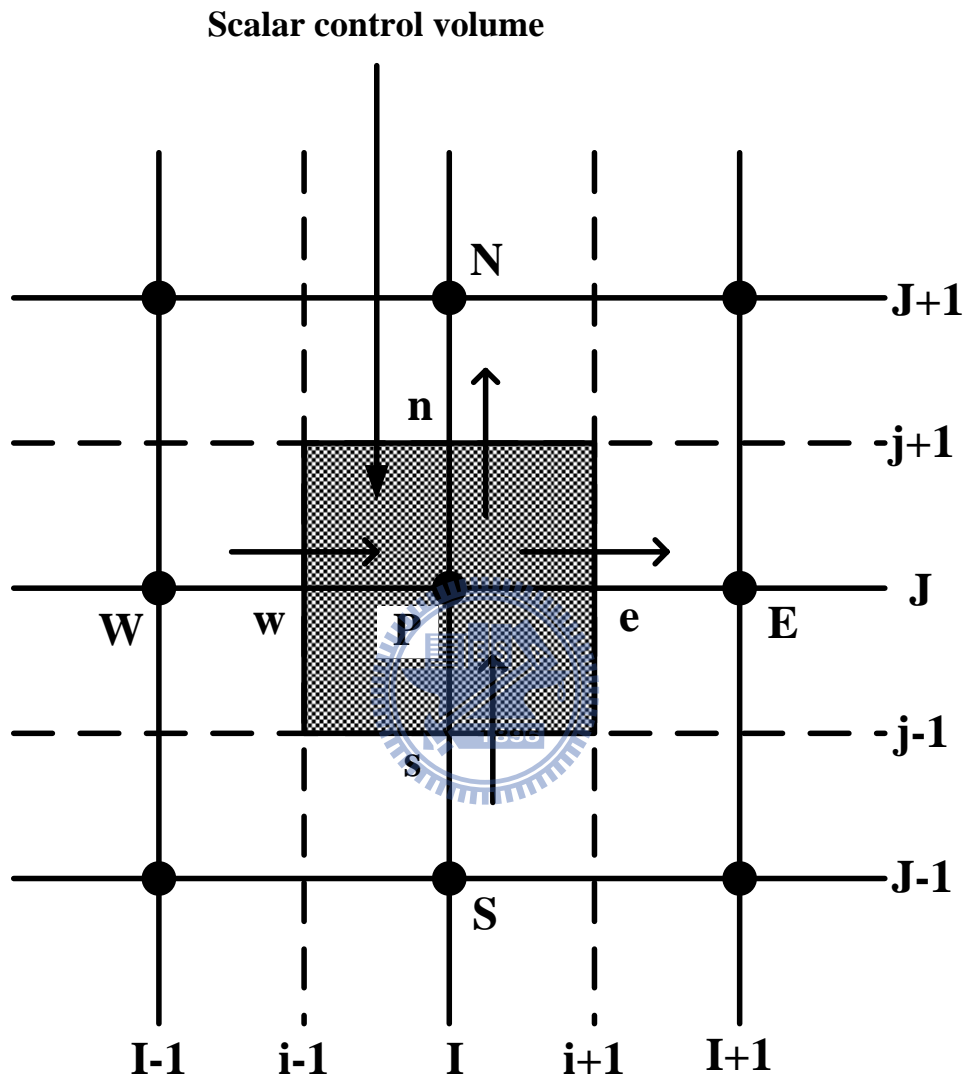


Fig. 3-2 The scalar control volume used for the discretization of the governing equation

CHAPTER 4

RESULTS AND DISCUSSION

4.1 Two-Dimensional Channel Model of a Plate Methanol Steam Micro-Reformer

In this section, the effects of the geometric and thermo-fluid parameters on the plate methanol steam micro-reformer performance and the heat and mass transfer are numerically investigated in detail. In this work, a two-dimensional numerical model was developed to study the methanol conversion and local heat and mass transfer in the channel of a micro-reformer. The information reported here would be useful in improving plate methanol steam reformer performance. When working in micro-reformers, it is very important to check the validity of the continuum model and evaluate possible rarefied gas flow effects. To this end, the Knudsen number (Kn) has been evaluated. This number compares the molecular mean free path with the characteristic geometric dimension of the system. The molecular mean free path has been evaluated according to Arzamendi et al.[63] for both the methanol steam reforming and combustion gases in the 250-350°C range resulting values between 93 and 115 nm. In my base case, the characteristic dimension is the channel height ($H = 0.2$ mm), the Knudsen numbers are between 1.86×10^{-4} and 5.75×10^{-4} . These values are lower than 10^{-3} which assures the validity of the continuum model and the Navier-Stokes equations for the systems considered in this work. The parameters used in the work are listed in Table 4-1. Then, the effects of the number of gridlines on the numerical results are shown in Table 4-2 for three different grids. The predicted methanol mole fraction distributions show that the deviations of the methanol mole fraction among these three grids are 1%. Therefore, the 91x26 grid is used in this work. The accuracy of the numerical results was validated by

comparing the predicted methanol conversion with experimental results of Park et al. [16]. Figure 4-1 compares numerical and experimental results under various wall temperature and inlet velocities. The results show that the numerical results agree reasonably well with the experimental data.

4.1.1 Effects of the Geometric Parameters on the Heat and Mass Transfer and Methanol Conversion in a Micro-Reformer Channel

The influences of the geometric parameters and thermo-fluid parameters on the performance of micro-reformer are considered of great importance. To this end, the effects of the channel length ($L=22$ mm, 33 mm, and 44 mm), channel height ($H=0.1$ mm, 0.2 mm, and 1.0 mm), catalyst thickness ($\delta_2=10$ μm , 30 μm and 50 μm) and catalyst porosity ($\varepsilon=0.28$, 0.38, and 0.48) on the methanol conversion and CO concentration in the micro-reformer were investigated.

For fixed Reynolds number ($Re=2.2$), the effects of geometric parameters on methanol conversion of micro-reformer channel are presented in Fig. 4-2(a). The results show that the methanol conversion increases with an increase in the wall temperature T_w for all geometric conditions, implying that a better micro-reformer performance can be archived at higher wall temperature. By comparing the results of $T_w = 200$ $^{\circ}\text{C}$ and $T_w = 260$ $^{\circ}\text{C}$ with $L=33$ mm, $H=0.2$ mm, $\delta_2=30$ μm and $\varepsilon=0.38$, it shows that the methanol conversion for $T_w = 260$ $^{\circ}\text{C}$ could be improved by 49% relative to that of $T_w = 200$ $^{\circ}\text{C}$. Comparison of the corresponding curves of the channel lengths of $L=22$ mm, 33 mm, and 44 mm indicates that better methanol conversion is found for a longer micro-reformer channel. This is due to the longer residence time of the fuel in the longer channel. As for the effects of channel heights ($H=0.1$ mm, 0.2 mm, and 1.0 mm), the results reveal that all the three micro-channels possess a similar

methanol conversion. Additionally, it is seen in Fig. 4-2(a) that the methanol conversion in the micro-reformer is enhanced by the increased catalyst thickness. The channel with thicker catalyst layer has a larger chemical reaction area, which in turn causes a better methanol conversion. The results show that methanol conversion improves from 80% to 99% at $T_w = 260\text{ }^\circ\text{C}$ with the catalyst thickness ranging from $10\mu\text{m}$ to $50\mu\text{m}$. The effects of the porosity of catalyst layer ($\epsilon=0.28, 0.38, \text{ and } 0.48$) on methanol conversion of micro-reformer channel are also shown in Fig. 4-2(a). It is found that the methanol conversion increases with an increase in the porosity of catalyst layer. This means that reaction surface is enlarged via an increase in the catalyst porosity. In addition, the best methanol conversion is noted for the case with $L=33\text{ mm}$, $H=0.2\text{ mm}$, $\delta_2=50\text{ }\mu\text{m}$ and $\epsilon=0.38$ at $T_w = 260\text{ }^\circ\text{C}$. This implies that the appropriate channel geometry and catalyst thickness are very critical for improving methanol conversion.

The CO concentration must be reduced for further use in a PEM fuel cell. Therefore, the CO concentration distributions for various geometric parameters are presented in Fig. 4-2(b). It is clearly observed that the CO concentration increases with increasing wall temperature. This is because the endothermic reverse water-gas-shift reaction increases as the wall temperature increases. It is clear in Fig. 4-2(b) that lower CO concentration is found for a micro-reformer with a shorter channel length. A detailed comparison of the corresponding curves shows that lower CO concentration is noted for a micro-reformer with a thinner catalyst thickness or a lower porosity. It is clearly seen that the CO concentration is about 16000ppm for the case with $L=33\text{ mm}$, $H=0.2\text{ mm}$, $\delta_2=30\text{ }\mu\text{m}$, $\epsilon=0.38$ and a wall temperature of $260\text{ }^\circ\text{C}$.

The effects of inlet fuel ratio on the CO concentration (ppm) at the outlet were also investigated. The effect of the molar ratio of $\text{H}_2\text{O}/\text{CH}_3\text{OH}$ on the CO concentration for various geometric parameters and wall temperatures are shown in Fig 4-3. A careful inspection of Fig. 4-3 discloses that the CO concentration decreases with an increase in the

inlet molar ratio of $\text{H}_2\text{O}/\text{CH}_3\text{OH}$. This is due to the fact that the higher H_2O concentration enhances the water-gas-shift reaction which, in turn, reduces the CO concentration. The results also show that the CO concentration would be reduced from 1.72% to 0.95% at $T_w = 260\text{ }^\circ\text{C}$ with the $\text{H}_2\text{O}/\text{CH}_3\text{OH}$ molar ratio values ranging from 1.0 to 1.6. However, the higher molar ratio of $\text{H}_2\text{O}/\text{CH}_3\text{OH}$ also reduces the H_2 concentration at the channel outlet. It is also found that the effects of the $\text{H}_2\text{O}/\text{CH}_3\text{OH}$ molar ratio on the CO concentration are more significant for a case with a higher wall temperature.

The impact of channel height on temperature distribution along the centerline of the channel, at a fixed Reynolds number, was examined for the heights 0.1 mm, 0.2 mm and 1cm. The hydraulic diameters of channel vary depending on channel heights. A higher channel height has a greater hydraulic diameter. Fig. 4-4 illustrates that the centerline temperature increases along the channel as a consequence of the heated wall. For a smaller channel height, the temperature distribution is much more uniform due to the shorter thermal entrance length. This kind of uniform temperature distribution improves the chemical reaction rate. Therefore, as shown in Fig. 4-2 (a), the methanol conversion of the micro-reformer is slightly enhanced with the smaller channel height at higher wall temperature. A comparison of the temperature distributions for wall temperatures of $200\text{ }^\circ\text{C}$ and $260\text{ }^\circ\text{C}$ indicates that the centerline temperature increases with an increase in the wall temperature.

Figure 4-5 shows the effects of wall temperature on the cross-sectioned temperature at different axial locations for $H=1.0\text{mm}$ at the wall temperatures of $200\text{ }^\circ\text{C}$ and $260\text{ }^\circ\text{C}$. It is clearly found that near the entrance ($X=0.076$), the cross-sectioned temperature shows a significant variation. As the flow move downstream, the cross-sectioned temperature becomes uniform with a slight variation. When $X>0.606$, the results show that the temperature variation disappears. Figure 4-6 presents the cross-sectioned velocity in the catalyst layer and flow channel for different axial locations at the wall temperatures of $200\text{ }^\circ\text{C}$ and $260\text{ }^\circ\text{C}$. As

expected, there is a large difference on the velocity scale between the catalyst layer and flow channel. The velocity distributions in the catalyst layer are down to two orders of magnitude smaller than that in the flow channel, indicating that gas diffusion is the dominant transport mechanism in the porous media. The results also indicate the wall temperature of 260 °C generates higher gas velocity distributions than that of 200 °C.

Figure 4-7 shows the local distributions of the different species at wall temperatures of 200 °C and 260 °C along the centerline of the channel for the same operating conditions. Fig. 4-7 discloses that both the mole fractions of the CH₃OH and H₂O decrease as the fluid moves downstream, while the H₂, CO₂ and CO mole fractions increase with axial location. Fig. 4-7 clearly demonstrates that the mole fractions of the products increase with an increase in the wall temperature. In addition, Fig. 4-7 (b) shows that the methanol conversion is greater than 99% at a wall temperature of 260 °C, with a product gas composition of 74.7% H₂, 23.6% CO₂ and 1.7% CO at the outlet of the channel. The results agree reasonably with experimental data [16]. For the PEM fuel cell, the CO concentration should be less than 10 ppm, so cleanup step is required after reforming. The utilization of the PrOx or water-gas-shift reaction equipment can reduce the CO concentration in the gas from the micro-reformer.

Studies of the reactant gas transport in micro-reformer channels have shown that a detailed understanding of the local distribution of the CH₃OH mole fraction along the channel is important for designing the micro-reformer. Therefore, the effects of geometric parameters on the local distributions of the CH₃OH mole fraction along the channel center line are presented in Fig. 4-8. The results reveal that geometric parameters have a considerable impact on the local CH₃OH distributions. It is found that the CH₃OH mole fractions decrease as the fluid moves downstream due to the chemical reaction. For various channel heights, there appears to be little variation in the CH₃OH mole fraction distributions. The higher methanol concentration is noted for a system with a longer channel length or with a lower catalyst layer

thickness and porosity. This implies that the chemical reaction rate is weaker for a system with a shorter channel length or with a lower catalyst layer thickness and porosity. The effect of wall temperature on the local CH_3OH mole fraction can be found by comparing the corresponding curves in Figs. 4-8 (a) and (b). It is clear that smaller methanol concentration is noted for a case with a higher wall temperature. This can be explained by the fact that a stronger chemical reaction is experienced for a micro-reformer channel with a higher wall temperature.

The distributions of the H_2 mole fraction along the channel are shown in Fig. 4-9 for various geometric parameters and wall temperatures. A higher H_2 mole fraction along the channel represents a higher methanol conversion. Thus, the variation of the H_2 fraction is opposite to that of the CH_3OH mole fraction in Fig. 4-8. In Fig. 4-9, a higher H_2 mole fraction is found for a micro-reformer channel with a longer channel length or with a higher catalyst thickness, porosity and wall temperature. Figure 4-10 presents the effects of the geometric parameters on the local CO mole fraction distribution along the center line at wall temperatures of $200\text{ }^\circ\text{C}$ and $260\text{ }^\circ\text{C}$. The trends of the variations in Fig. 4-10 can be interpreted in a similar way as for the results in Fig. 4-8 since a higher methanol conversion results in a higher CO production.

4.1.2 Effects of Thermo-Fluid Parameters on the Heat and Mass transfer and Methanol Conversion in a Micro-Reformer Channel

Additionally, the Reynolds number ($\text{Re}=2.2, 4.4$ and 8.8), fuel ratio ($\text{S/C}=1.0, 1.3$ and 1.6) and inlet temperature ($T_0=100\text{ }^\circ\text{C}, 120\text{ }^\circ\text{C},$ and $140\text{ }^\circ\text{C}$) are the key thermo-fluid parameters in micro-reformer channels which would affect the micro-reformer performance. The Reynolds number increases with increasing fuel velocities at the same inlet area. Figure

4-11 shows the effects of the Reynolds number on the local distributions of the CH₃OH mole fraction along the channel at the same catalyst layer thickness and porosity. Three cases with Reynolds number of 2.2, 4.4 and 8.8 are presented in Fig. 4-11. It is clearly observed a lower methanol concentration (better methanol conversion) is found for a micro-reformer channel with a lower Reynolds number. This is due to the fact micro-reformer channel with a lower Reynolds number would experience a longer reactant gas resident time and reaction time, which in turn causes a better methanol conversion. In this work, we considered the H₂O/CH₃OH molar ratio values 1.0, 1.3 and 1.6. The predicted results in Fig. 4-11 show that the CH₃OH concentration decreases with an increase in the H₂O/CH₃OH molar ratio. Also, the impact of different inlet fuel temperatures was examined for the values of 100 °C, 120 °C and 140 °C. It is found that a lower CH₃OH concentration (a better methanol conversion) is found for a system with a higher inlet fuel temperature which increases the reaction rate. Comparison of the local CH₃OH mole fractions in Figs. 4-11 (a) and (b) for the wall temperatures of 200 °C and 260 °C for the various operating parameters shows that the local CH₃OH mole fraction decreases with increasing wall temperature due to a strong chemical reaction for a high wall temperature.

The dependence of the local H₂ mole fraction distribution on the Reynolds number, fuel ratio and inlet temperature are presented in Fig. 4-12. The results show that a higher H₂ mole fraction is noted for a micro-reformer channel with a lower Reynolds number. This is due to the longer gas resident time which results in a better methanol conversion and a higher H₂ production. The influences of the H₂O/CH₃OH molar ratio on the H₂ mole fraction are presented in Fig. 4-12. The results show that a higher molar ratio of H₂O/CH₃OH causes the H₂ mole fraction to fall. Additionally, the H₂ mole fraction increases with increasing inlet fuel temperature. Comparison of Figs. 4-12 (a) and (b) indicates that a higher local H₂ mole fraction is experienced for a micro-reformer channel with a higher wall temperature owing to

a stronger chemical reaction.

Figure 4-13 presents the variations of the CO mole fractions along the channel for the various thermo-fluid parameters. By comparing Figs. 4-12 and 4-13, it is found that the CO distributions in Fig. 4-13 have the same trends as the H₂ distributions in Fig. 4-12. This confirms the common concept that a micro-reformer with a H₂ production indicates a higher CO concentration.

4.2 Three-Dimensional Channel Model of a Plate Methanol Steam Micro-Reformer

In this section, the numerical results are obtained for a channel of a plate methanol steam micro-reformer. A three-dimensional channel model was developed to investigate the geometric sizes (aspect ratios and channel size) and thermo-fluid parameters (Reynolds number and wall temperature) on methanol conversion and local transport phenomena in the channel of a plate steam methanol micro-reformer.

In past studies of heat and mass transfer in a micro-reformer, simplified models without wall conduction effects have been developed. In this work, a detailed analysis of the 3-dimensional modeling with wall conduction effects has been proposed to examine the transport phenomena of heat and mass transfer in a micro-reformer channel. Figure 4-14 presents the effects of wall conduction on the local temperature distributions and CH₃OH mole fraction distributions along the centerline of the channel. In this plot, X denotes the dimensionless distance from the channel inlet to outlet. It is clearly seen that the temperature distribution is affected by the wall thermal conduction and shows a rapid and uniform development compared with that without a wall conduction effect. This implies that the effects of wall conduction on the thermal development in a micro-reformer are important. In

addition, it is found in Fig. 4-14 that the effects of wall conduction on the methanol distribution are negligible, whereas their effect on the temperatures distribution is remarkable and cannot be neglected in the modeling. Therefore, wall conduction effects are taken into account in this work. This is the different between two-dimensional channel model and three-dimensional channel model.

The validation of the numerical results is performed by comparing the present predictions with previous experimental results. Figure 4-15 shows the comparison of the present predictions and experimental results. The solid symbols denote the experimental results of Park et al. [16] and the curve is the present prediction. The results show that the numerical results agree reasonably well with the experimental data.

4.2.1 Effects of Channel with Various Height and Width Ratios on Micro-Reformer Performance and Local Transport Phenomena

Using previously stated the numerical model, the effects of aspect ratios of channel on methanol conversion and transport phenomena were emphasized. The various cases for different aspect ratios are shown in Table 4-3. The aspect ratios, γ , are defined as follows:

$$\gamma = \frac{\delta_1 + \delta_2}{W_R} \quad (4-1)$$

Where $(\delta_1 + \delta_2)$ and W_R are the channel height and width, respectively. The corresponding hydraulic diameters in Table 4-3 are fixed to be 0.286 mm.

In the present study, the mass fractions of the inlet reactant gas including methanol vapor and water vapor of 0.38 and 0.62, respectively, were tested. Thus, the molar ratio of H_2O/CH_3OH was kept constant at 1.1. The inlet flow velocity of 0.266 m/s used and therefore, the corresponding Reynolds number Re was 3.14 for each test. The geometric dimensions and

physical properties of the channel are listed in Table 4-4.

The grid independence was examined in preliminary test runs. Three grid configurations were evaluated for the channel of the plate methanol steam micro-reformer at a wall temperature of 200°C. The numbers of grid lines in the x, y and z directions were: 41x16x18, 51x21x23, and 71x31x33. The influence of grid lines on the local methanol mole fraction is shown in Table 4-5. The deviations of methanol mole fraction are 0.4% for grids 41x16x18 and 51x21x23, and 0.4% for grids 51x21x23 and 71x31x33. Grid 51x21x23 was, therefore, chosen for the simulation in the present study as a tradeoff between accuracy and CPU computation time.

For aspect ratio of $\gamma=0.5$, Fig. 4-16 presents the local distributions of the different species at wall temperatures of 200 °C and 260 °C along the center of the channel. Overall inspection of Fig. 4-16 disclosed that the CH₃OH and H₂O mole fractions decrease along the channel, while the H₂, CO₂ and CO mole fractions increase along the center of the channel. The results demonstrate that as the mole fractions of the products increase as the wall temperature increases. The results also show that the methanol conversion is about 49% for a wall temperature of 200 °C, with a gas composition of 24% CH₃OH, 28% H₂O, 36% H₂, and 12% CO₂ at the channel outlet. However, the CO concentration is only 244 ppm. For a wall temperature of 260 °C, the results indicate that the methanol conversion is greater than 96%, with a product gas composition of 74.05% H₂, 24.28% CO₂, and 1.67% CO at the channel outlet. For the PEMFC, the CO concentration must be less than 10 ppm which can be achieved using a CO oxidation reactor. The utilization of the preferential oxidizer (PrOx) reactor or water-gas-shift reaction can reduce the CO concentration in the gas from the methanol micro-reformer. Kwon et al. [26] used a reformer and PrOx reactor, and showed that the CO produced was totally removed from the gas by the PrOx device.

Figure 4-17 presents the effects of the aspect ratios of channel on methanol conversion

and CO concentration (ppm). In this work, the catalyst thicknesses are fixed to be $30\mu\text{m}$. A careful examination of Fig. 4-17 reveals that the methanol conversion increases with an increase in wall temperature. Thus, the methanol conversion can be improved by increasing wall temperature, which in turn, increases the chemical reaction rate. It is also found from Fig. 4-17 that the methanol conversion increases with a decrease in aspect ratio due to the large chemical reaction area for a low aspect-ratio channel. This implies that better performance is noted for a lower aspect-ratio channel of micro-reformer. The CO concentration (ppm) leaving the channel was also studied. In Fig. 4-17, the results show that the CO concentration increases with increasing wall temperature. This can be made plausible by noting the fact that the reaction rate of the endothermic reverse water-gas-shift reaction increases as the wall temperature increases. Additionally, it is also found that the CO concentration (ppm) increases with decreasing aspect ratios. A height/width ratio of $\gamma=0.25$ and a wall temperature of $260\text{ }^{\circ}\text{C}$ yielded the better methanol conversion (greater than 98%), but the CO concentration was also higher, and was greater than 16000 ppm. Hence, the CO concentration in the outlet gases must be reduced for further use in a PEMFC.

The effects of aspect ratios on local methanol conversion distributions along the channel center line at $T_w=200\text{ }^{\circ}\text{C}$ and $T_w=260\text{ }^{\circ}\text{C}$ are presented in Fig. 4-18. An overall inspection of Fig. 4-18 reveals that the aspect ratios of channel have a considerable impact on the local methanol conversion distributions along the center line. It is found that the predicted methanol conversion increases along the channel. In addition, methanol conversion efficiency increases with decreasing aspect ratios of channel. As for the effects of wall temperature, better methanol conversion is noted for a case with a higher wall temperature owing to a stronger chemical reaction rate.

Figure 4-19 shows the effects of the aspect ratios of channel on the distribution of the H_2 and CO mole fractions, respectively, along the channel center line. It is clear in Fig. 4-19(a)

that the H_2 mole fraction along the channel center line represents the methanol conversion, with a higher H_2 fraction indicating higher methanol conversion rates. Thus, the variation of the H_2 fraction is opposite to that of the CH_3OH mole fraction. It is clearly observed from Fig. 4-19(a) the H_2 mole fraction increases as the aspect ratio decreases and wall temperature increases. The trends of the variations in Fig. 4-19(b) can be interpreted in a similar way to the data in Fig. 4-19(a). This is because that a higher methanol conversion results in a higher CO production. These phenomena are more obvious at a higher wall temperature ($260\text{ }^\circ\text{C}$), because the methanol micro-reformer produces more CO for a higher wall temperature.

Figure 4-20(a) presents the reactant gas velocity distributions in the center of the channel along the direction of flow from the inlet to the outlet for wall temperatures of $200\text{ }^\circ\text{C}$ and $260\text{ }^\circ\text{C}$ for the various aspect ratios. It is clearly seen in Fig. 4-20(a) that the velocity slowly increases from the inlet to the outlet. The wall temperature of $260\text{ }^\circ\text{C}$ generates higher gas velocity distributions than that of $200\text{ }^\circ\text{C}$. The results show that the methanol conversion of the micro-reformer is independent of the velocity distributions in the center of the channel due to the chemical reaction dominating methanol conversion. Then, to explore the pressure loss caused by the various aspect ratios, the local pressure losses (the difference between local and inlet pressures) along the channel center line for wall temperatures of $200\text{ }^\circ\text{C}$ and $260\text{ }^\circ\text{C}$ under various aspect ratios are presented in Fig. 4-20(b). In Fig. 4-20(b), it is found that the local pressure loss increases along the flow channel. A careful examination of Fig. 4-20(b) discloses that larger pressure loss is noticed for a case with a higher wall temperature ($260\text{ }^\circ\text{C}$). Additionally, the results show that larger pressure loss is found for a smaller aspect ratio ($\gamma=0.25$). The higher pressure losses mean that excess work has to be done in pushing the gases through. Therefore, reducing pressure losses is one of the most important issues.

Effects of the aspect ratios on the temperature distributions are shown in Fig. 4-21(a). It is clearly seen that the fluid temperature increases along the channel as a consequence of

chemical reaction. When $X > 0.03$, the fluid temperature increase insignificantly along channel because there is a thermal equilibrium beyond this point. It is also shown that the temperature rises with the decrease in aspect ratios, γ . As the γ decreases, the temperature distributions become much more uniform. Therefore, a smaller aspect ratio leads to a better methanol conversion. Afterwards, to explore the change in steam reforming reaction rate caused by the various aspect ratios of the channels, the local steam reforming reaction rates along the interface between the catalyst layer and the flow channel are presented in Fig. 4-21(b). For a wall temperature of 260°C , larger aspect ratios can improve the steam reforming reaction rate, as a result of the methanol being consumed in the forward region of channel inlet. For a lower wall temperature of 200°C , the change in steam reforming reaction rate follows a similar trend to that of the wall temperature 260°C . In addition, it is found that a higher steam reforming reaction rate is found for a case with a higher wall temperature due to a stronger steam reforming reaction.

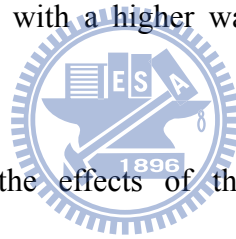


Figure 4-22 demonstrates the effects of the Reynolds number on the methanol conversion and the H_2 production rate of the channel in the plate methanol steam micro-reformer for wall temperatures of 260°C . An overall inspection of Fig.4-22 discloses that the methanol conversion increases with decreasing Reynolds number Re . This can be made plausible by noting the fact that the fuel can spend more time in the channel for a lower Reynolds number Re . As for the H_2 production rate, the results show that the H_2 production rate increases as the Re increases. Additionally, the effects of the aspect ratios on the methanol conversion and H_2 production rate are shown in Fig. 4-22. It is clear that the methanol conversion increases with a decrease in aspect ratio. When $\gamma=0.5$ with a Re of 3.14, the methanol conversion was greater than 86%, and the H_2 production rate was $184\text{ cm}^3/\text{min}$. The plate methanol steam micro-reformer produced hydrogen to supply fuel cell, Park et al. [16] presented that the H_2 production rate was only $186\text{ cm}^3/\text{min}$, which could supply a 15W

fuel cell.

4.2.2 Effects of Geometric Size on the Transport Phenomena and Performance of Micro-Reformer

Effects of geometric size on the transport phenomena and performance of micro-reformer are important. To this end, the effects of channel size on temperature distributions are shown in Fig. 4-23. In Fig. 4-23, two channel sizes were tested: channel (I) 33mm(L), 1.5mm(W_R), 0.75mm($\delta_1 + \delta_2$) and channel (II) 33mm(L), 0.429mm(W_R), 0.214mm($\delta_1 + \delta_2$), respectively. The aspect ratios were all fixed to be 0.5, with the catalyst thickness being 30 μ m. Different channel sizes have different hydraulic diameters. Channel (I) has a greater hydraulic diameters than channel (II). It is found from Fig. 4-23 that the temperature distribution increases along the channel as a consequence of the chemical reaction. For a smaller channel size, the temperature distribution is much more uniform due to the shorter thermal entrance length. This kind of uniform temperature distribution improves the chemical reaction rate. As a result, the smaller channel leads to better methanol conversion. Comparing the local temperature distributions for wall temperatures of 200 $^{\circ}$ C and 260 $^{\circ}$ C, it can be shown that the local temperature distribution increases with increasing wall temperature.

The effects of the Reynolds number Re on the methanol mole fraction distributions of two channel sizes (I) 33mm(L), 1.5mm(W_R), 0.75mm($\delta_1 + \delta_2$) and (II) 33mm(L), 0.429mm(W_R), 0.214mm($\delta_1 + \delta_2$) for wall temperatures of 200 $^{\circ}$ C and 260 $^{\circ}$ C are examined in Fig. 4-24. The results show that a larger CH_3OH mole fraction is noted for a case with a higher Reynolds number Re . Additionally, it is clearly observed that for fixed Re , channel (I) shows similar methanol distributions to those of channel (II). Therefore, channels (I) and (II)

have similar methanol conversion, but channel (I) requires more catalyst loading and a slower velocity than channel (II). This is because that channel (II) has a more uniform temperature distribution which increases the chemical reaction rate. Comparison of Figs. 4-24 (a) and (b) shows that the CH₃OH consumption increases with increasing wall temperature, which in turn, increases the reaction rate.

4.3 Three-Dimensional Model of a Plate Methanol Steam Micro-Reformer with Serpentine Flow Field Design

The research above has shown that micro-reformer performance can be enhanced by suitable thermo-fluid parameters. However, there has been a limited amount of work investigating the effects of the different flow field designs on thermo-fluid parameters, especially for the serpentine flow field. Therefore, the objective of this section is to establish a three-dimensional serpentine flow field model of the plate methanol steam micro-reformer to investigate its transport phenomena and methanol conversion efficiency.

Figure 2-3 presents schematics of the three-dimensional plate methanol steam micro-reformer considered in this work. The inlet cross-section of the channel is 1 mm x 1 mm. The thicknesses of the catalyst layers are set at 50 μm. The base conditions of the properties are as follows; the operating pressure is 1 atm and the inlet temperature is 120°C. The inlet flow velocity is 1 m/s and the molar ratio of H₂O/CH₃OH is 1.3 in the first example. The physical properties of the channels are listed in Table 4-6.

In order to study the effect of grid number on the numerical results, the grid independence was examined in preliminary test runs. For simplification of the analysis, three grid configurations were evaluated for the single channel of the plate methanol steam micro-reformer at a wall temperature of 230°C. The single channel length is 33 mm, and the

cross-section of the channel is 1 mm x 1 mm. The thicknesses of the catalyst layer are set at 50 μm . The inlet flow velocity is 1 m/s and the molar ratio of $\text{H}_2\text{O}/\text{CH}_3\text{OH}$ is 1.3. The physical properties of the channel are listed in Table 4-6. The numbers of grid lines in the x, y and z directions were 265x36x9, 133x26x5, and 67x16x3. The influence of grid lines on the local temperatures is shown in Table 4-7. The deviations of local temperatures are 0.04-1.1% for grids 67x16x3 and 133x26x5, and 0.4-2.8% for grids 133x26x5 and 265x36x9. Therefore, Grid 132x25x4 was chosen for the simulation in the present study as a tradeoff between accuracy and CPU computation time.

In order to compare the numerical results and experimental data, a micro-reformer with parallel flow field is tested. Fig. 4-15 shows a comparison of the present prediction with previous experimental data. The solid symbols denote the experimental results of Park et al. [16] and the curve is the present prediction. Only small discrepancies between the numerical results and the experimental data have been found. The numerical model accurately predicted the methanol conversion and the gas distributions. Hence, the proposed three-dimensional numerical model is adequate for analyzing the heat and mass transfer in a micro-reformer.

4.3.1 Effects of Thermo-Fluid Parameters on the Plate Methanol Steam Micro-Reformer with Serpentine Flow Field Performance

The wall temperature, T_w , on the heated wall is important. To this end, the effects of wall temperatures on the dimensionless temperature distributions along the centerline of the serpentine flow field at a Reynolds number of 41 and a $\text{H}_2\text{O}/\text{CH}_3\text{OH}$ molar ratio of 1.3 are examined in Fig. 4-25(a). In Fig. 4-25(a), the fluid temperature shows a significant increase when the fuel moves downstream. The fluid temperature increases along the serpentine flow channel due to the heated wall. The dimensionless temperature experiences a negligible

variation when $X > 0.3$. This is due to thermal equilibrium for $X > 0.3$, in which the temperature has a more uniform distribution. In addition, it is found in Fig. 4-25(a) that the dimensionless temperature distributions are almost the same for various values of wall temperature. Figure 4-25(b) shows the effects of the wall temperature T_w on the distribution of CH_3OH and H_2 mole fraction along the centerline of the serpentine flow field. The CH_3OH mole fraction gradually decreases along the flow directions due to the chemical reaction, whereas the H_2 mole fractions increase when the flow moves downstream. It is also clearly seen that the CH_3OH consumption and the H_2 mole fractions increase with an increase in the wall temperature. A lower CH_3OH mole fraction and a higher H_2 mole fraction along the serpentine flow field represent a higher methanol conversion.

The velocity distributions along the centerline of the serpentine flow field for various values of wall temperature are presented in Fig. 4-26(a). Significant variations are seen clearly at the turning points of the flow channel due to the change of velocity direction. The fuel flow velocity increases from the inlet to outlet, due to increases in the temperature caused by significant density variation. The rise in fuel velocity becomes relatively insignificant since it is fully developed thermally at $X > 0.3$. The thermo-fluid parameters affect not only the methanol conversion efficiency, but also pressure loss (the difference between local and inlet pressures) in the serpentine flow channel. Large pressure drops in the channel mean that more pumping work is needed to pump the reactants. Thus, pressure loss is a significant issue. An exploration of pressure loss for various wall temperatures along the centerline of the serpentine flow field is presented in Fig. 4-26(b). Local pressure loss increases along the serpentine flow field. A larger pressure loss occurs at higher wall temperatures. In addition, clearly observed variations in the pressure loss appear at the turning points, due to the velocity change. The pressure losses are higher for the serpentine flow field than for the parallel flow channel, so reducing them is a priority for future use with the plate methanol micro-reformer.

The effects of the Reynolds number (Re) on the local dimensionless temperature, CH_3OH and H_2 mole fraction distributions at $T_w=230^\circ C$ are analyzed in Fig. 4-27. A careful examination of Fig. 4-27(a) reveals that the dimensionless temperature increases as the fluid moves downstream due to the heated wall. In addition, the dimensionless temperature rise is lower for a higher Re . This is due to the fact that a higher Reynolds number significantly increases the heat leaving the flow channel, which decreases the temperature rise. In Fig. 4-27(b), the CH_3OH mole fraction clearly decreases along the serpentine flow field. This is due to the temperature rise caused by the strong chemical reaction, which in turn increases the methanol consumption. Also, the methanol mole fraction distributions decrease with a lower Reynolds number. The results also show that a higher H_2 mole fraction is noted for the lower Reynolds number. This is due to the longer gas resident time which results in a better methanol conversion and a higher H_2 production.

Figure 4-28 presents the effects of the H_2O/CH_3OH (S/C) molar ratio on the CH_3OH , H_2 and CO mole fraction distributions at $T_w=230^\circ C$. Figure 4-28(a) shows that more efficient methanol conversion is noted at a higher H_2O/CH_3OH molar ratio. It is also found that a higher molar ratio of H_2O/CH_3OH causes the H_2 mole fraction to fall. The CO mole fraction distributions are also shown in Fig. 4-28(b). The CO concentration decreases with an increase in H_2O/CH_3OH molar ratio. This is because the higher H_2O concentration would enhance the water-gas-shift reaction, which in turn reduces the CO concentration. However, the higher H_2O/CH_3OH molar ratio also reduces the H_2 concentration at the channel outlet.

Figures 4-29 and 4-30 present the CH_3OH , H_2 and CO mole fraction distributions for $T_w=230^\circ C$ along the middle cross-section of the serpentine flow field ($Y=0.5$) and the interface between flow channel and catalyst layer ($Y=0.95$), respectively. An overall inspection of Figs. 4-29 and 4-30 reveals that the mole fraction of CH_3OH decreases along both the middle cross-section of the channel and the interface between the flow channel and

catalyst layer. A comparison between Figs. 4-29 and 4-30 shows that the methanol consumption is higher at the interface compared with the middle cross-section. This is because the interface has a higher temperature and chemical reaction rate. It is evident that the mass fraction of H₂ and CO increases along the middle cross-section of the serpentine flow field and along the interface between the flow channel and catalyst layer. This confirms that a methanol micro-reformer with a higher CH₃OH consumption indicates a higher H₂ and CO concentration, as would be expected.

Figure 4-31 presents the effects of the Reynolds number Re on the methanol conversion η and H₂ production rate Q_{H_2} for various values of wall temperature T_w . In Fig. 4-31, the value of Q_{H_2} increases and η decreases with an increase in Re . This can be attributed to the fact that a lower Re implies an increase in the fuel residence time and temperature distributions in the micro-reformer, which in turn improves the methanol conversion. As for the Q_{H_2} , a higher Q_{H_2} is found for the case with a higher Re due to the higher inlet flow rate. In addition, η and Q_{H_2} increase with an increase in wall temperature T_w . Besides, it is important to note that a higher Reynolds number will not necessarily provide a better H₂ production rate. When the methanol conversion is too small, a higher Reynolds number may provide a lower H₂ production rate.

4.3.2 Effects of Various Heated Plates on Micro-Reformer Performance

The effects of various heated plates of the channel on the temperature distributions and CH₃OH mole fraction distributions are examined in Fig. 4-32. In Fig. 4-32, two cases of heated plates were tested, top heated plate ($Y=1$) or bottom heated plate ($Y=0$). The effects of top versus bottom heated plates of the channel on temperature distributions along the center line of the serpentine flow field are shown in Fig. 4-32. A top heated plate has a higher

temperature distribution than a bottom heated plate. This is because a bottom heated plate has a smaller temperature rise due to fuel convection effects, while a top heated plate with the heated position near the catalyst layer has a more significant temperature rise. For a bottom heated plate, it is also apparent that marked temperature variations occur at the turning points of the flow channel due to the change of the heat flow direction. The top heated plate clearly has a larger methanol consumption than the bottom heated plate. These phenomena make it obvious that the stronger chemical reaction for the case with the top heated plate is due to a higher temperature distribution.

4.4 Three-Dimensional Channel Model of a Plate Methanol Steam Micro-Reformer with Methanol Catalytic Combustor

A three-dimensional numerical model of a micro-reformer with combustor is developed to examine the effects of various flow configurations, geometric parameters and Reynolds number (Re) on micro-reformer performance. The geometrical dimensions and parameters used are listed in Table 4-8.

In this work, a grid system of 121x81x21 points was used. To examine the grid independence of the predictions, three grid systems were considered and their influences on the prediction of local temperature distributions for a typical case are presented in Table 4-9. It is found that the maximum deviation among the computations using grids of 101x62x11, 121x81x21 and 141x100x31 are less than 1.3% and the results on the 121x81x21 and the 141x100x31 grids are quite close. Therefore, the grid system of 121x81x21 points seems sufficient to resolve the behaviors of local temperature distributions in the present micro-reformer model. To further check the adequacy of the numerical scheme, it is clearly seen from Fig. 4-33 that the present predictions agree reasonably well with the experimental

data of Won [24]. The above preliminary runs confirm that the present model and the numerical method used are generally appropriate for the analysis of the problem.

4.4.1 Effects of Various Flow Configurations and Geometric Parameters on Micro-Reformer Performance

In the present section, a three-dimensional channel model of a micro-reformer with combustor is developed to examine the effects of various flow configurations and geometric parameters on micro-reformer performance. A three dimensional model is analyzed to understand heat and mass transfer in the channels of a methanol steam micro-reformer with methanol catalytic combustor. The influences of wall conduction effects on the transport phenomena of heat and mass transfer in a micro-reformer with combustor are important. Therefore, the local temperature distributions along the centerline of the top reforming channel ($Y=0.333$) and the CH_3OH mole fraction distributions along the centerline of the reforming channel ($Y=0.167$) are presented in Fig. 4-34. In this work, X denotes the dimensionless distance from the flow channel inlet to the outlet. It is clearly seen in Fig. 4-34(a) that the temperature distributions with the wall thermal conduction effect show a lower and more uniform distribution than that without a wall conduction effect. This implies that the effects of wall conduction on the thermal development in a micro-reformer with combustor are important. It is also found in Fig. 4-34 that the effects of wall conduction lead to a higher methanol distribution than without a wall conduction effect due to a smaller value of the temperature distribution. However, the wall conduction effects on the heat and mass transport phenomena are remarkable and cannot be neglected in the modeling. Therefore, their effect should be considered in this work.

The influences of the flow configurations on the transport phenomena and the

performance of micro-reformers are important. To this end, the effects of the flow configurations for co- and counter-current flow on the temperature distributions along different axial location lines and on the local distributions of the mole fractions of various species along the centerline of the reforming channel are presented in Fig. 4-35. Fig. 4-35(a) discloses that the temperature distributions are much more uniform due to the shorter thermal entrance length. It is also obvious that a higher temperature distribution is noted for the counter-current flow. This is due to the fact that counter-current flow leads to better thermal management. Figure 4-35(b) shows the local distributions of the different species for co- and counter-current flow along the centerline of the reforming channel ($Y=0.167$). An overall inspection of Fig. 4-35(b) reveals that both the mole fractions of CH_3OH and H_2O decrease as the fluid moves downstream, while the H_2 , CO_2 and CO mole fractions increase with axial location. In addition, a lower CH_3OH mole fraction along the centerline of the channel represents a higher methanol conversion rate. The methanol conversion rate is greater than 91% for the counter-current flow, with a product gas composition of 73.2% H_2 , 25.1 % CO_2 and 1.7% CO at the outlet of the reforming channel. Comparing co- and counter-current flow via numerical simulation, the results show that the methanol conversion efficiency for counter-current flow could be improved by 10% due to a higher temperature distribution.

In order to explain the effectiveness of the geometric parameters for a micro-reformer with combustor in the thermal management, the temperature and CH_3OH mole fraction distributions for various geometric parameters were investigated. For a fixed Reynolds number, Figure 4-36 demonstrates the effects of the combustion flow channel heights on the temperature distributions along the centerline of the top reforming channel and on the CH_3OH mole fraction distributions along the centerline of the reforming channel with counter-current flow. It is shown in Fig. 4-36(a) that along the reforming channel, the temperature distributions are very uniform. Overall inspection of Fig. 4-36(b) disclosed that a

lower CH₃OH mole fraction is noted for a system with a greater combustion flow channel height due to a stronger chemical reaction for a higher temperature distribution. This means that a higher efficiency methanol conversion is enhanced via a greater combustion flow channel height.

An exploration of the temperature distributions for various reforming flow channel heights along the centerline of the top reforming channel is presented in Fig. 4-37(a). For fixed Re, the results show that a higher temperature distribution is found for a micro-reformer channel with a lower reforming flow channel height. This is because a higher channel height has a greater hydraulic diameter. As for the effects of reforming flow channel heights on the CH₃OH mole fraction distributions along the centerline of the reforming channel, an overall inspection of Fig. 4-37(b) reveals that better micro-reformer performance is noted for a lower reforming channel height. This implies that the chemical reaction rate is slower for a system with a greater reforming channel height. This seems plausible as a stronger chemical reaction is experienced for a micro-reformer channel with a higher wall temperature.

The effects of the channel widths on the temperature distributions and CH₃OH mole fraction distributions for a fixed Reynolds number were also investigated. Figure 4-38(a) presents the effects of channel widths on the temperature distributions along the centerline of the top reforming channel ($Y=0.333$). It is shown in Fig. 4-38(a) that the local temperature distribution increases with a decrease in the channel width. This may be because a rather narrow channel decreases the heat leaving the flow channel. In Fig. 4-38(b), the methanol conversion of the micro-reformer is slightly enhanced with a wider channel width. It is important to note that a higher temperature distribution will not necessarily provide better methanol conversion, because the channel width increases with increasing catalyst reaction area, which in turn increases the chemical reaction rate.

Figure 4-39 shows the effects of the steel widths on the temperature distributions and

CH₃OH mole fraction distributions. Fig. 4-39 (a) presents the effects of the steel widths on the temperature distributions along the centerline of the top reforming channel (Y=0.333). Comparison of the corresponding curves of the steel widths $W_L=0.25$ mm, 0.5 mm, and 1.0 mm indicates that a higher temperature distribution is found with wider steel. As for the effects of the steel width on the CH₃OH mole fraction distributions along the centerline of the reforming channel (Y=0.167), the results reveal that they have similar CH₃OH mole fraction distributions. This is due to having similar temperature distributions. Therefore, the steel width does not have a significant impact on the methanol conversion.

4.4.2 Effects of the Reynolds Number (Re) on Heat and Mass Transfer Phenomena and Micro-Reformer Performance

In the study of the effects of the Reynolds number (Re) on the transport phenomena and micro-reformer performance, understanding the detailed distributions of heat and mass transfer is important to the design of a micro-reformer with a combustor. The Reynolds number (Re) is one of the key thermo-fluid parameters in the micro-reformer and combustor channels which would affect the micro-reformer performance. Therefore, effects of the Reynolds number (Re_C) on the combustion channel side on the temperature distributions along the centerline of the top reforming channel (Y=0.333) and CH₃OH mole fraction distributions along the centerline of the reforming channel (Y=0.167) with counter-current flow are examined in Figure 4-40. A careful examination of Fig. 4-40(a) shows that the temperature increases with an increase in the Reynolds number (Re_C) on the combustor side due to a higher inlet flow rate. This is because higher combustion energy is released for a higher inlet flow rate (Reynolds number). Afterwards, an overall inspection of Fig. 4-40(b) reveals that the CH₃OH mole fractions decrease as the fluid moves downstream due to the

reforming chemical reaction. It is also shown that the CH_3OH mole fraction distributions decrease with increasing Reynolds number in the combustor channels. This can be made plausible by noting the fact that the chemical reaction increases as the temperature distributions increase.

Figure 4-41 presents the effects of the Reynolds number (Re_R) on the micro-reformer side on the temperature distributions along the centerline of the top reforming channel ($Y=0.333$) and CH_3OH mole fraction distributions along the centerline of the reforming channel ($Y=0.167$) with counter-current flow. The results in Fig. 6(a) reveal that the temperature distributions are enhanced by the decreased Reynolds number (Re_R) on the micro-reformer channels. This is due to a higher Reynolds number (Re_R) significantly increasing the heat leaving the flow channel, which decreases the temperature rise. In addition, it is seen in Fig. 4-41(b) that the CH_3OH mole fraction distributions decrease with a lower Reynolds number due to a longer time of gas residence and a higher temperature, which results in a better methanol conversion.

Figure 4-42 demonstrates the effects of the Reynolds number (Re_C) for the combustor on the methanol conversion and wall temperature of the reforming channel in the plate methanol steam micro-reformer. For comparison, the results without the wall conduction effect in the model are also presented. An overall inspection of Fig. 4-42 shows that the wall temperature increases with increase of the Reynolds number (Re_C) on the combustion channel side. This is plausible because the inlet fuel velocity increases in the channel as the Reynolds number increases. As for the methanol conversion, the results show that the methanol conversion increases as the Reynolds number of the combustion channel increases, which in turn increases the wall temperature. In addition, the wall conduction effect is also shown in Fig. 4-42. The deviations in the methanol conversion between the results with and without consideration of wall conduction effects are larger. This means that the wall conduction effect

on the methanol conversion and wall temperature become significant and cannot be neglected in the modeling.

4.5 Three-Dimensional Model of a Plate Methanol Steam Micro-Reformer with Methanol Catalytic Combustor for Parallel Flow Field and Serpentine Flow Field

This section is to establish the three-dimensional computational models of a plate methanol steam micro-reformer with a methanol catalytic combustor to investigate the performance and transport phenomena for the parallel flow field and serpentine flow field. The dimensions of a plate methanol steam micro-reformer with a methanol catalytic combustor in this section are 40mm(L)x15mm(W)x2.5mm(H), the inlet and outlet cross-sections of the flow channel are 1.0mmx0.5mm, and the rib width is 2 mm. The thicknesses of the catalyst layer are set to be 0.05mm. Because of the discrepancies in the flow channel design, the flow channel length and the turning points among various flow field designs, the fuel consumption and temperature distributions inside the micro-reformer are different. The effects of the flow field designs on the temperature, CH₃OH mole fraction, H₂ mole fraction and CO mole fraction distributions are presented in this section. The base conditions of the properties are in the following: the operating pressure and temperature of both micro-reformer and combustor are 1 atm and 393 °C, respectively. The inlet flow rates at the reforming side and at the combustion side are 7.5 cm³/min and 75 cm³/min as the base case, respectively. The parameters used in this section are listed in Table 4-10.

The Reynolds number (Re_R) on the micro-reformer side is a significant issue to be considered in choosing the flow field designs. Fig. 4-43(a) shows the effects of the Reynolds number (Re_R) on the micro-reformer side on the wall temperature of the reforming channel

for various flow field designs. The results reveal that the wall temperature is enhanced by the decreased Reynolds number (Re_R) on the micro-reformer. This is due to a higher Reynolds number (Re_R) significantly increasing the heat leaving the flow channel, which decreases the temperature rise. The serpentine flow field with combustor and the serpentine flow field with micro-reformer have a higher wall temperature of the reforming channel than any other flow fields. In addition, it is seen in Fig. 4-43(b) that a higher methanol conversion increases with a lower Reynolds number due to a longer time of gas residence and a higher temperature. The methanol conversion for the serpentine flow field with combustor and the serpentine flow field with micro-reformer is the best due to a higher wall temperature.

The effects of the flow field designs on the Reynolds number (Re_C) of the combustor and wall temperature of the reforming channel are presented in Fig. 4-44(a). It indicates that the temperature increases with an increase in the Reynolds number (Re_C) on the combustor side due to a higher inlet flow rate. This is because higher combustion energy is released for a higher inlet flow rate. The wall temperature increases in the following order: (I) the parallel flow field with combustor and the parallel flow with micro-reformer; (II) the serpentine flow field with combustor and the parallel flow field with micro-reformer; (III) the parallel flow field with combustor and the serpentine flow with micro-reformer field with combustor; (IV) the serpentine flow field with combustor and the serpentine flow field with micro-reformer. It is due to the improvement of the heat transport with the flow field design. In addition, the effects of the flow field designs on the Reynolds number (Re_C) of the combustor and methanol conversion in the plate methanol steam micro-reformer are shown in Fig. 4-44(b). As for the methanol conversion, the results indicate that the methanol conversion increases as the Reynolds number of the combustion channel increases. Therefore, it is concluded that increasing the corner number and the channel length to the various flow fields can effectively raise the temperature distribution, and enhance the methanol conversion.

The temperature distributions on the top cross-section of reforming channel are presented in Fig. 4-45. Constant flow rate approach is utilized in this analysis. The temperature distribution increases along the channel for each flow field designs. Fig. 4-46 presents the CH₃OH mole fraction distributions on the middle cross-section of the reforming channel for the various flow fields. It shows that the CH₃OH mole fraction decreases along the channel for the four flow fields. The methanol conversion at the exit of channel are 52%, 62%, 68%, and 79% for (I) the parallel flow field with combustor and the parallel flow with micro-reformer, (II) the serpentine flow field with combustor and the parallel flow field with micro-reformer, (III) the parallel flow field with combustor and the serpentine flow with micro-reformer field with combustor, (IV) the serpentine flow field with combustor and the serpentine flow field with micro-reformer, respectively. Therefore, it is expected that the methanol conversion would be highest for the serpentine flow field with combustor and the serpentine flow field with micro-reformer.

The distributions of the H₂ mole fraction on the middle cross-section of the reforming channel are shown in Fig. 4-47 for the various flow fields. A higher H₂ mole fraction along the flow channel represents a higher methanol conversion. Thus, the variation of the H₂ fraction is opposite to that of the CH₃OH mole fraction. A higher H₂ mole fraction is found for the serpentine flow field with combustor and the serpentine flow field with micro-reformer. Figure 4-48 presents the variations of the CO mole fractions on the middle cross-section of the reforming channel for the various flow fields. It is found that the CO distributions have the same trends as the H₂ distributions. This confirms the common concept that a micro-reformer with a H₂ production indicates a higher CO concentration.

Figure 4-49 demonstrates the effects of the inlet flow rate ($Q_{0,R}$) on the micro-reformer side on the H₂ production rate of the channel for various flow fields. An overall inspection of Fig.4-49 discloses that the H₂ production rate increases with decreasing the Reynolds number

(Re_R) on the micro-reformer side. The serpentine flow field with combustor and the serpentine flow field with micro-reformer is the best design by considering the H_2 production rate.



Table 4-1 Parameters used in the two-dimensional channel model of a plate methanol steam micro-reformer

Channel length L (m) [16]	3.3×10^{-2}
Channel height H (m) [16]	2.0×10^{-4}
Flow channel height δ_1 (m)	1.7×10^{-4}
Catalyst layer thickness δ_2 (m)	3.0×10^{-5}
Inlet average velocity u_0 (m s^{-1}) [16]	0.266
Inlet average temperature T_0 ($^{\circ}\text{C}$) [16]	393
Operation pressure (atm) [16]	1
Activation energy for steam reforming (kJ mol^{-1}) [66]	76
Activation energy for reverse water gas shift (kJ mol^{-1}) [66]	108
Catalyst density (kg m^{-3}) [51]	1480
Catalyst thermal conductivity ($\text{W m}^{-1} \text{K}^{-1}$) [51]	0.3
Catalyst layer porosity [52]	0.38
Catalyst permeability (m^2) [52]	2.379×10^{-12}
Mass diffusion coefficient ($\text{m}^2 \text{s}^{-1}$) [51]	6.8×10^{-5}

Table 4-2 Methanol mole fractions for the various grids

x(m)	0.005	0.010	0.015	0.020	0.025	0.030
Gridlines						
71x16	0.377	0.309	0.261	0.224	0.194	0.171
91x26	0.378	0.309	0.261	0.224	0.194	0.171
111x41	0.378	0.309	0.261	0.224	0.194	0.173

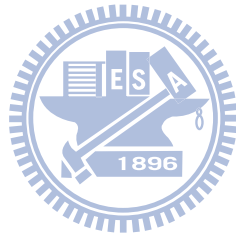


Table 4-3 The cases with various aspect-ratio channels used in this work

	Case 1	Case 2	Case 3	Case 4
γ	0.25	0.5	1.0	2.0
$\delta_1 + \delta_2$ (mm)	0.179	0.214	0.286	0.429
W_R (mm)	0.714	0.429	0.286	0.214

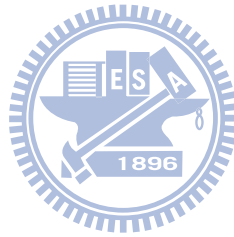


Table 4-4 Parameters used in the three-dimensional channel model of a plate methanol steam micro-reformer

Channel length L (m)	3.3×10^{-2}
Channel width W_R (m)	4.29×10^{-4}
Channel height $\delta_1 + \delta_2$ (m)	2.14×10^{-4}
Flow channel height δ_1 (m)	1.84×10^{-4}
Catalyst layer thickness δ_2 (m)	3.0×10^{-5}
Average inlet temperature ($^{\circ}\text{C}$)	120
Operating pressure (atm)	1
Activation energy for steam reforming (kJ/mol) [66]	76
Activation energy for reverse water gas shift (kJ/mol) [66]	108
Catalyst density (kg m^{-3}) [51]	890
Catalyst layer porosity [52]	0.38
Catalyst permeability (m^2) [52]	2.379×10^{-12}

Table 4-5 Mole fractions of methanol for the various grid tests at different axial locations

$I_x J_x K$	$x(m)$	0.005	0.010	0.015	0.020	0.025	0.030
41x16x18		0.381	0.314	0.266	0.230	0.200	0.176
51x21x23		0.382	0.316	0.269	0.232	0.203	0.179
71x31x33		0.382	0.316	0.269	0.233	0.204	0.179

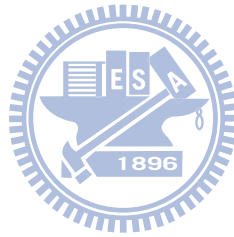


Table 4-6 Parameters used in the three-dimensional model of the plate methanol steam micro-reformer with serpentine flow field design

Channel width W_C (m)	1.0×10^{-3}
Channel height H (m)	1.0×10^{-3}
Flow channel height δ_1 (m)	9.5×10^{-4}
Catalyst layer thickness δ_2 (m)	5.0×10^{-5}
Average inlet temperature ($^{\circ}\text{C}$)	120
Operating pressure (atm)	1
Catalyst density (kg m^{-3}) [51]	1480
Catalyst thermal conductivity ($\text{W m}^{-1} \text{K}^{-1}$) [51]	0.3
Activation energy for steam reforming (kJ mol^{-1}) [66]	76
Activation energy for reverse water gas shift (kJ mol^{-1}) [66]	108
Catalyst layer porosity [52]	0.38
Catalyst permeability (m^2) [52]	2.379×10^{-12}
Mass diffusion coefficient ($\text{m}^2 \text{s}^{-1}$) [51]	6.8×10^{-5}

Table 4-7 Temperature distributions (°C) for the various grid tests at different axial locations

IxJxK	X	0	0.152	0.303	0.455	0.606	0.758	0.909
67x16x3		120	176	202	218	224	227	228
133x26x5		120	174	201	217	224	227	228
265x36x9		120	169	200	216	223	226	228

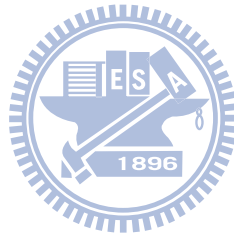


Table 4-8 Parameters used in the three-dimensional channel model of a plate methanol steam micro-reformer with methanol catalytic combustor

Flow channel length L (m)	4×10^{-3}
Combustion catalyst layer thickness δ_C (m)	5.0×10^{-5}
Reforming catalyst layer thickness δ_R (m)	5.0×10^{-5}
Combustion flow channel H_C (m)	4.5×10^{-4}
Reforming flow channel H_R (m)	4.5×10^{-4}
Average inlet temperature ($^{\circ}\text{C}$)	120
Operating pressure (atm)	1
Catalyst density (kg m^{-3}) [51]	1480
Catalyst thermal conductivity ($\text{W m}^{-1} \text{K}^{-1}$) [51]	0.3
Catalyst layer porosity [52]	0.38
Catalyst permeability (m^2) [52]	2.379×10^{-12}
Mass diffusion coefficient ($\text{m}^2 \text{s}^{-1}$) [51]	6.8×10^{-5}
Activation energy for steam reforming (kJ mol^{-1}) [41]	109
Activation energy for the reverse water gas shift (kJ mol^{-1}) [41]	115
Activation energy for decomposition reaction (kJ mol^{-1}) [41]	142
Activation energy for combustion reaction (kJ mol^{-1}) [80]	13

Table 4-9 Temperature distributions (°C) for the various grid tests at different axial locations

IxJxK	X								
	0.125	0.250	0.375	0.500	0.625	0.750	0.875	1.000	
101x62x11	239.0	239.8	240.6	241.4	241.9	242.1	241.7	210.0	
121x81x21	235.9	236.7	237.6	238.3	238.9	239.1	238.7	207.6	
141x100x31	233.4	234.2	235.1	235.8	236.3	236.6	236.1	205.7	

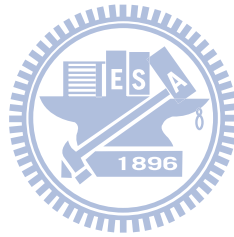


Table 4-10 Parameters used in the three-dimensional model of a plate methanol steam micro-reformer with methanol catalytic combustor

Flow channel length L (m)	4×10^{-3}
Combustion catalyst layer thickness δ_C (m)	5.0×10^{-5}
Reforming catalyst layer thickness δ_R (m)	5.0×10^{-5}
Combustion flow channel H_C (m)	4.5×10^{-4}
Reforming flow channel H_R (m)	4.5×10^{-4}
Steel width W_1 (m)	1×10^{-3}
Channel width W_2 (m)	1×10^{-3}
Rib width W_3 (m)	2×10^{-3}
Catalyst density (kg m^{-3}) [51]	1480
Catalyst thermal conductivity ($\text{W m}^{-1} \text{K}^{-1}$) [51]	0.3
Catalyst layer porosity [52]	0.38
Catalyst permeability (m^2) [52]	2.379×10^{-12}
Mass diffusion coefficient ($\text{m}^2 \text{s}^{-1}$) [51]	6.8×10^{-5}
Activation energy for steam reforming (kJ mol^{-1}) [41]	109
Activation energy for the reverse water gas shift (kJ mol^{-1}) [41]	115
Activation energy for decomposition reaction (kJ mol^{-1}) [41]	142
Activation energy for combustion reaction (kJ mol^{-1}) [80]	13



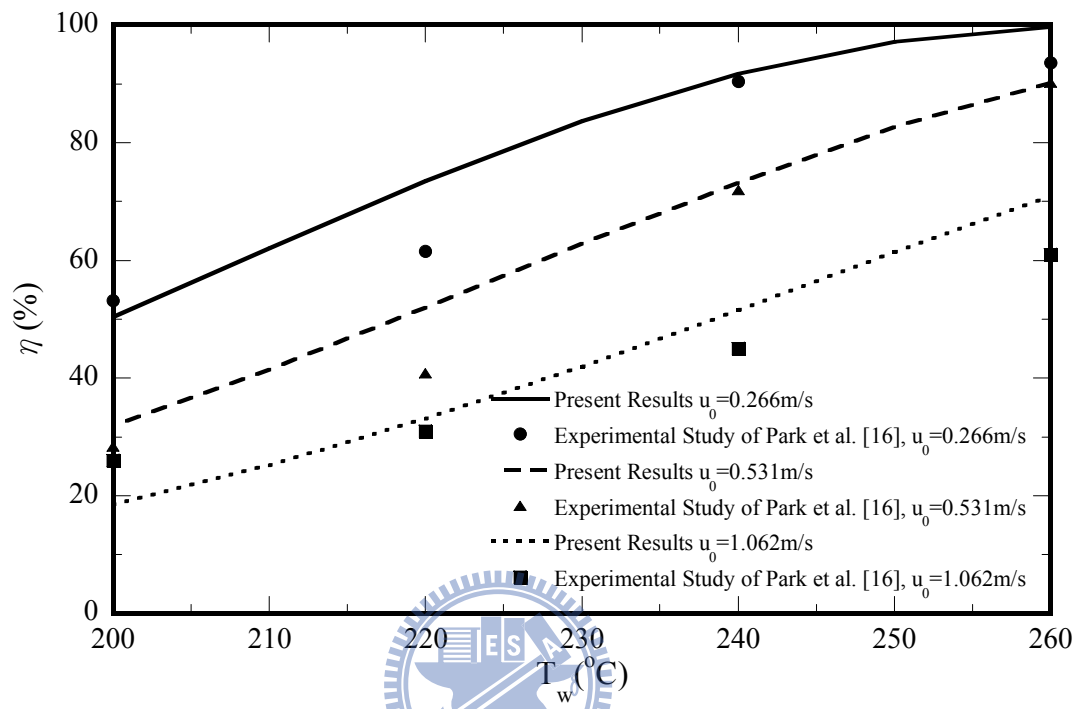


Fig. 4-1 Comparison of predicted methanol conversion with the experimental data of Park et al. [16]

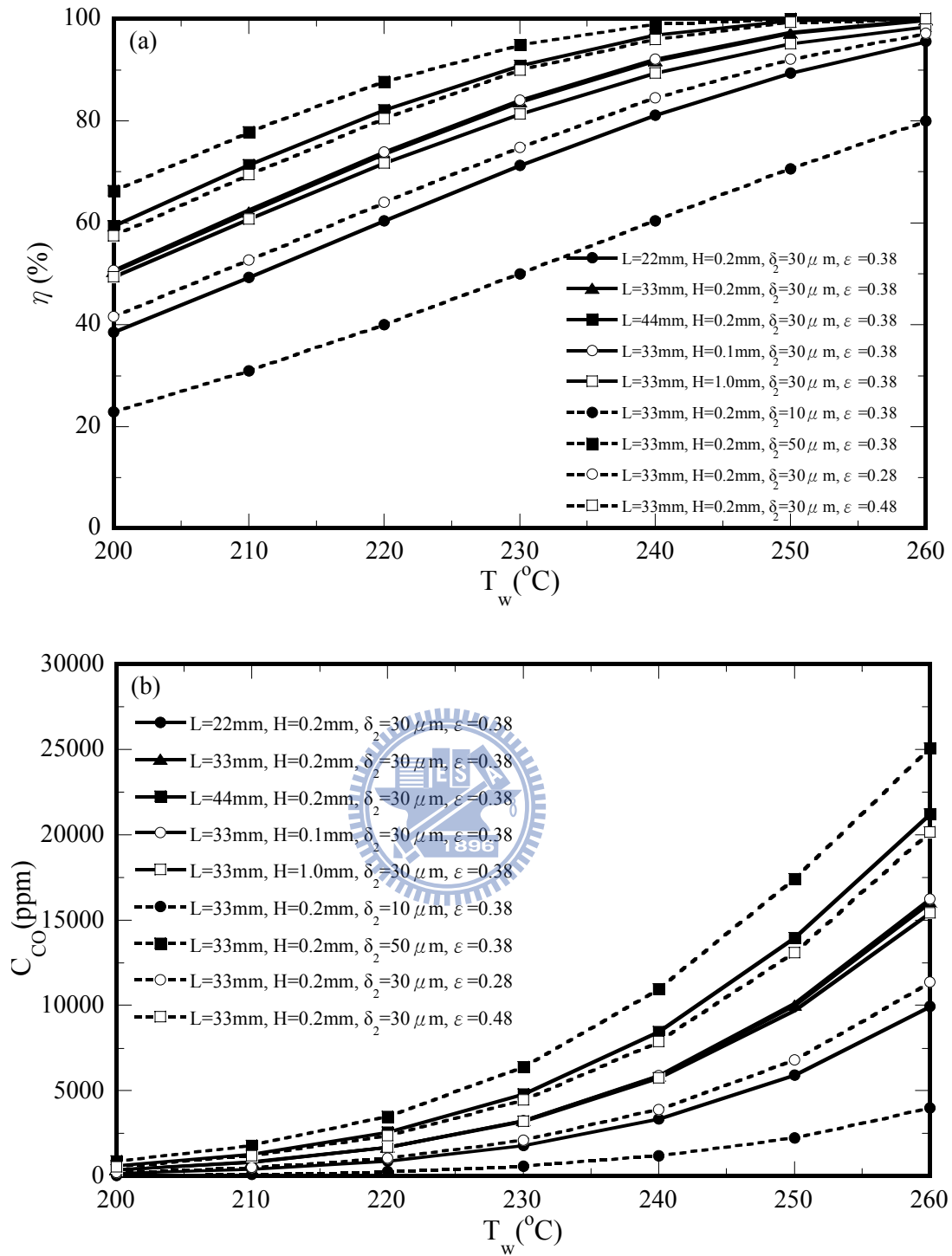


Fig. 4-2 Effects of geometric parameters and wall temperature on (a) the methanol conversion and (b) the CO concentration (ppm) at the outlet

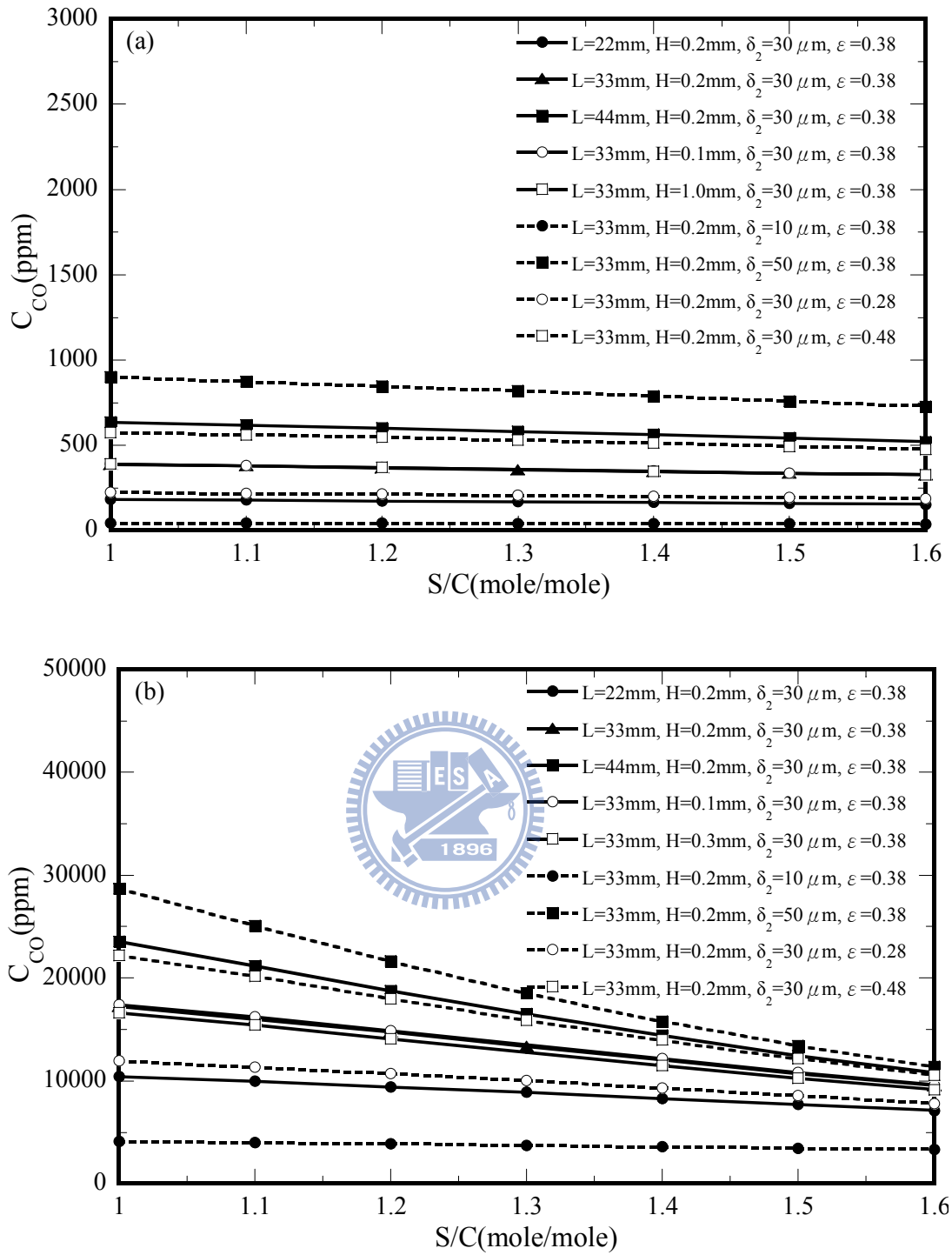


Fig. 4-3 Effects of geometric parameters and H_2O/CH_3OH molar ratio on the CO concentration at (a) $T_w=200\text{ }^\circ\text{C}$ and (b) $T_w=260\text{ }^\circ\text{C}$

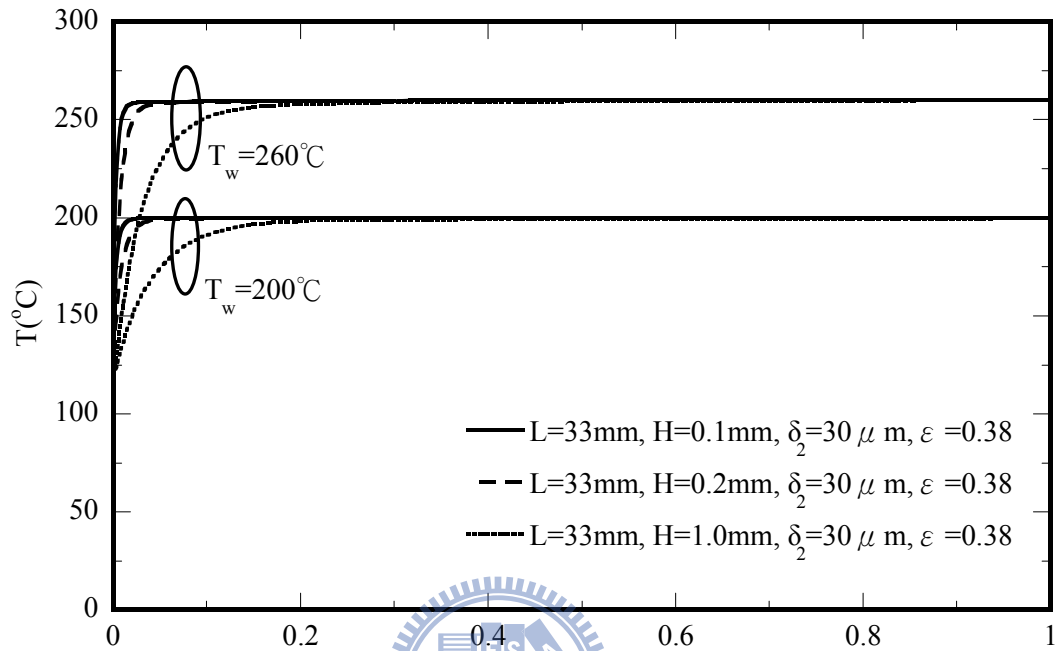


Fig. 4-4 Effects of the channel heights on temperature distributions along the centerline of the channel at $T_w=200^\circ\text{C}$ and $T_w=260^\circ\text{C}$

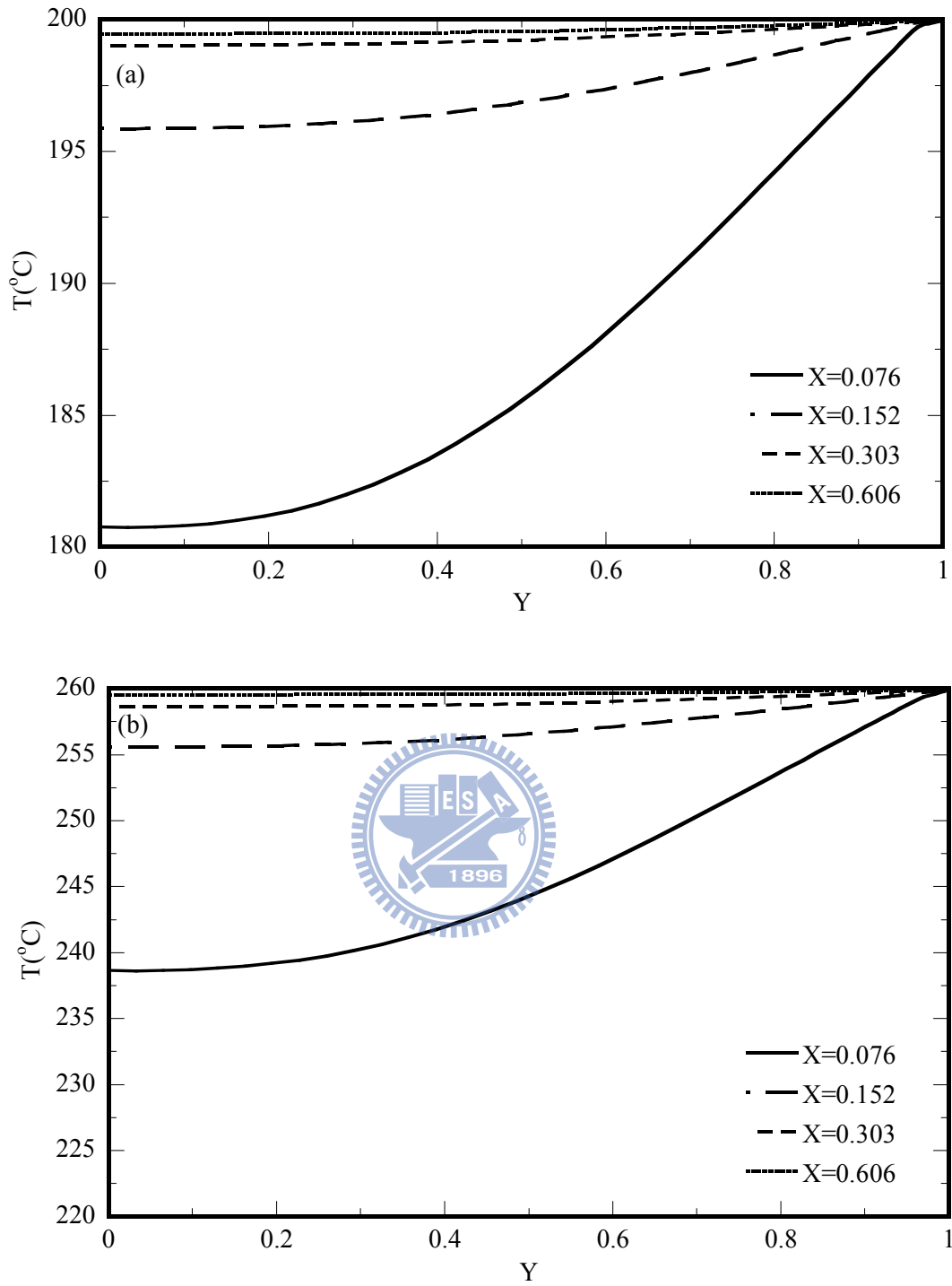


Fig. 4-5 Effects of wall temperature on the cross-sectioned temperature at different axial locations for $H=1.0\text{mm}$ (a) $T_w=200^{\circ}\text{C}$ and (b) $T_w=260^{\circ}\text{C}$

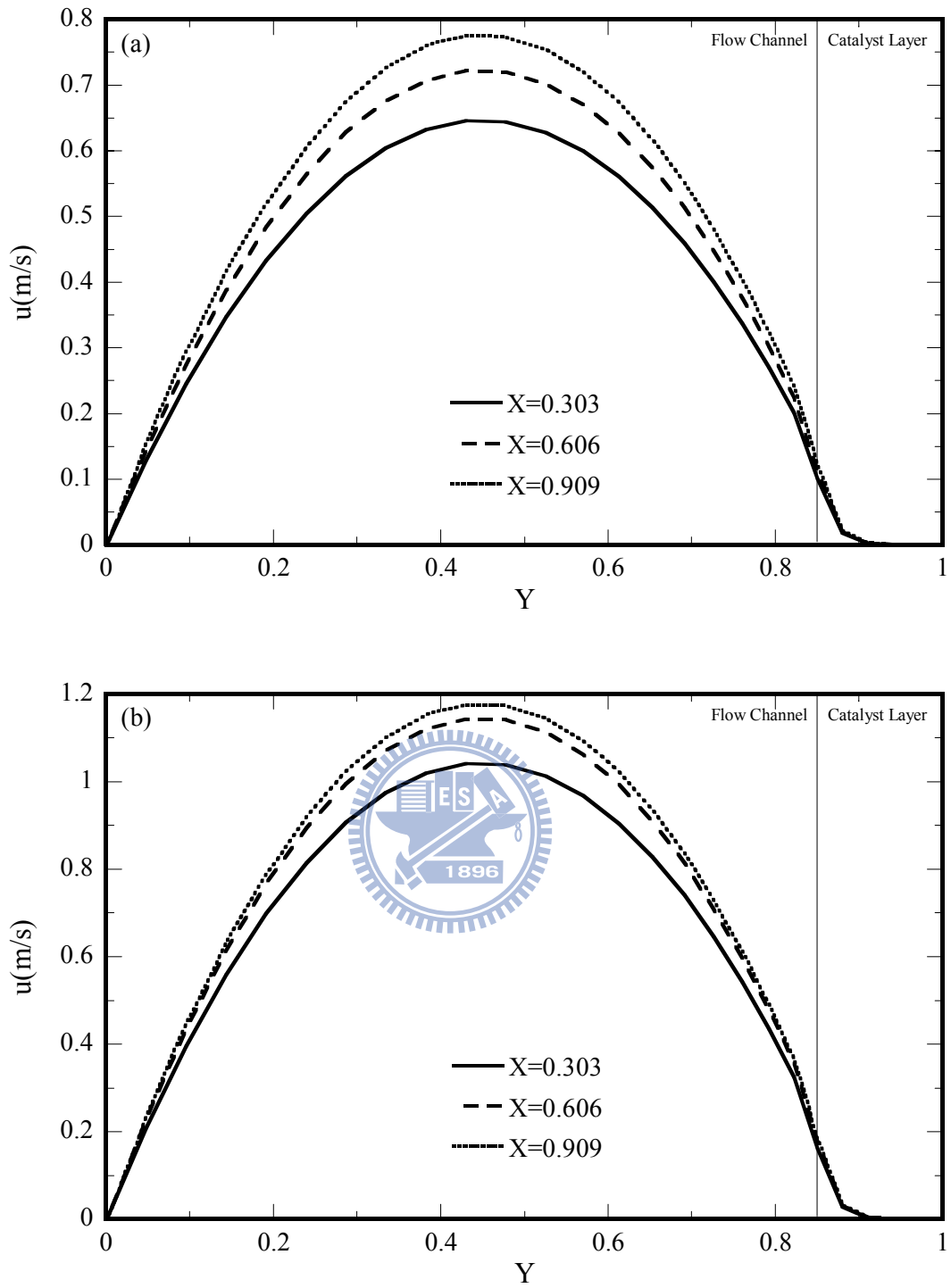


Fig. 4-6 Effects of wall temperature on the cross-sectioned velocity at different axial locations for $H=0.2\text{mm}$ (a) $T_w=200 \text{ }^\circ\text{C}$ and (b) $T_w=260 \text{ }^\circ\text{C}$

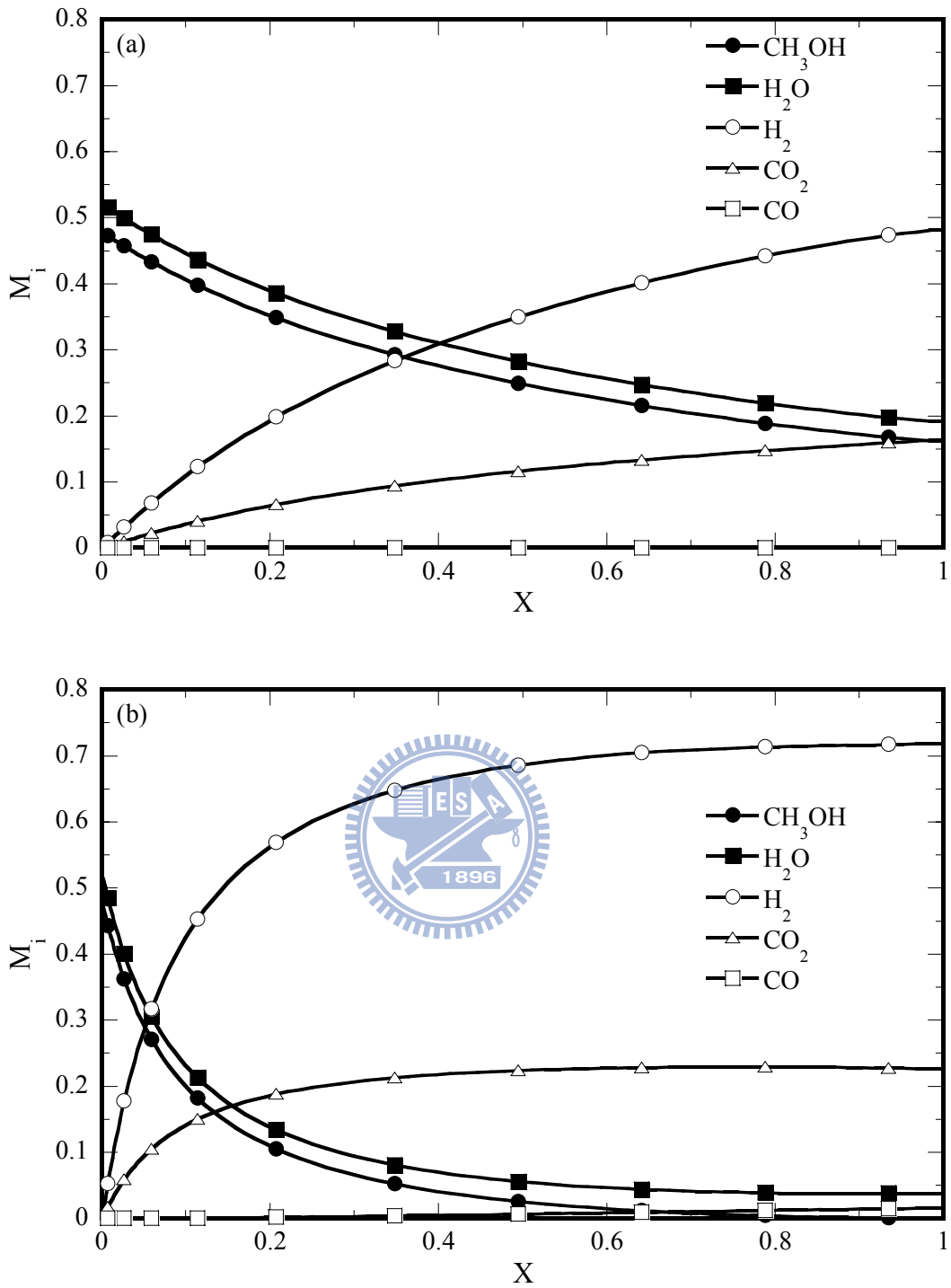


Fig. 4-7 Variations of the mole fraction of the various species along the channel (a) $T_w=200$ °C and (b) $T_w=260$ °C.

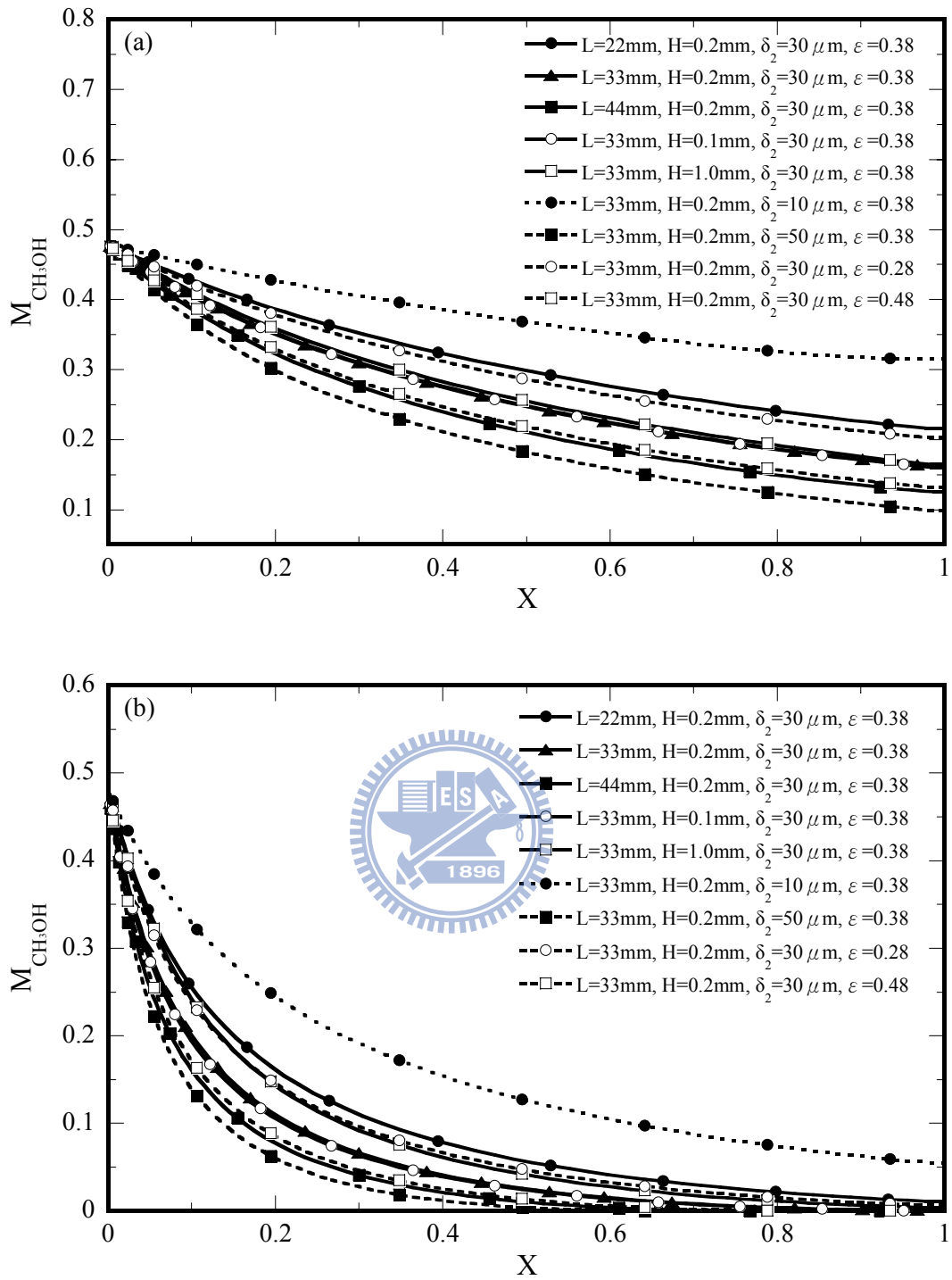


Fig. 4-8 Effects of geometric parameters on the local CH_3OH mole fraction along the channel

(a) $T_w = 200\text{ }^\circ\text{C}$ and (b) $T_w = 260\text{ }^\circ\text{C}$

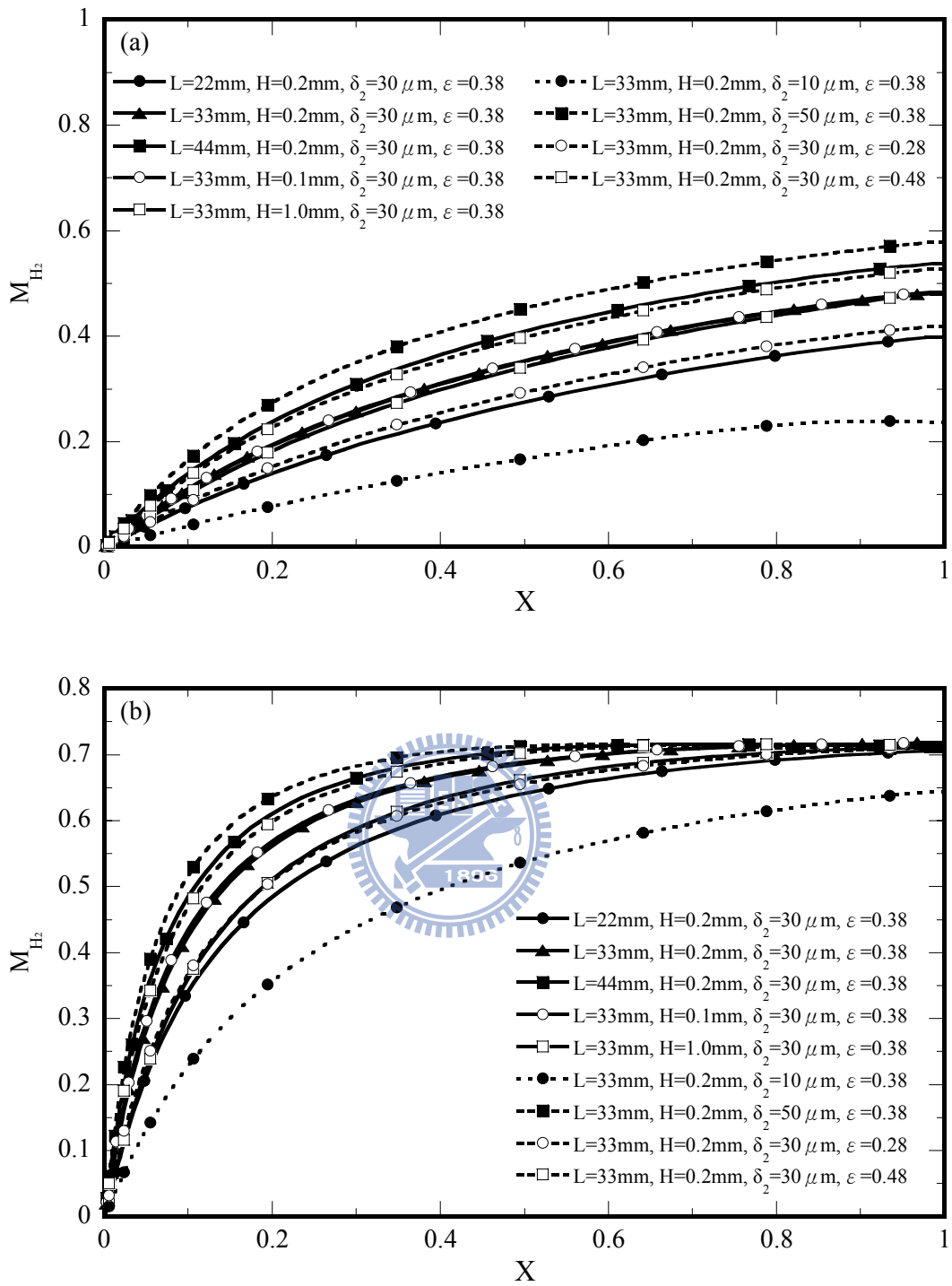


Fig. 4-9 Effects of geometric parameters on the local H_2 mole fraction along the channel at $T_w=200\text{ }^\circ\text{C}$ and (b) $T_w=260\text{ }^\circ\text{C}$

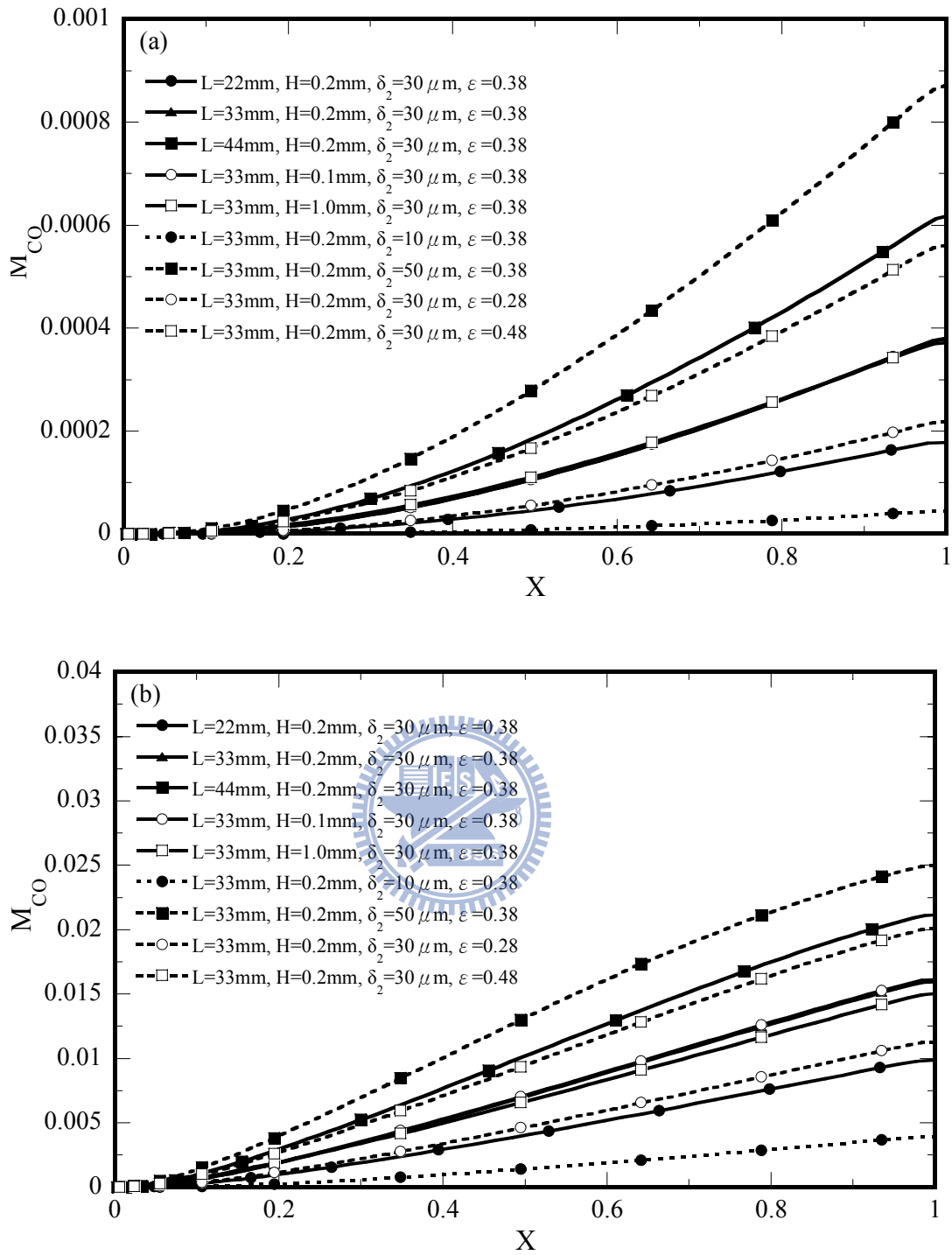


Fig. 4-10 Effects of geometric parameters on the local CO mole fraction along the channel at

(a) $T_w=200\ \text{°C}$ and (b) $T_w=260\ \text{°C}$

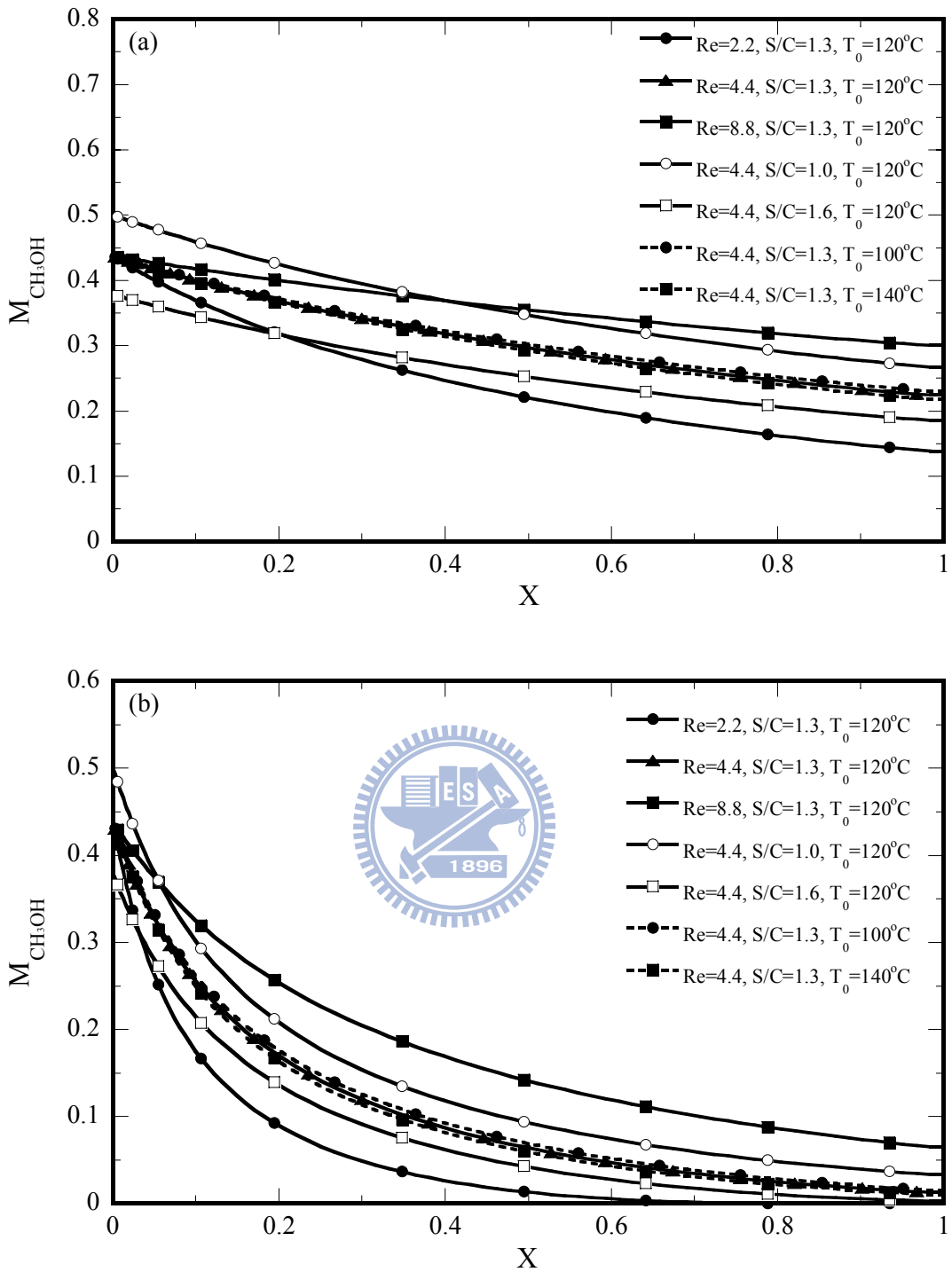


Fig. 4-11 Effects of thermo-fluid parameters on the local CH_3OH mole fraction along the channel at (a) $T_w=200\text{ }^\circ\text{C}$ and (b) $T_w=260\text{ }^\circ\text{C}$

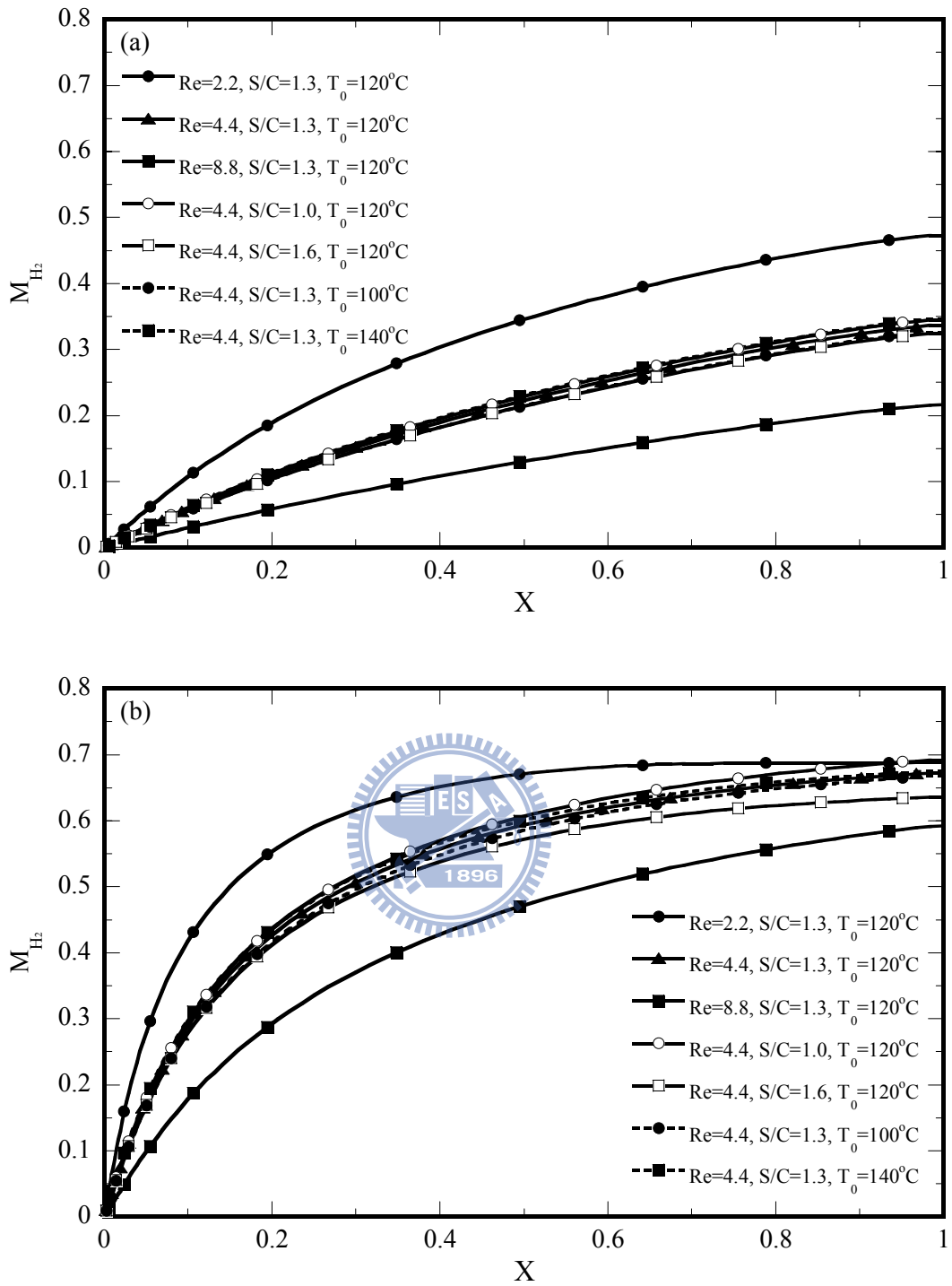


Fig. 4-12 Effects of thermo-fluid parameters on the local H_2 mole fraction along the channel

at (a) $T_w=200^\circ\text{C}$ and (b) $T_w=260^\circ\text{C}$

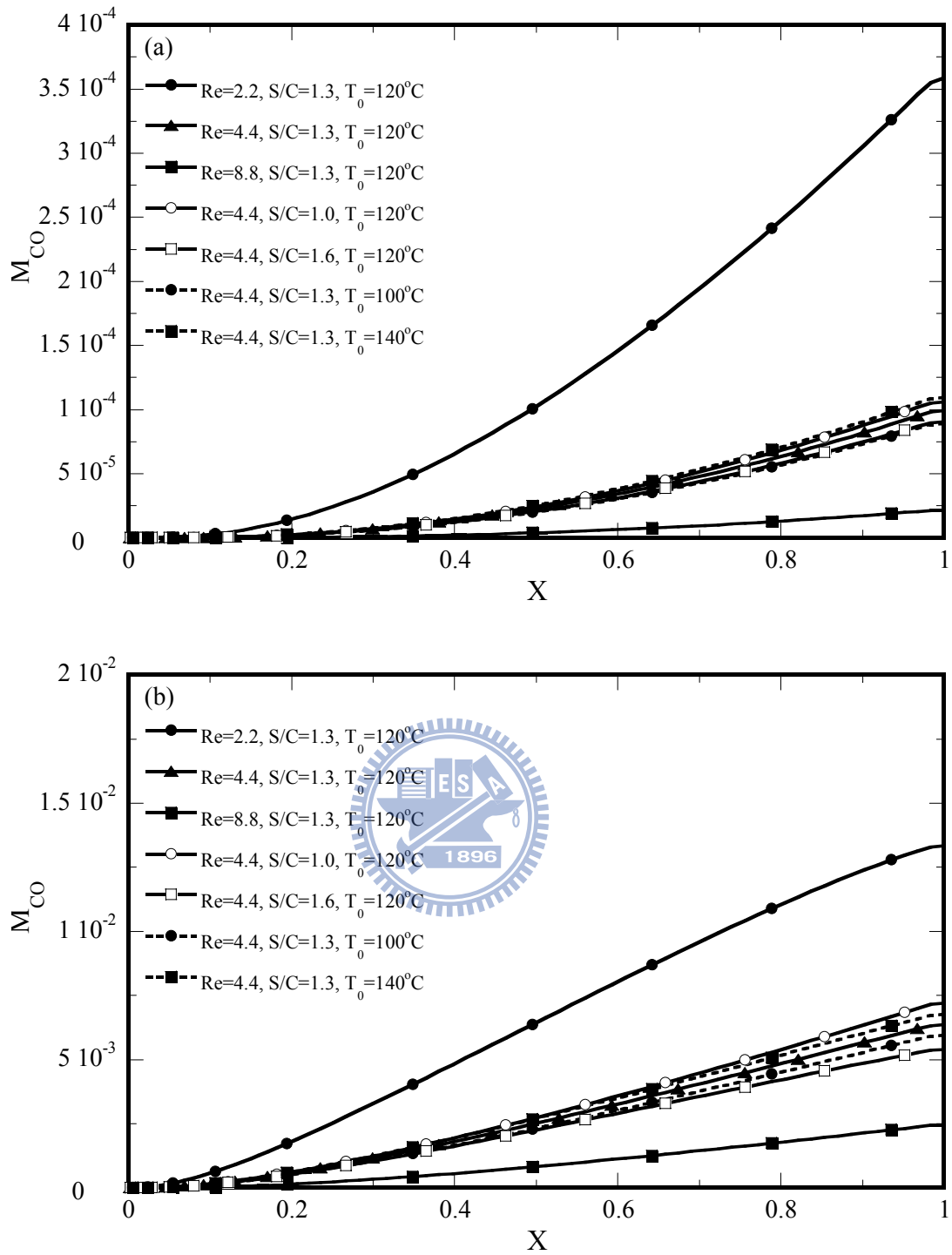


Fig. 4-13 Effects of thermo-fluid parameters on the local CO mole fraction along the channel

at (a) $T_w=200^\circ\text{C}$ and (b) $T_w=260^\circ\text{C}$

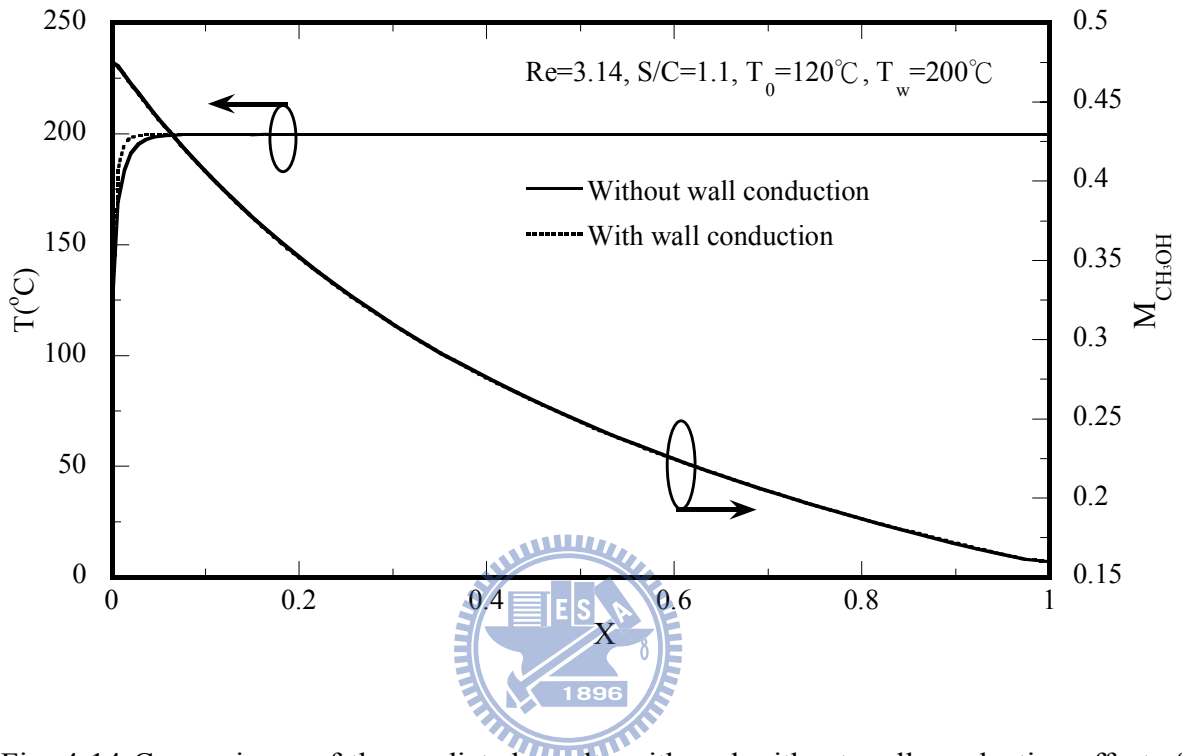


Fig. 4-14 Comparisons of the predicted results with and without wall conduction effects for the temperature and CH_3OH mole fraction distributions along the centerline of the channel ($Y=0.5$).

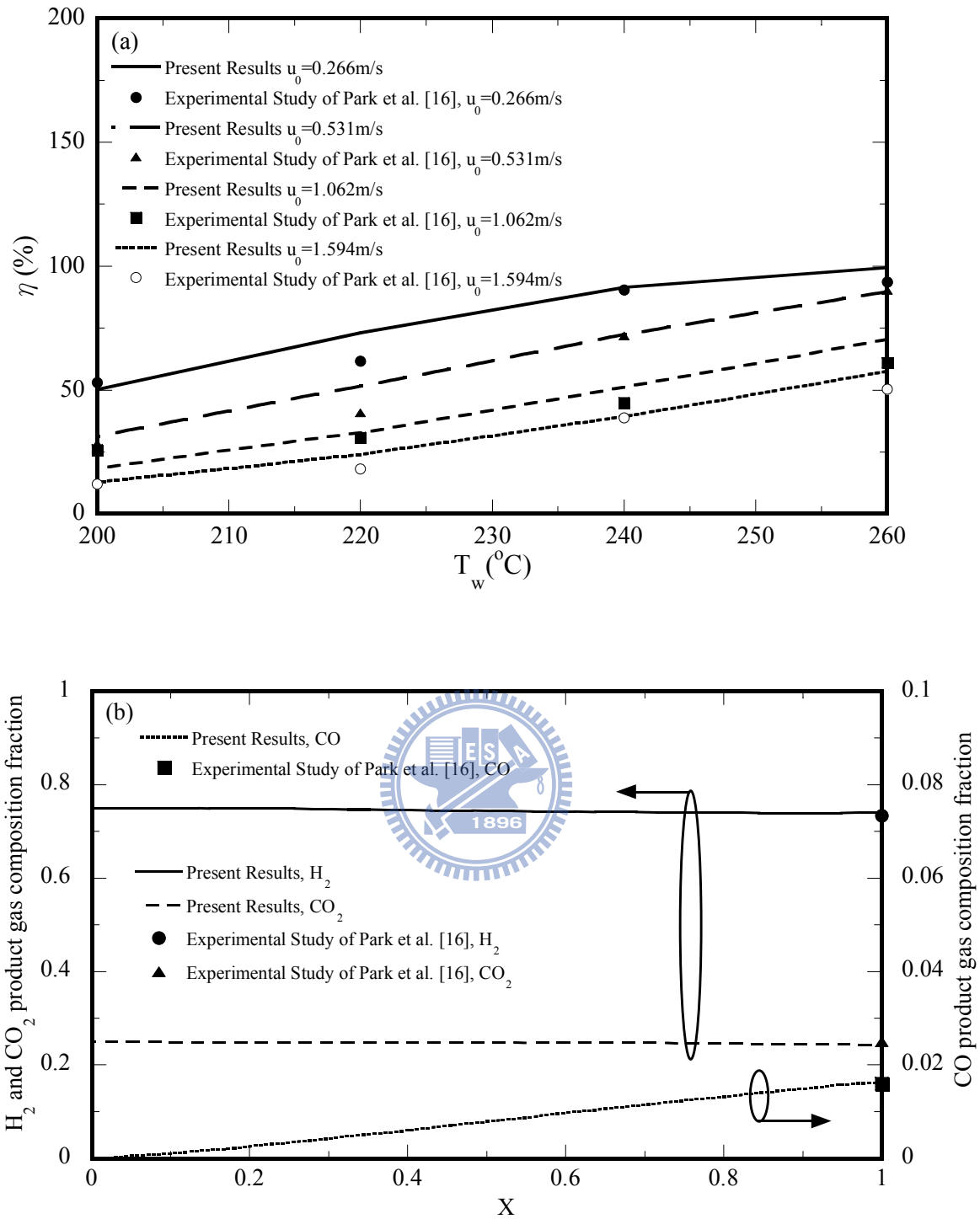


Fig. 4-15 Comparison of predicted methanol conversion with previous experimental data of Park et al. [16]

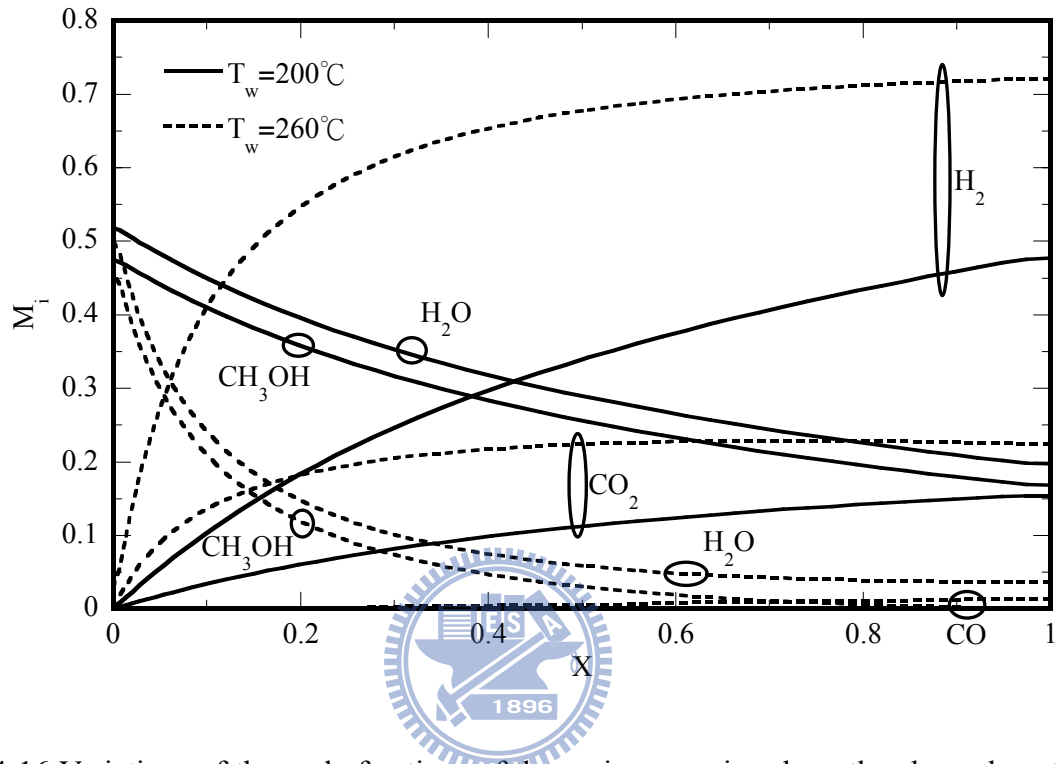


Fig. 4-16 Variations of the mole fractions of the various species along the channel center line ($\gamma=0.5$)

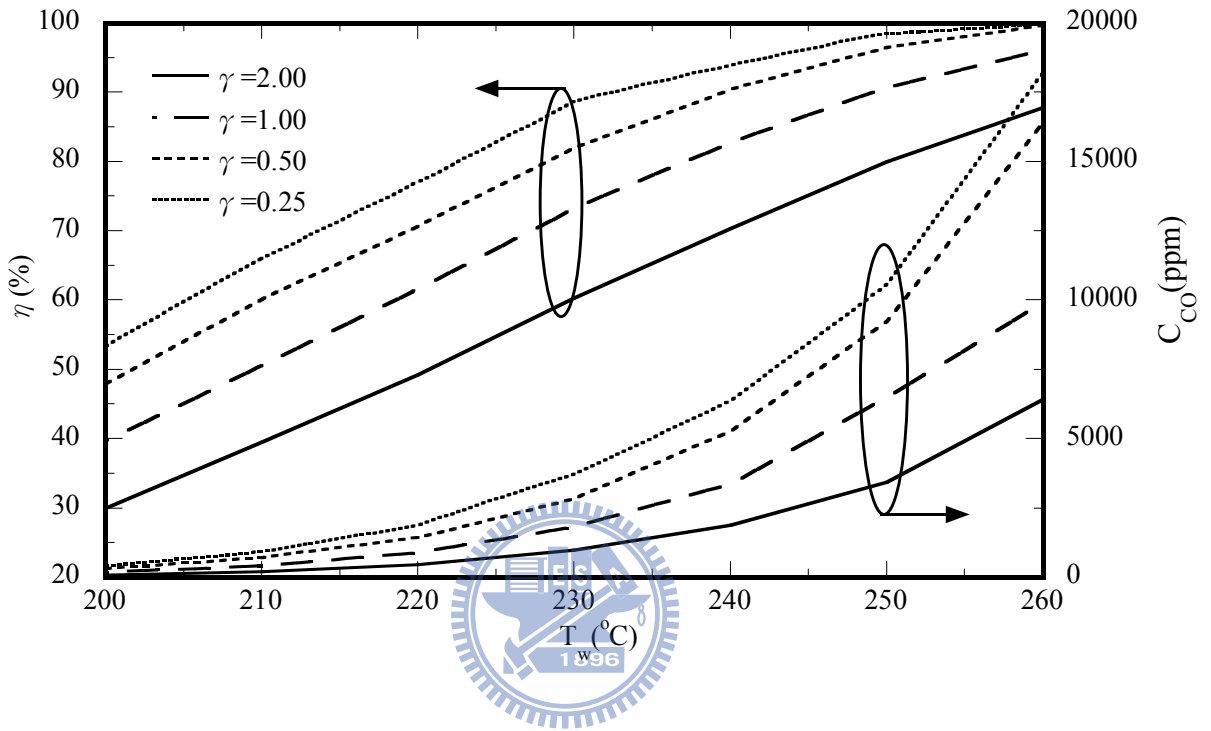


Fig. 4-17 Effects of aspect ratios of channel and wall temperature on methanol conversion and CO concentration (ppm) at outlet of channel

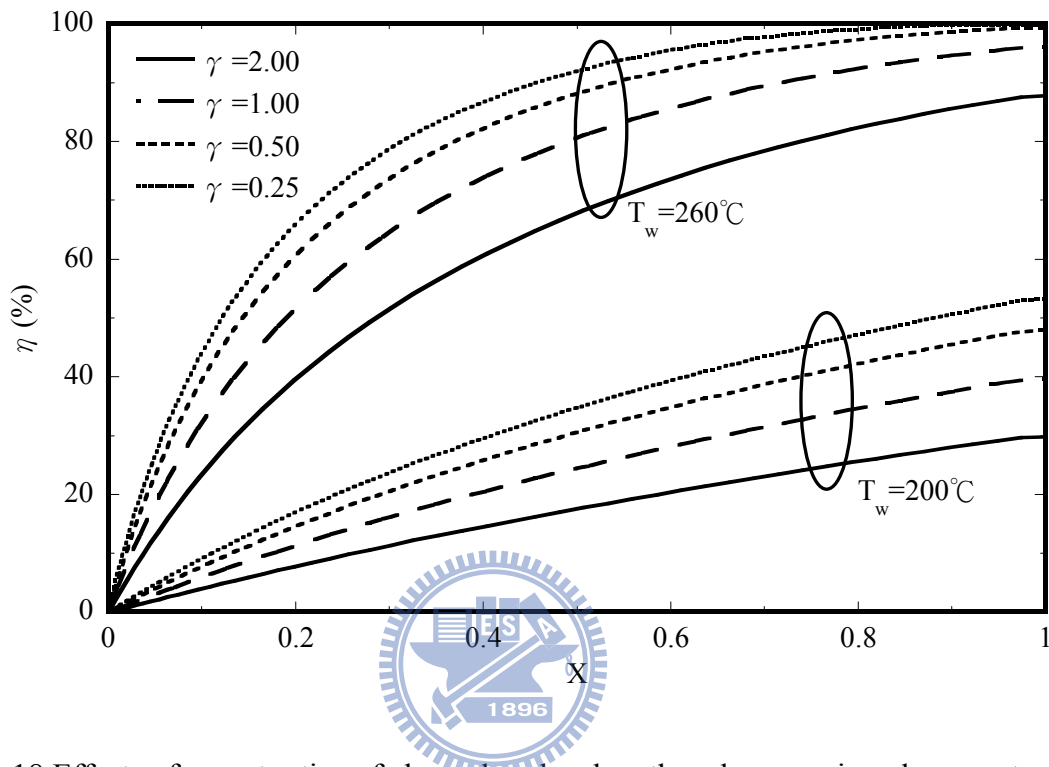


Fig. 4-18 Effects of aspect ratios of channel on local methanol conversion along center line of channel at $T_w=200^\circ\text{C}$ and $T_w=260^\circ\text{C}$

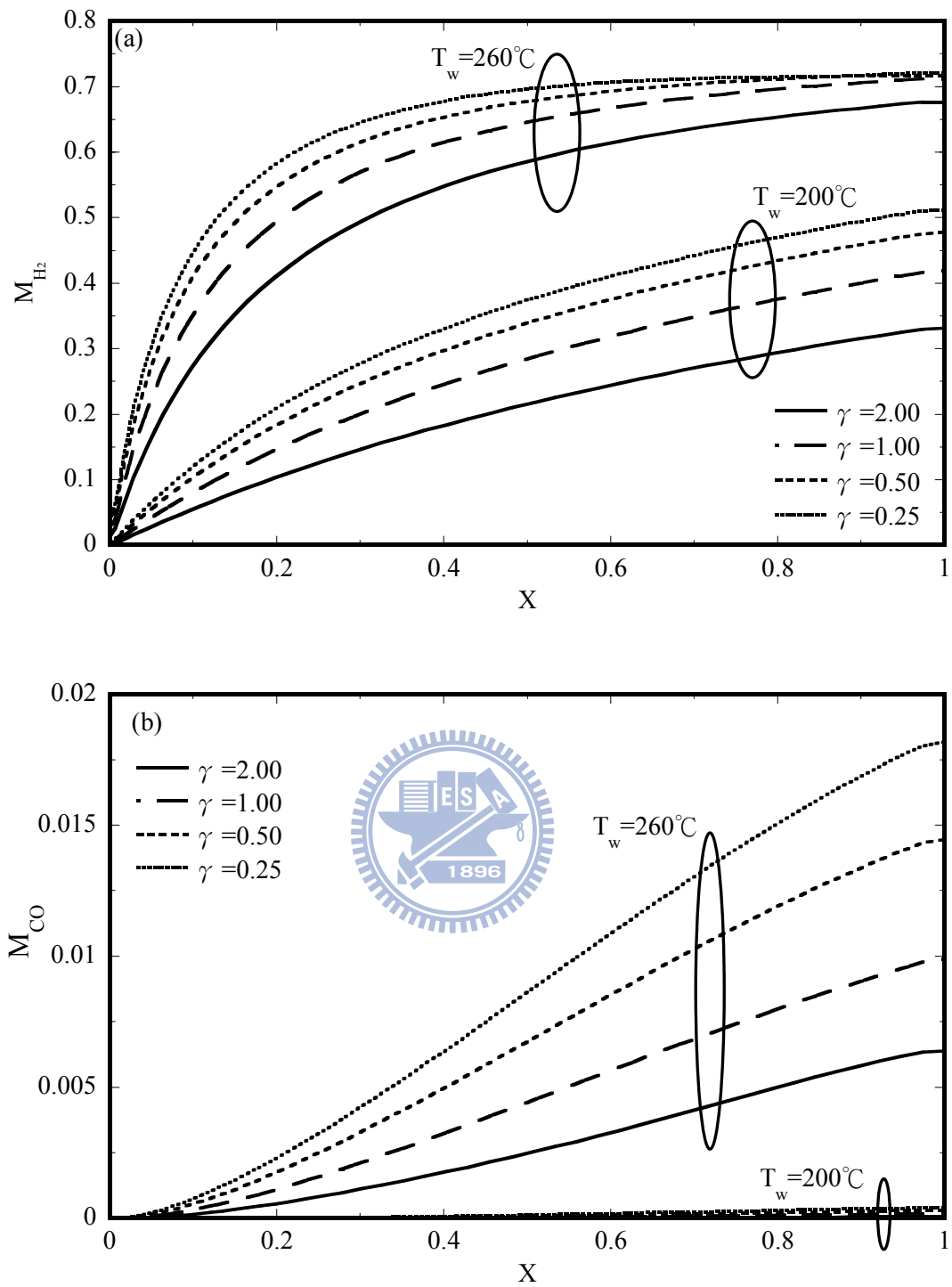


Fig. 4-19 Effects of aspect ratios of channel at $T_w=200\text{ }^\circ\text{C}$ and $T_w=260\text{ }^\circ\text{C}$ on (a) local H_2 mole fraction and (b) local CO mole fraction along center line of channel

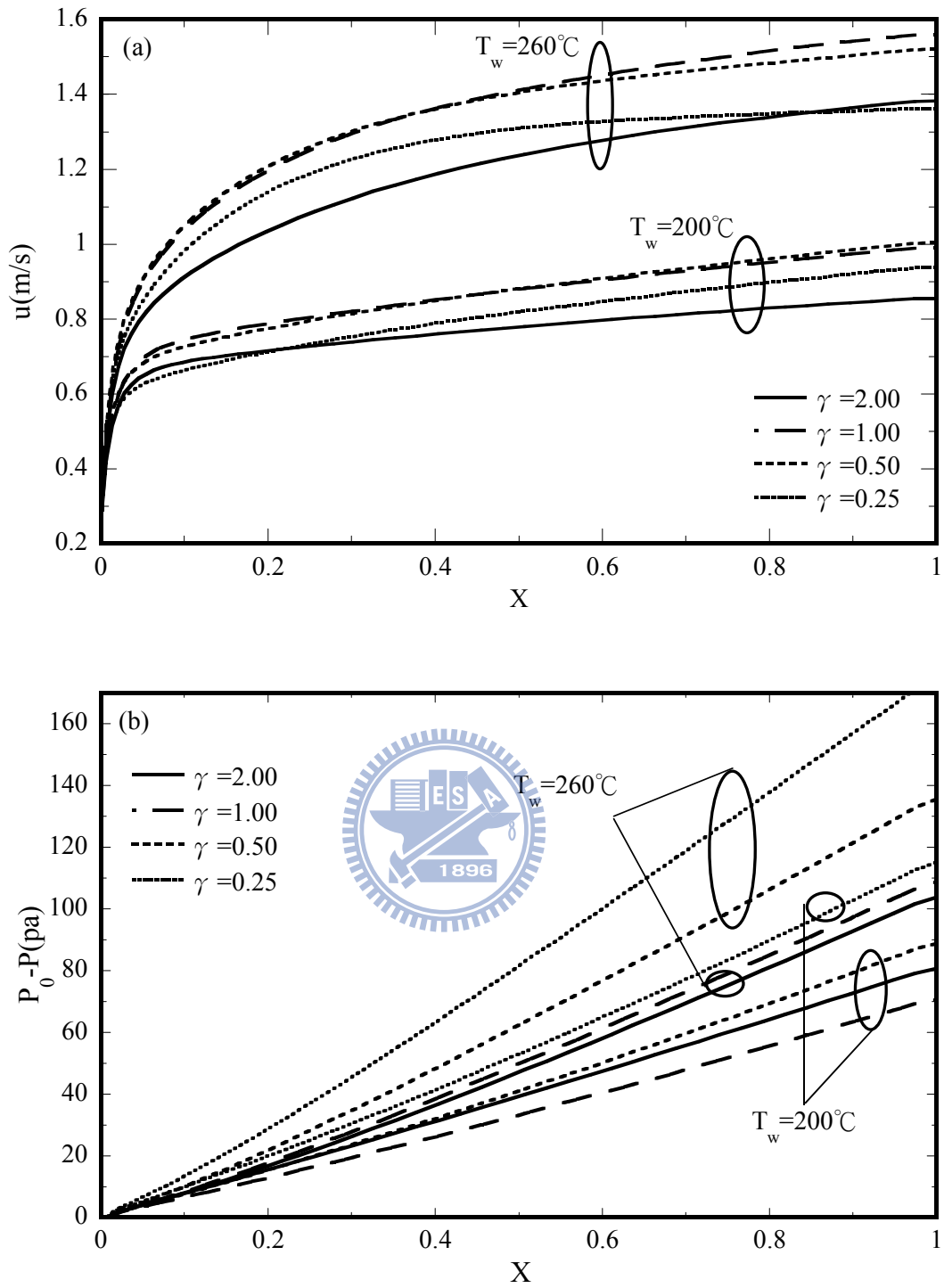


Fig. 4-20 Effects of aspect ratios of channel at $T_w=200^\circ\text{C}$ and $T_w=260^\circ\text{C}$ on (a) local velocity and (b) local pressure along center line of channel

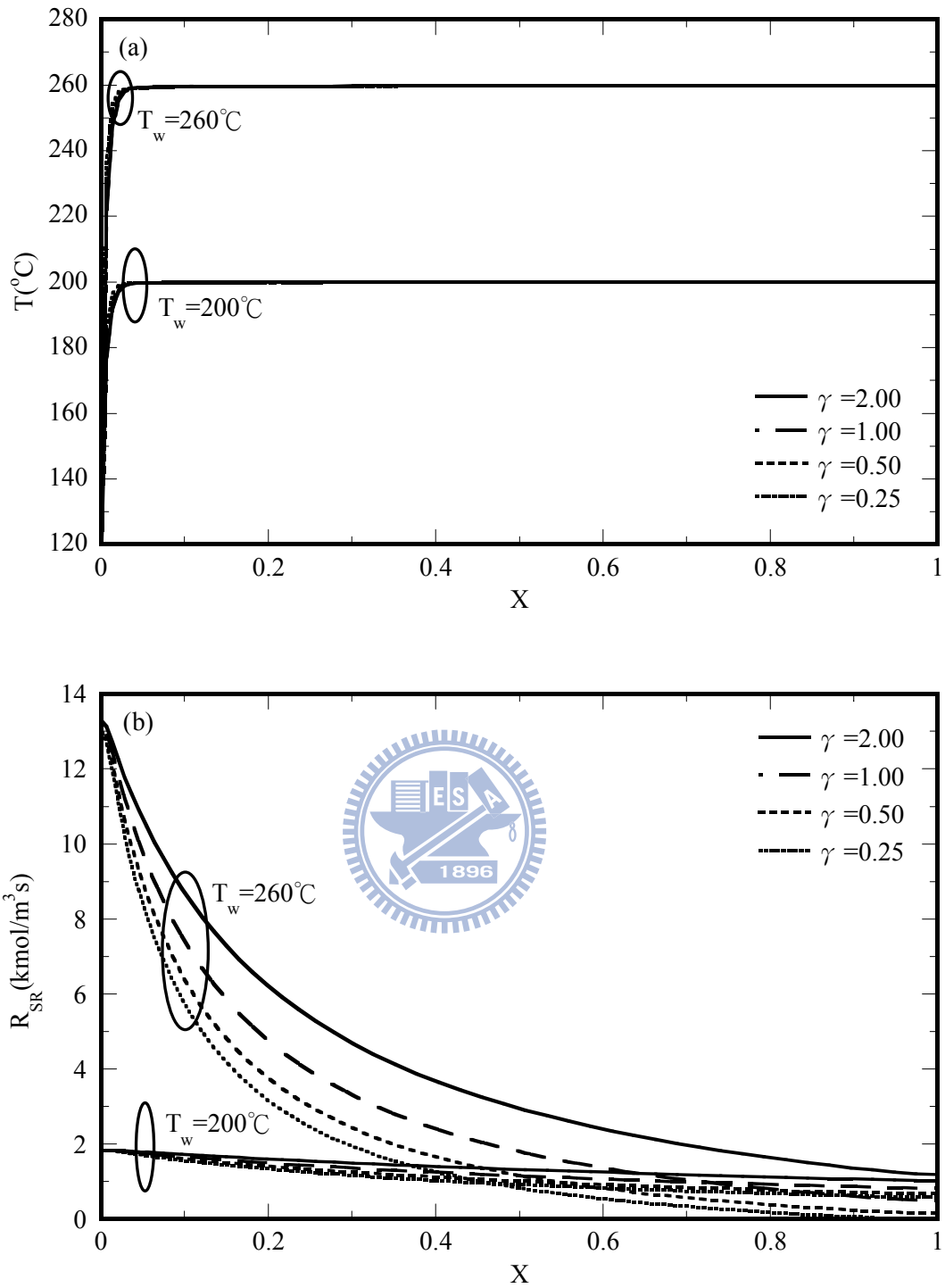


Fig. 4-21 Effects of aspect ratios of channel at $T_w=200^\circ\text{C}$ and $T_w=260^\circ\text{C}$ on (a) local temperature along center line of channel and (b) local reaction rates of methanol steam reforming along interface between flow channel and catalyst layer

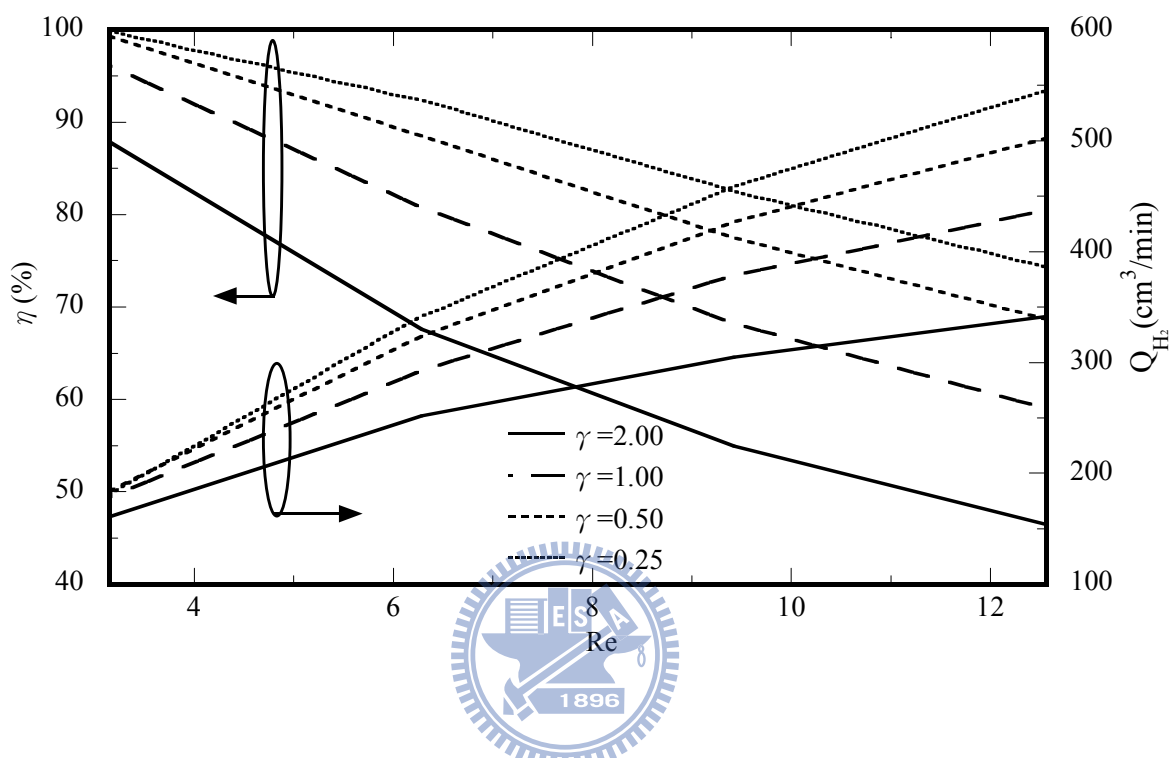


Fig. 4-22 Effects of aspect ratios of channel and Reynolds number on methanol conversion and H_2 production rate at $T_w=260\text{ }^\circ\text{C}$

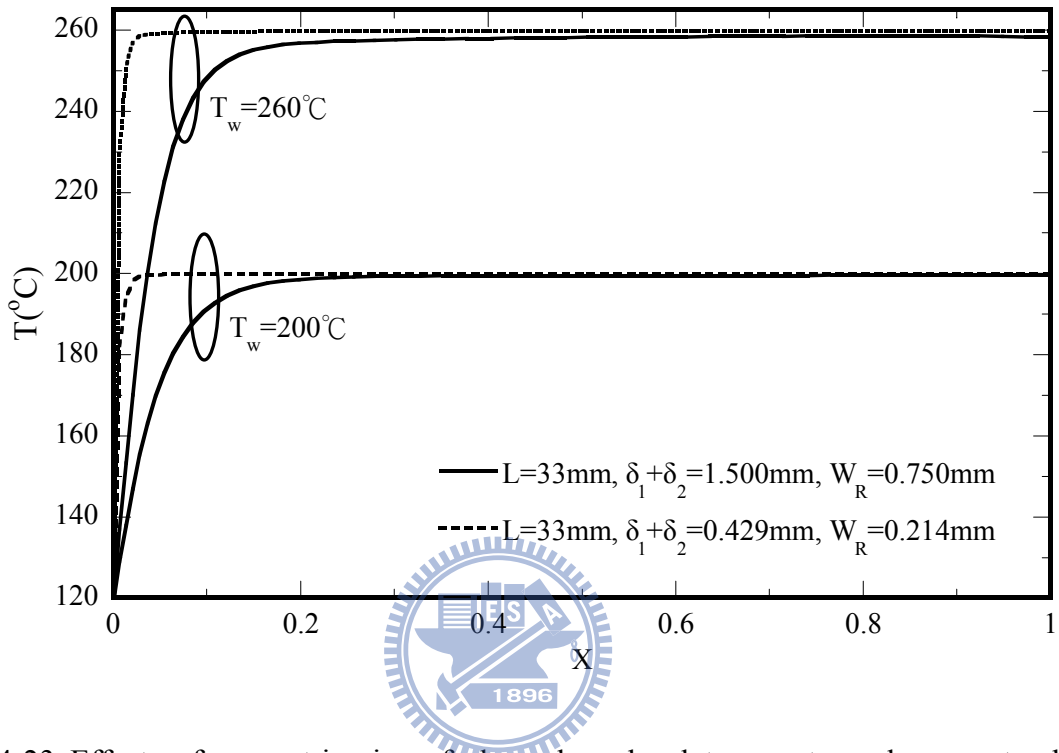


Fig. 4-23 Effects of geometric size of channel on local temperature along center line of channel at $T_w=200^{\circ}\text{C}$ and $T_w=260^{\circ}\text{C}$

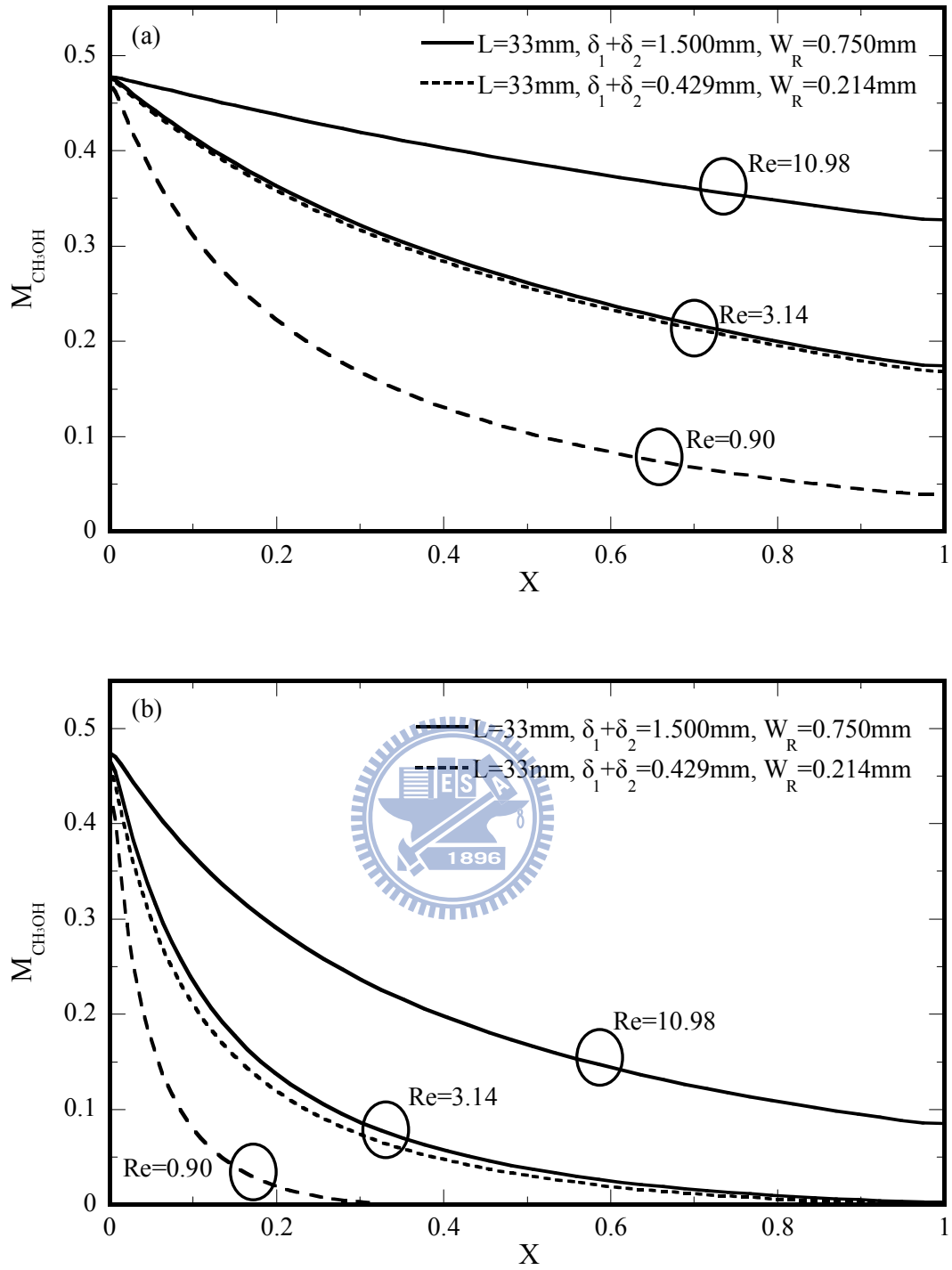


Fig. 4-24 Effects of geometric size of channel and Reynolds number on local CH_3OH mole fraction along center line of channel at (a) $T_w=200\text{ }^\circ\text{C}$ and (b) $T_w=260\text{ }^\circ\text{C}$.

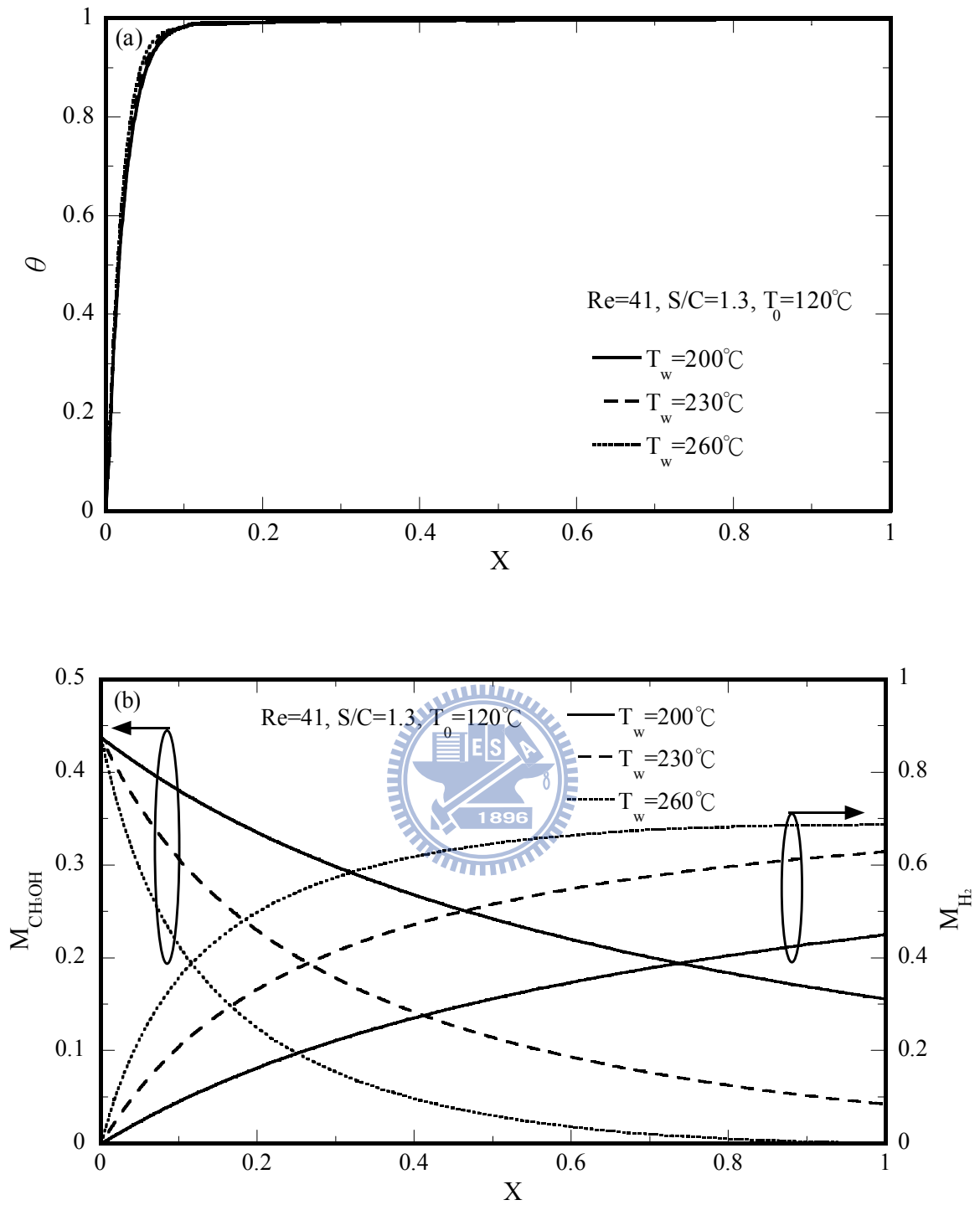


Fig. 4-25 Effects of various wall temperatures on (a) the temperature distributions and (b) the CH₃OH mole fraction and H₂ mole fraction distributions along the centerline of the serpentine flow field (Y=0.5).

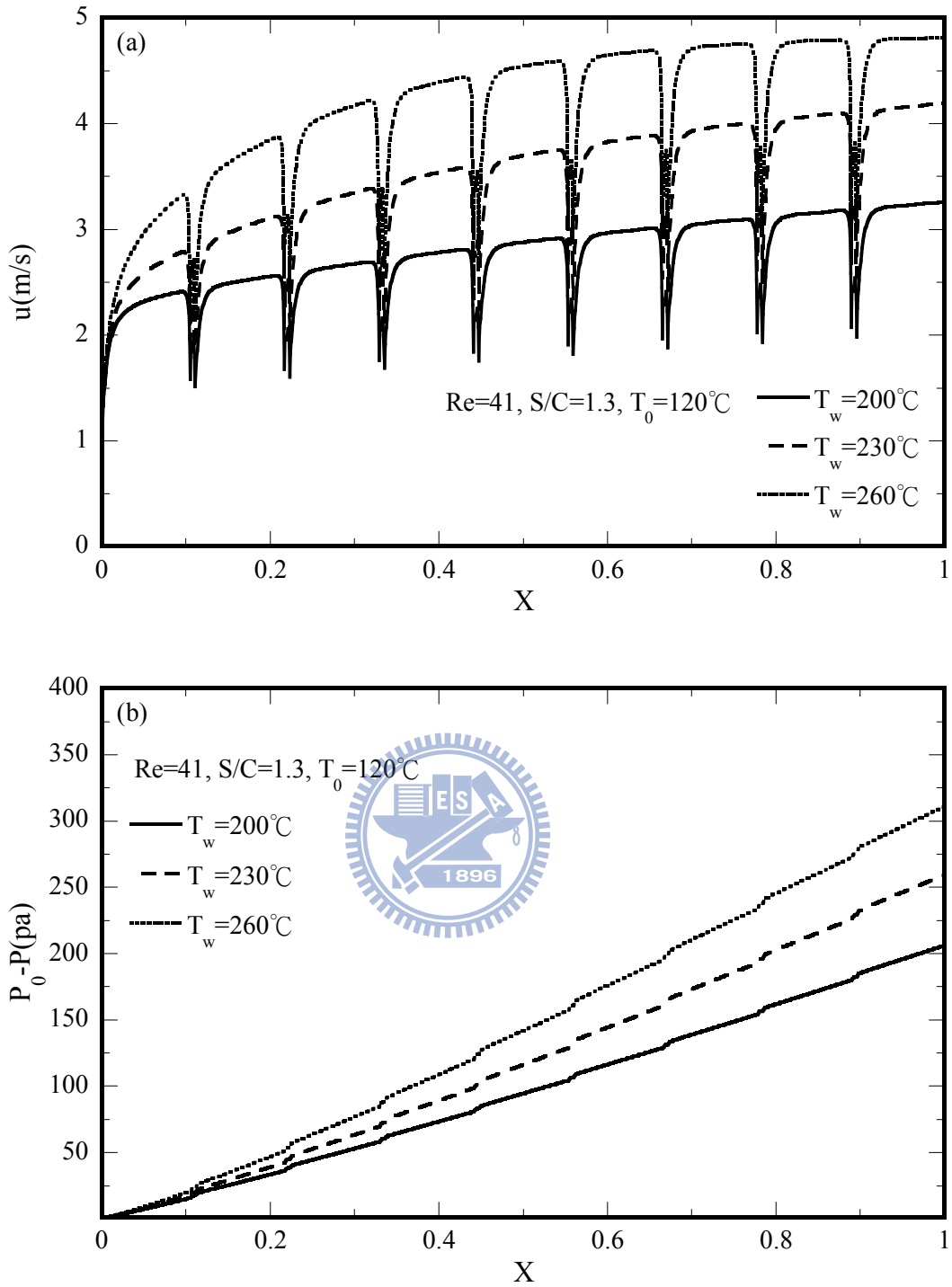


Fig. 4-26 Effects of various wall temperatures on (a) the local velocity and (b) the local pressure along the centerline of the serpentine flow field ($Y=0.5$).

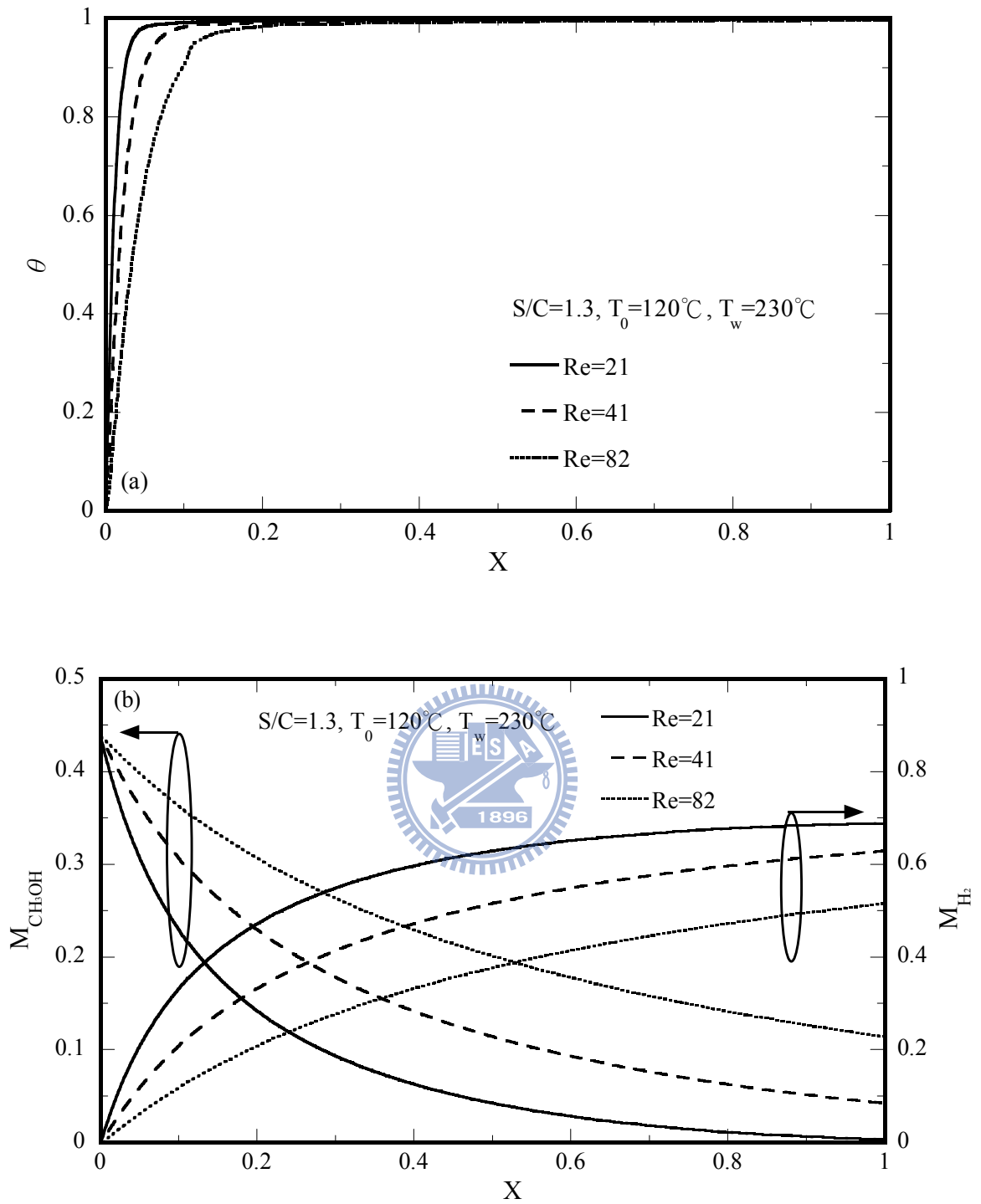


Fig. 4-27 Effects of Reynolds numbers at $T_w=230^\circ\text{C}$ on (a) the temperature distributions and (b) the CH_3OH mole fraction and H_2 mole fraction distributions along the center line of the serpentine flow field ($Y=0.5$)

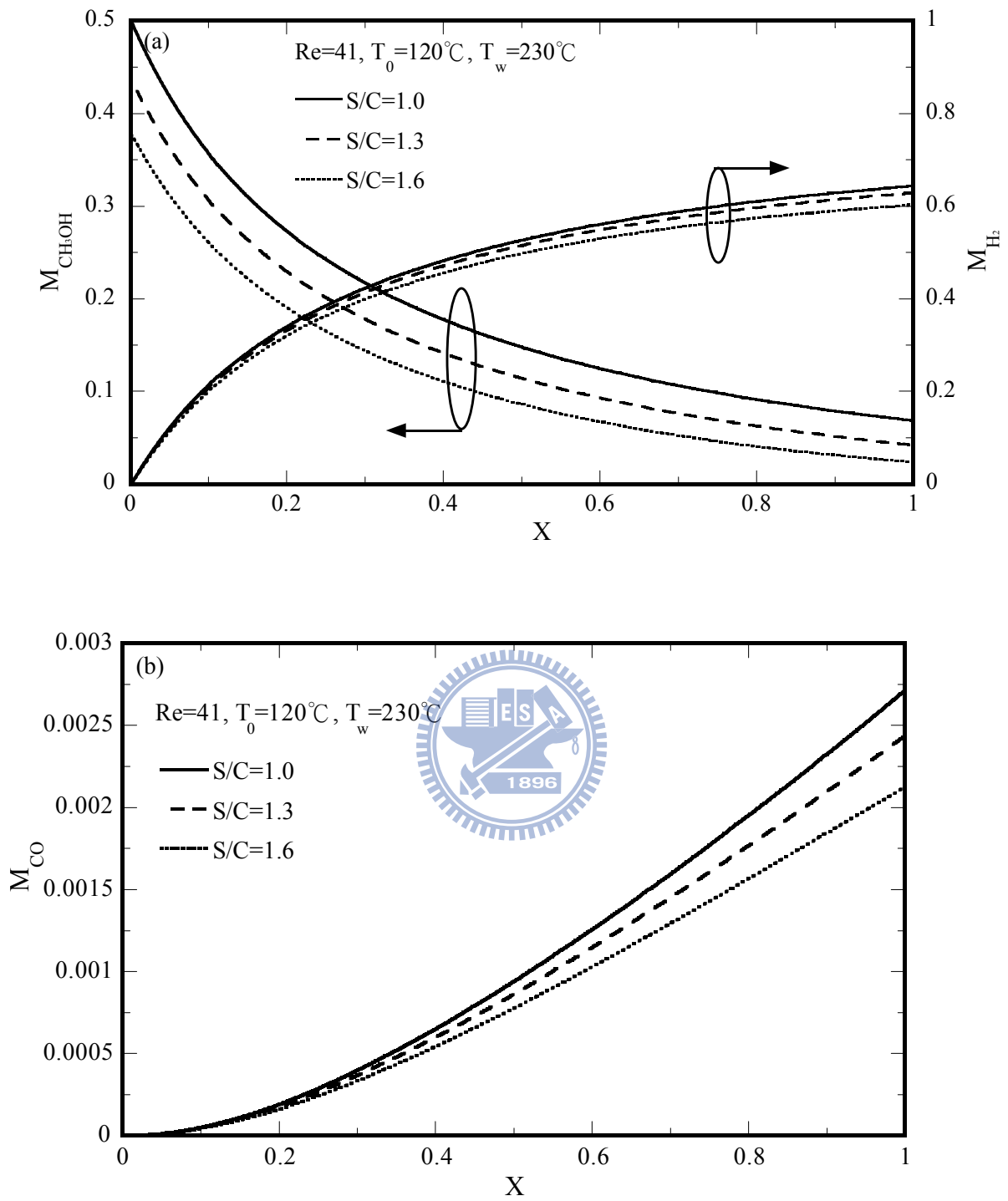


Fig. 4-28 Effects of H₂O/CH₃OH molar ratio (S/C) at T_w=230°C on (a) the temperature distributions and (b) the CH₃OH mole fraction and CO mole fraction distributions along the center line of the serpentine flow field (Y=0.5)

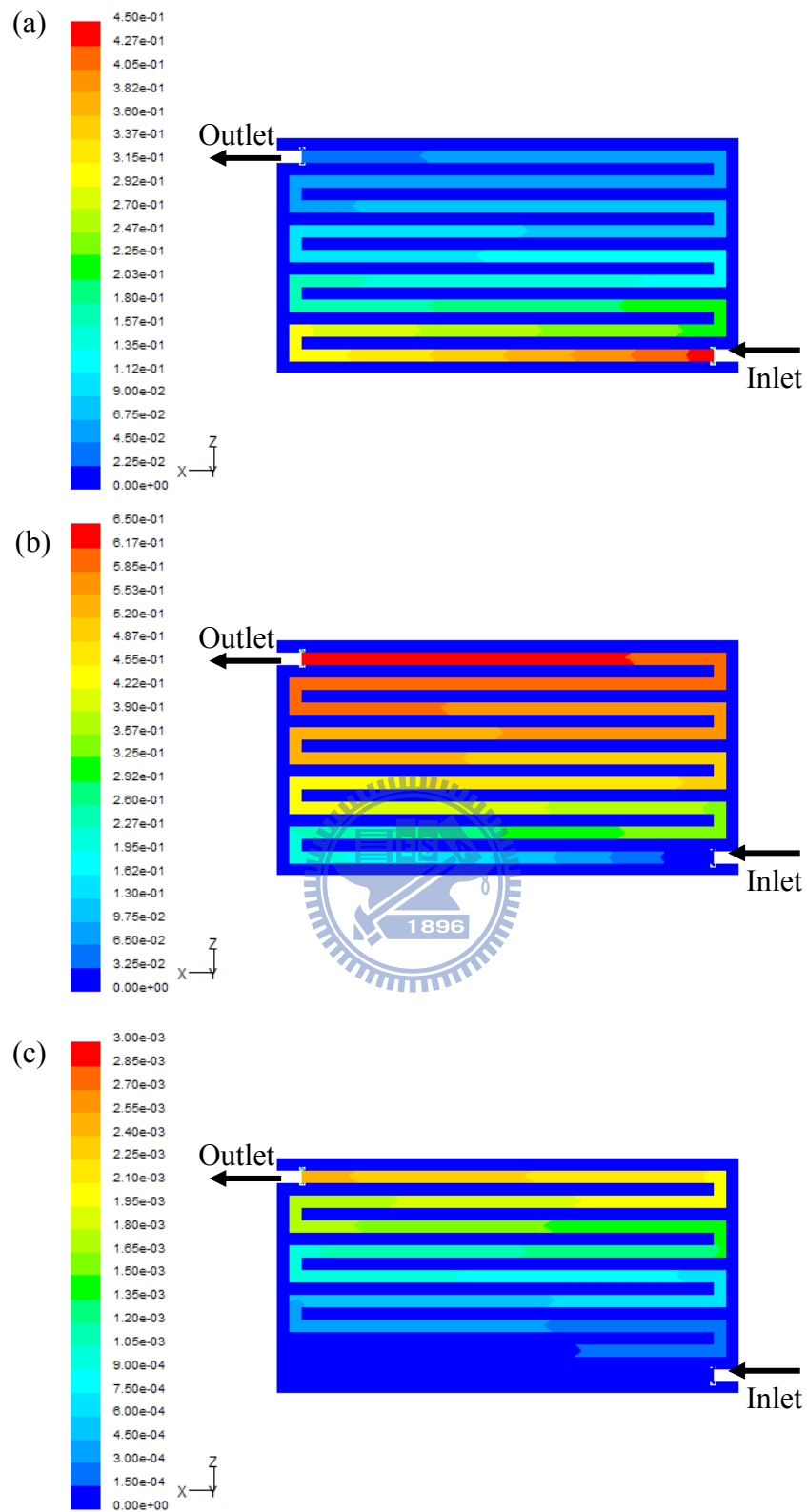


Fig. 4-29 Local distributions of (a) CH_3OH mole fraction, (b) H_2 mole fraction and (c) CO mole fraction along the cross-section of $Y=0.5$ at $T_w=230^\circ\text{C}$

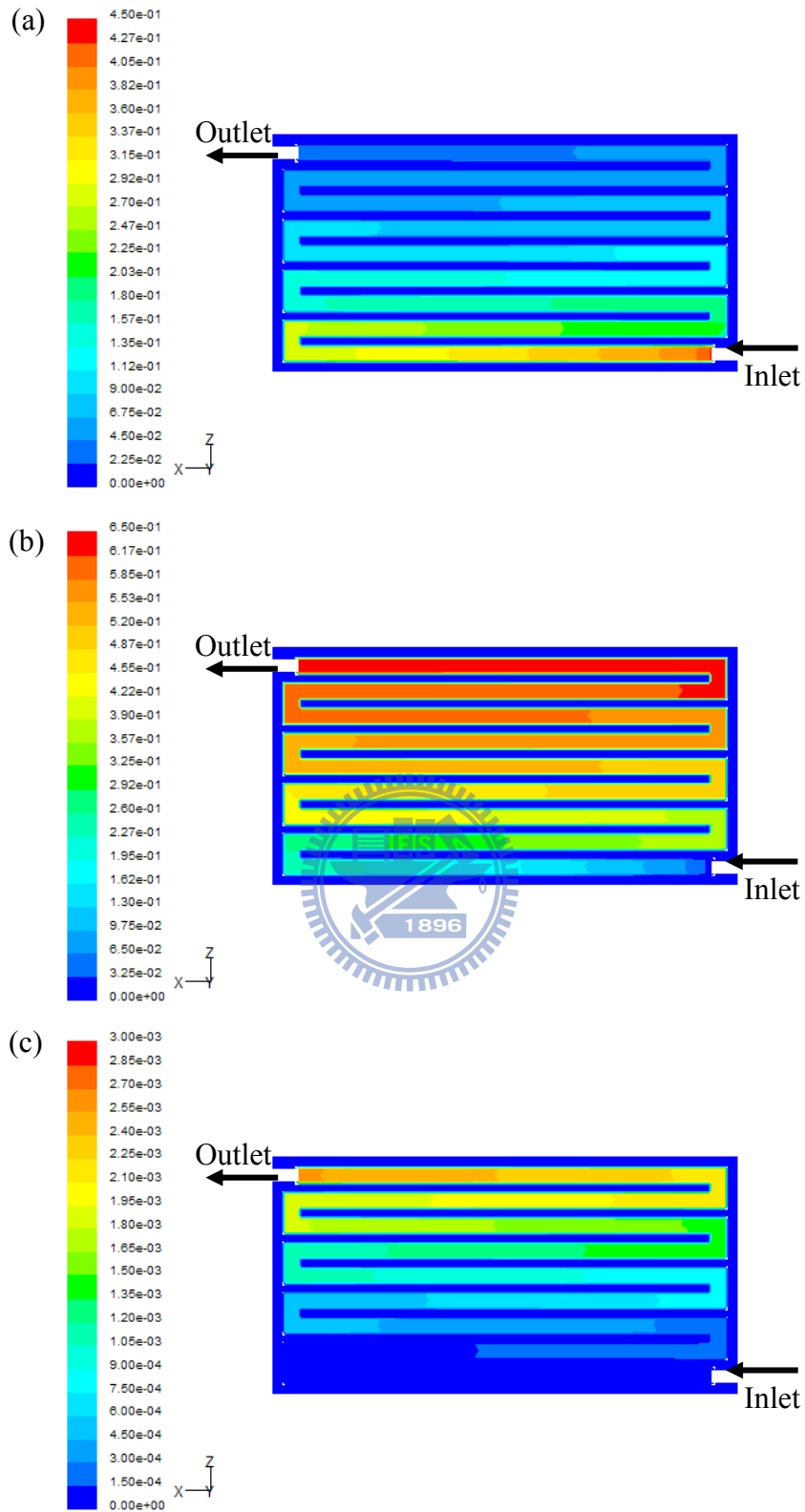


Fig. 4-30 Local distributions of (a) CH₃OH mole fraction, (b) H₂ mole fraction and (c) CO mole fraction along the interface between the flow channel and catalyst layer (Y=0.95) at T_w=230°

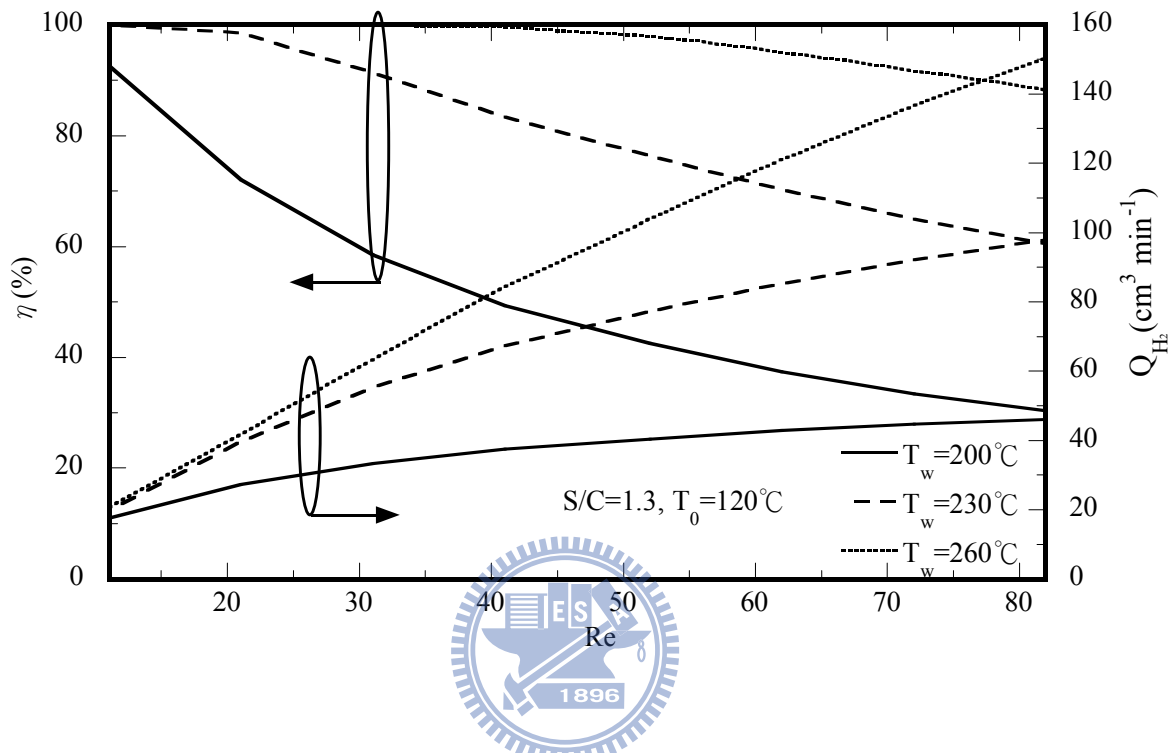


Fig. 4-31 Effects of wall temperature and inlet fuel Reynolds number on the methanol conversion and H_2 production rate

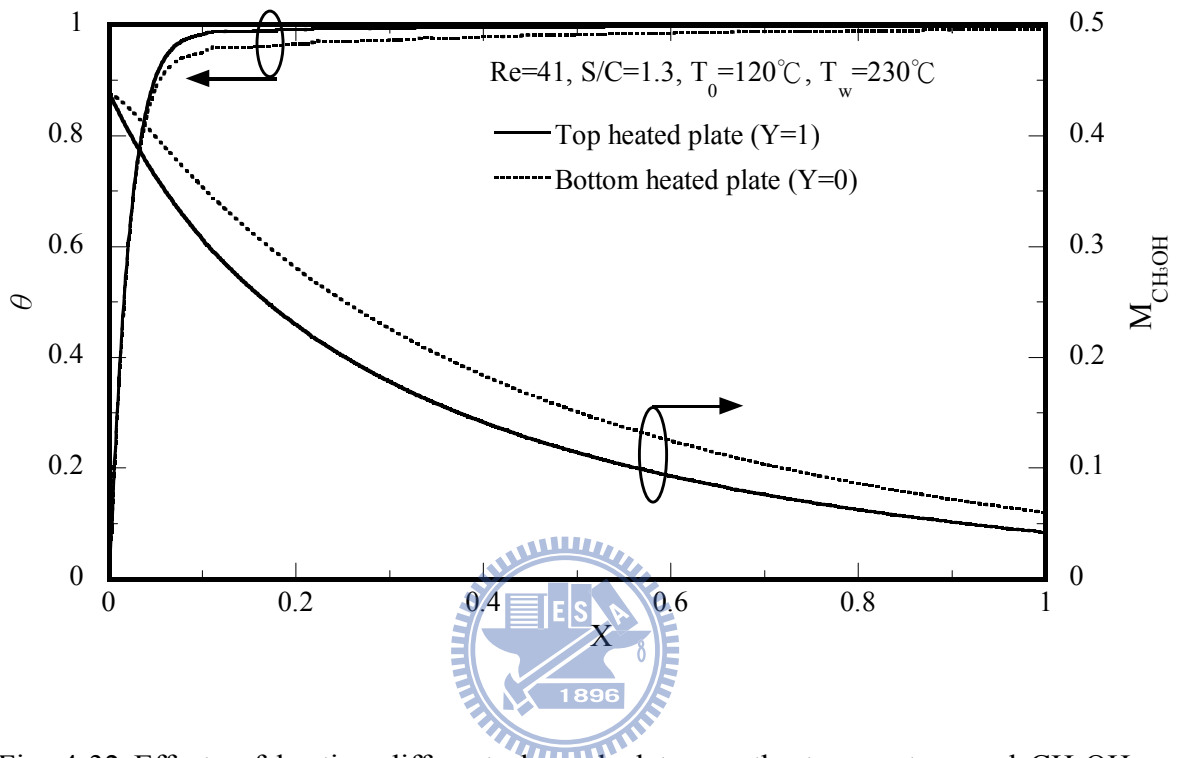


Fig. 4-32 Effects of heating different channel plates on the temperature and CH_3OH mole fraction distributions along the center line of the serpentine flow field ($Y=0.5$)

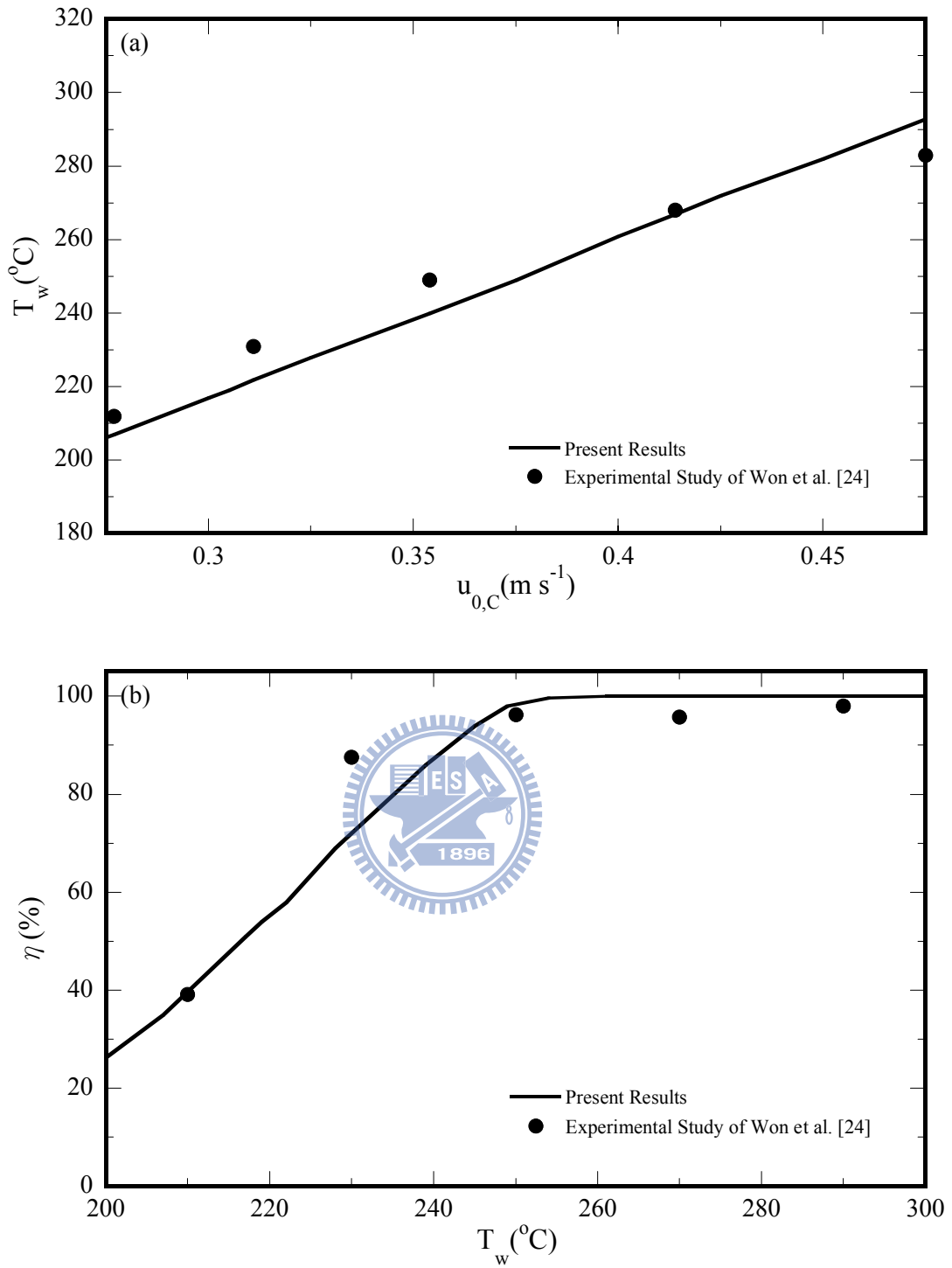


Fig. 4-33 Comparison of theoretical simulation of present results with previous experimental data by Won et al. [24]

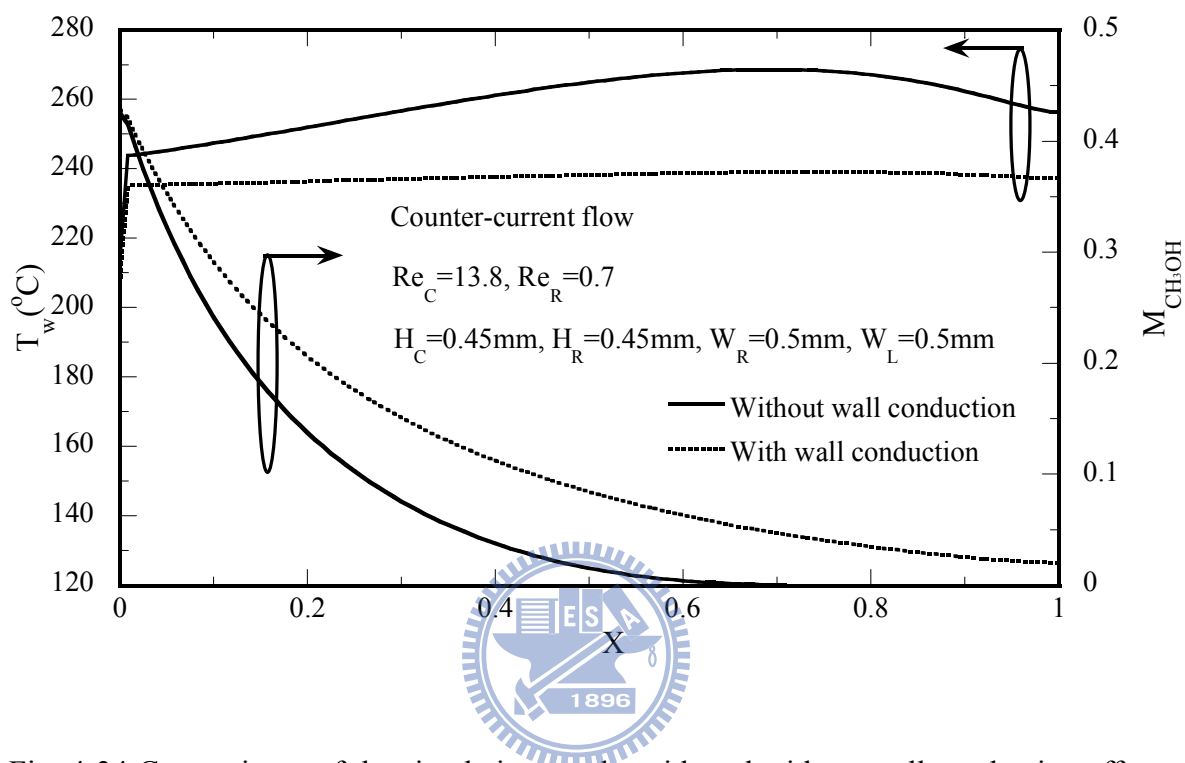


Fig. 4-34 Comparisons of the simulation results with and without wall conduction effects for the temperature distributions and CH_3OH mole fraction distributions along the centerline of the channel

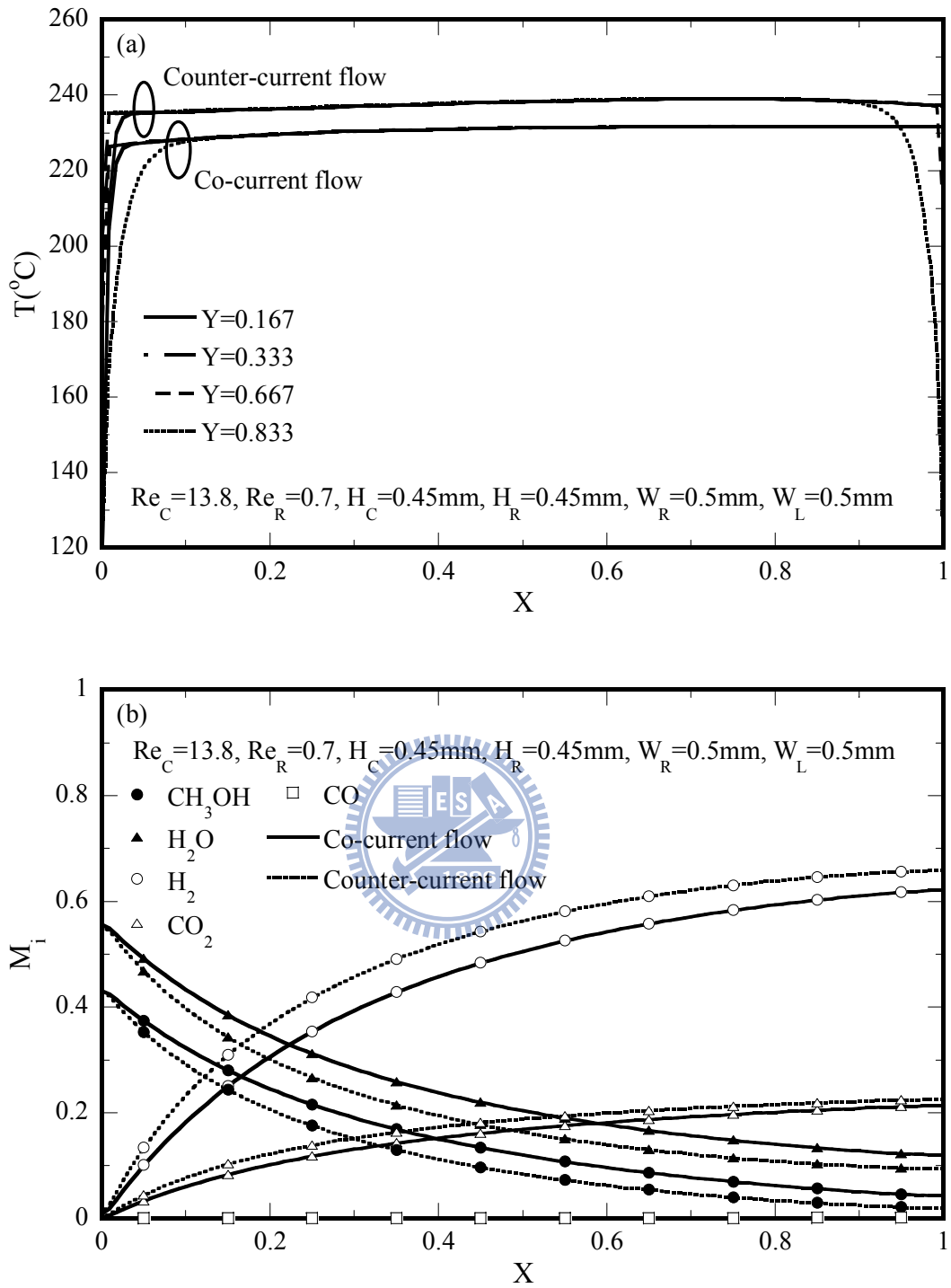


Fig. 4-35 Effects of co- and counter-current flow configurations on (a) the temperature distributions along different axial location lines and (b) the local distributions of the mole fractions of the various species along the center line of the reforming channel ($Y=0.167$)

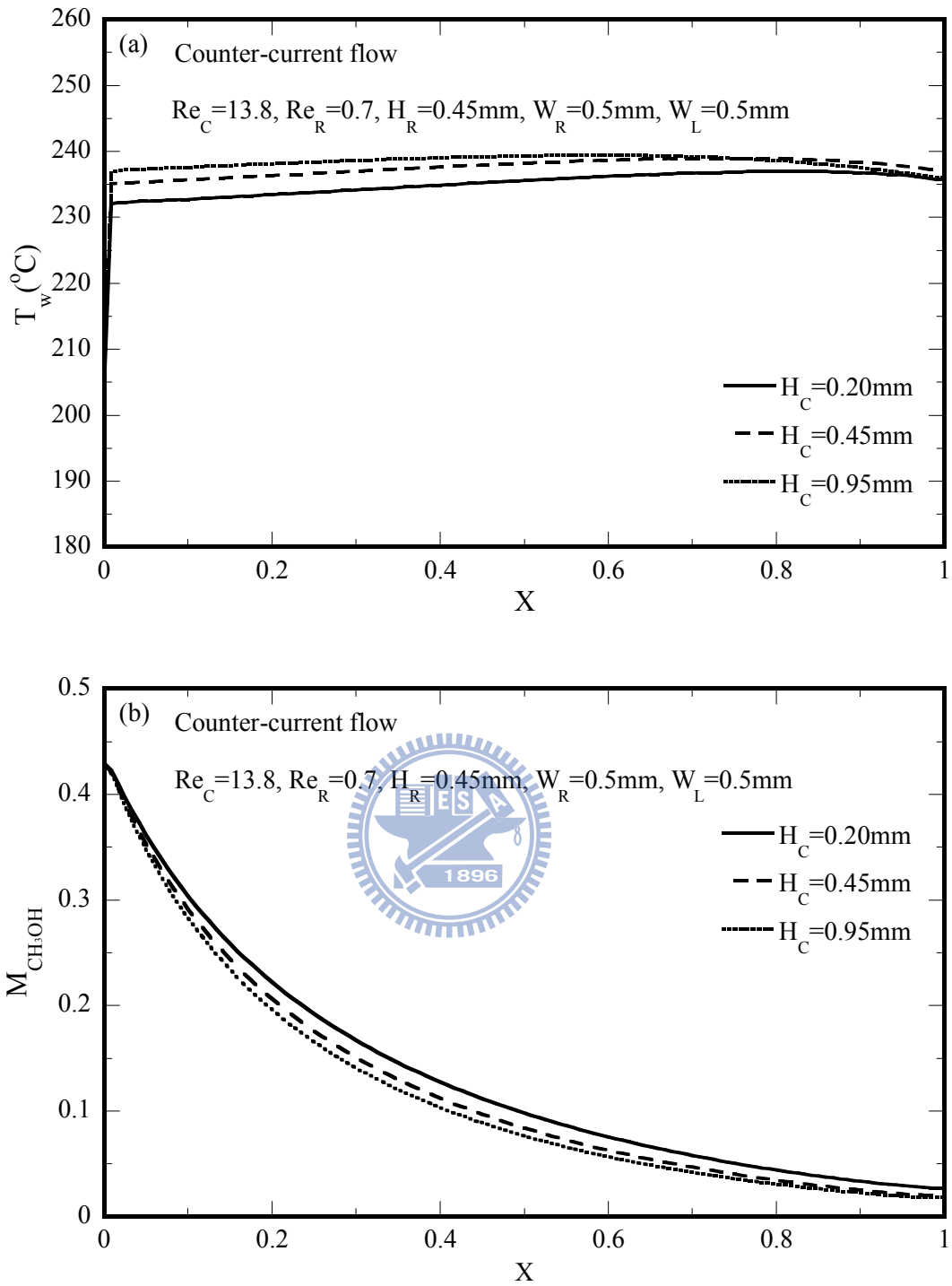


Fig. 4-36 Effects of the channel height of the combustor on (a) the temperature distributions along the top centerline of the reforming channel and (b) the CH_3OH mole fraction distributions along the center line of the reforming channel

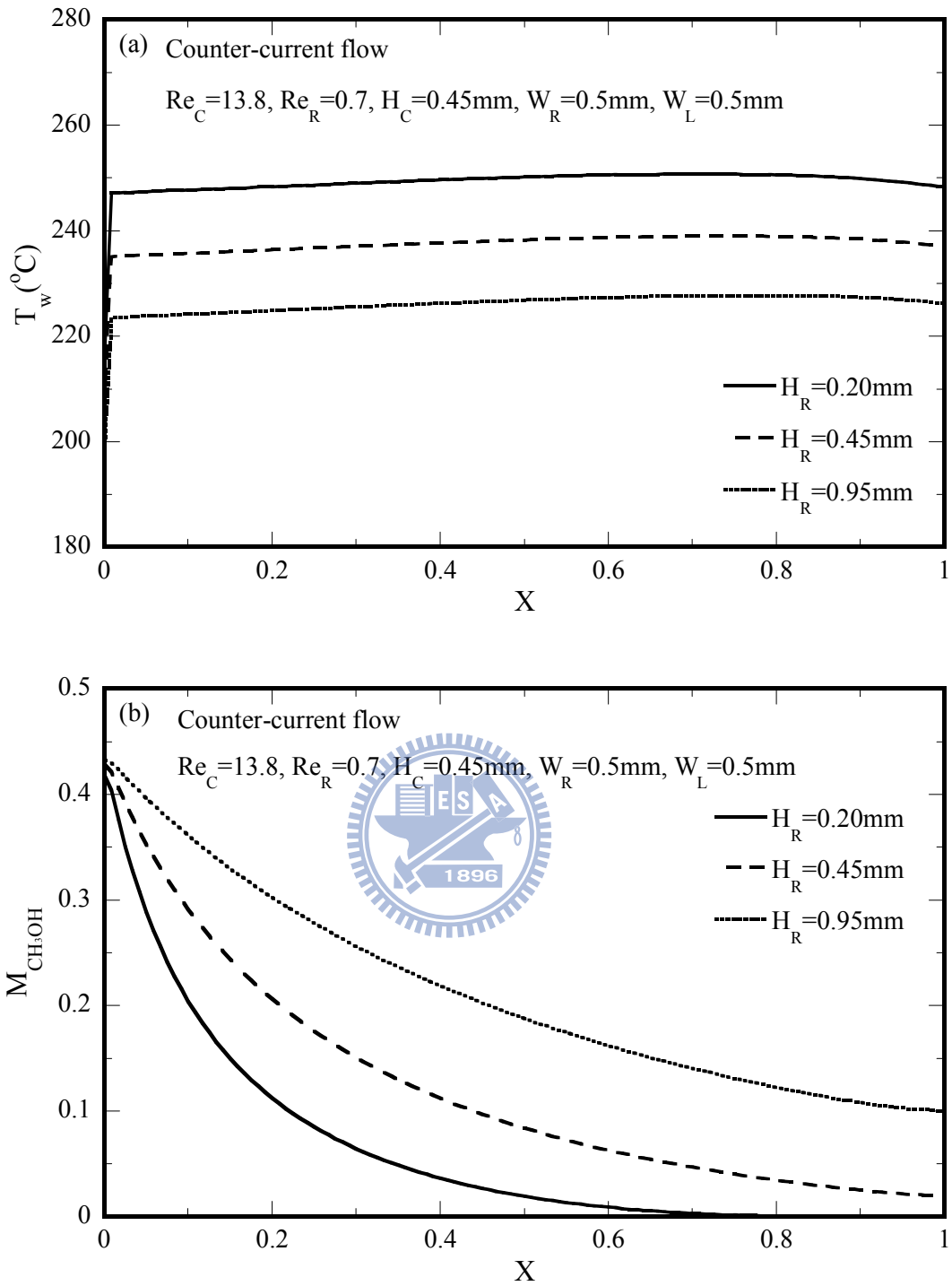


Fig. 4-37 Effects of the channel height of the reformer on (a) the temperature distributions along the top centerline of the reforming channel and (b) the CH_3OH mole fraction distributions along the center line of the reforming channel

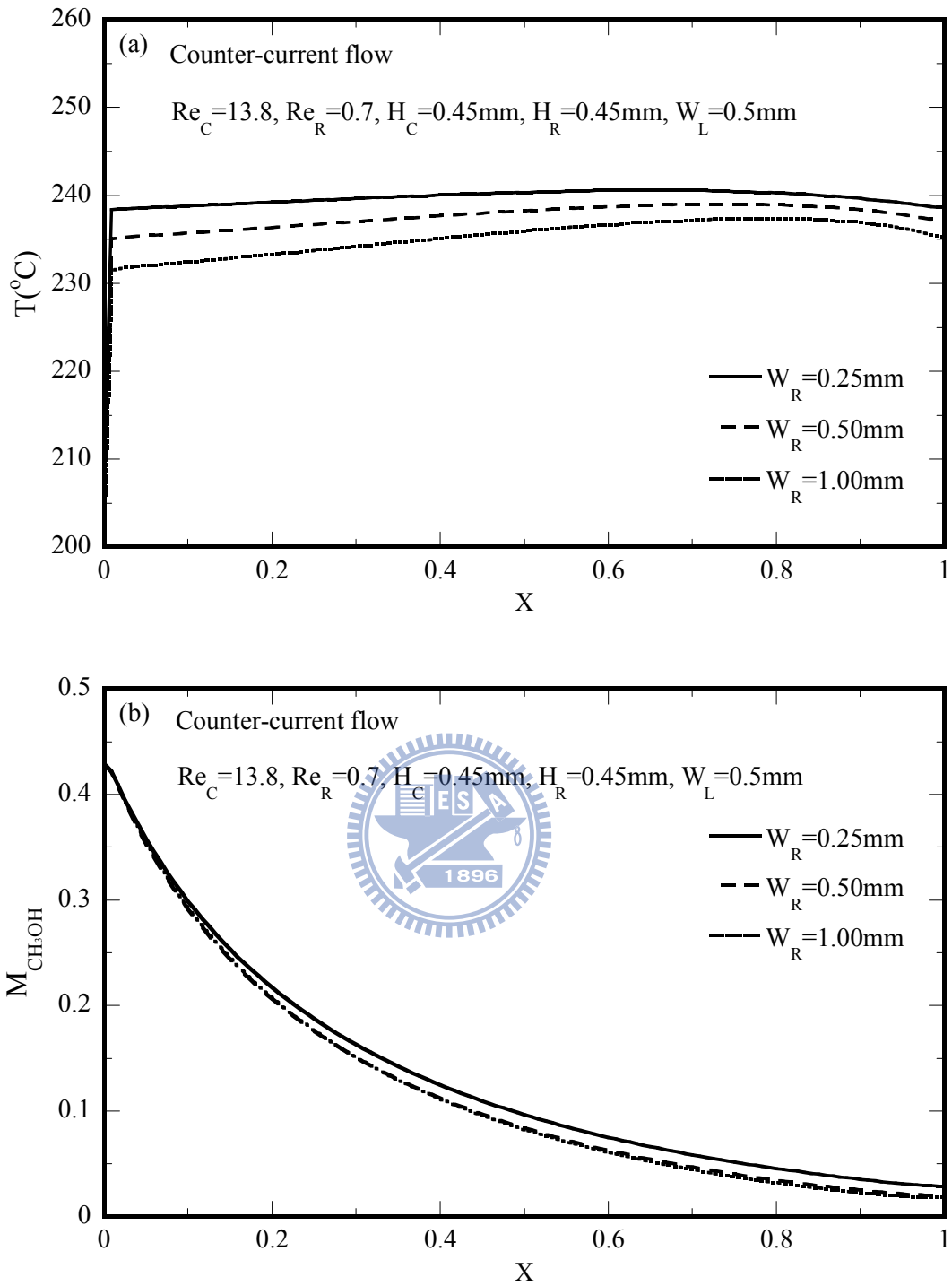


Fig. 4-38 Effects of the channel width on (a) the temperature distributions along the top centerline of the reforming channel ($Y=0.333$) and (b) the CH_3OH mole fraction distributions along the center line of the reforming channel ($Y=0.167$)

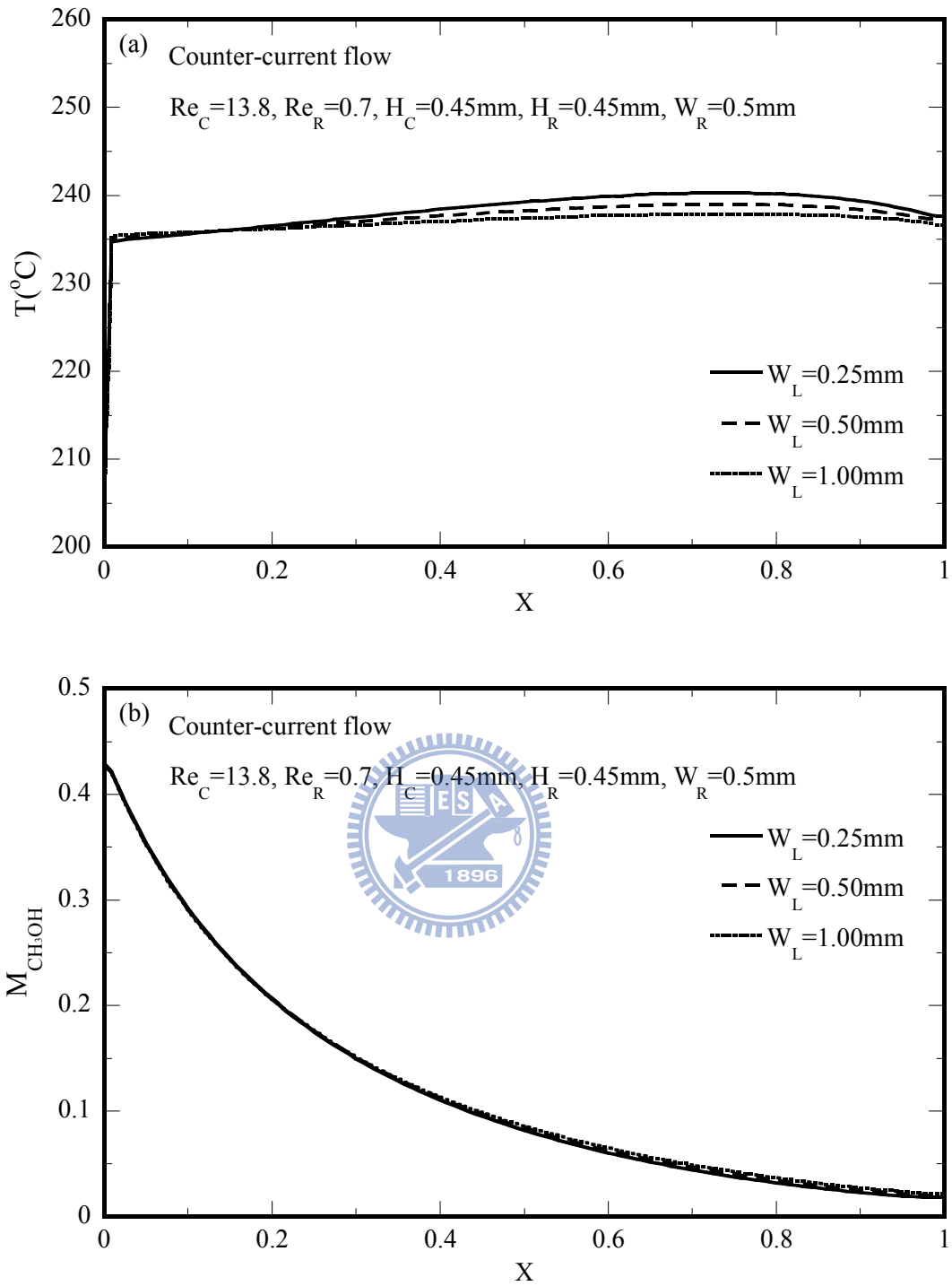


Fig. 4-39 Effects of the steel widths on (a) the temperature distributions along the top centerline of the reforming channel ($Y=0.333$) and (b) the CH_3OH mole fraction distributions along the center line of the reforming channel ($Y=0.167$)

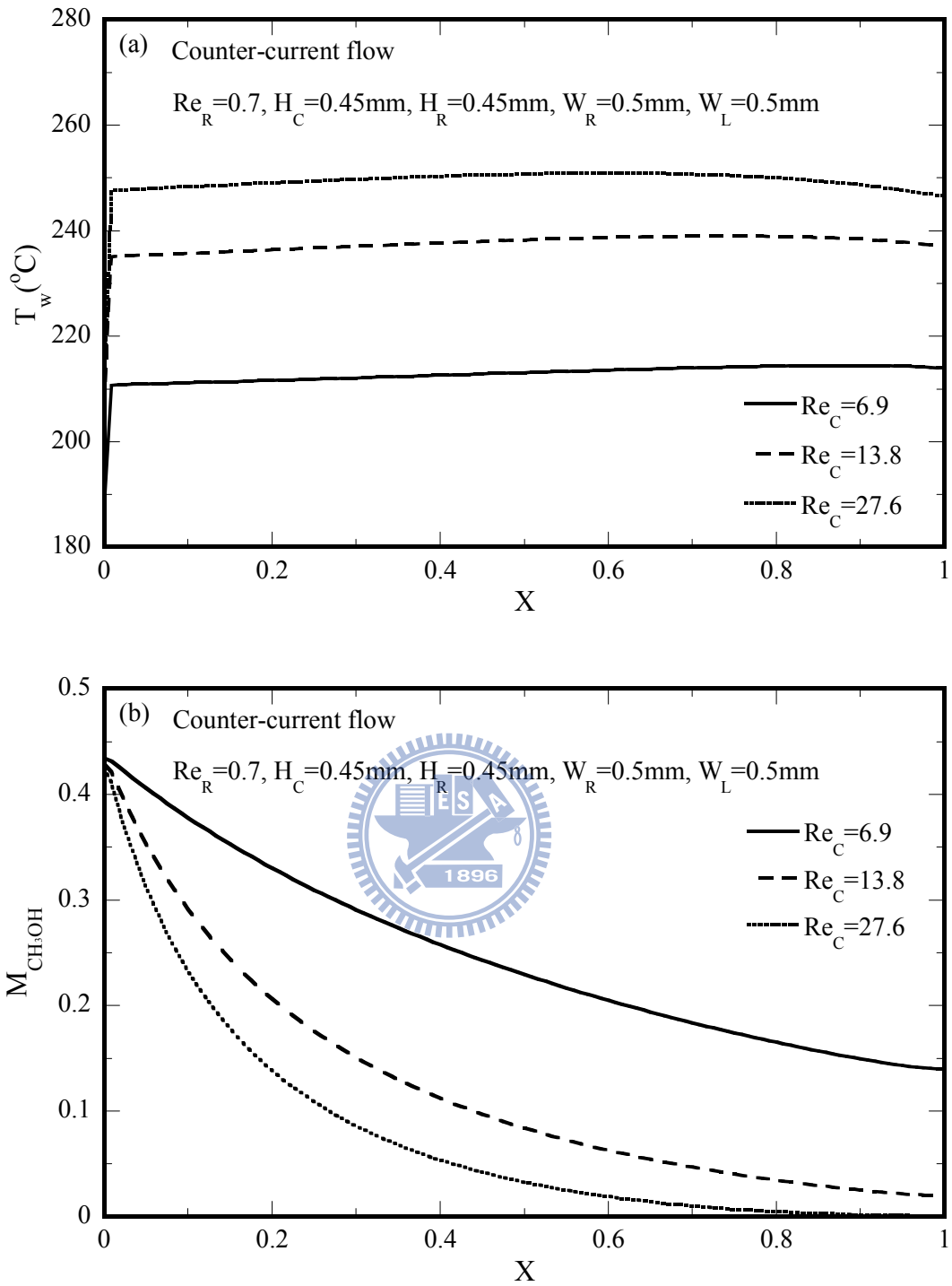


Fig. 4-40 Effects of the Reynolds number (Re) for the combustor on (a) the temperature distributions along the top centerline of the reforming channel ($Y=0.333$) and (b) the CH_3OH mole fraction distributions along the centerline of the reforming channel ($Y=0.167$)

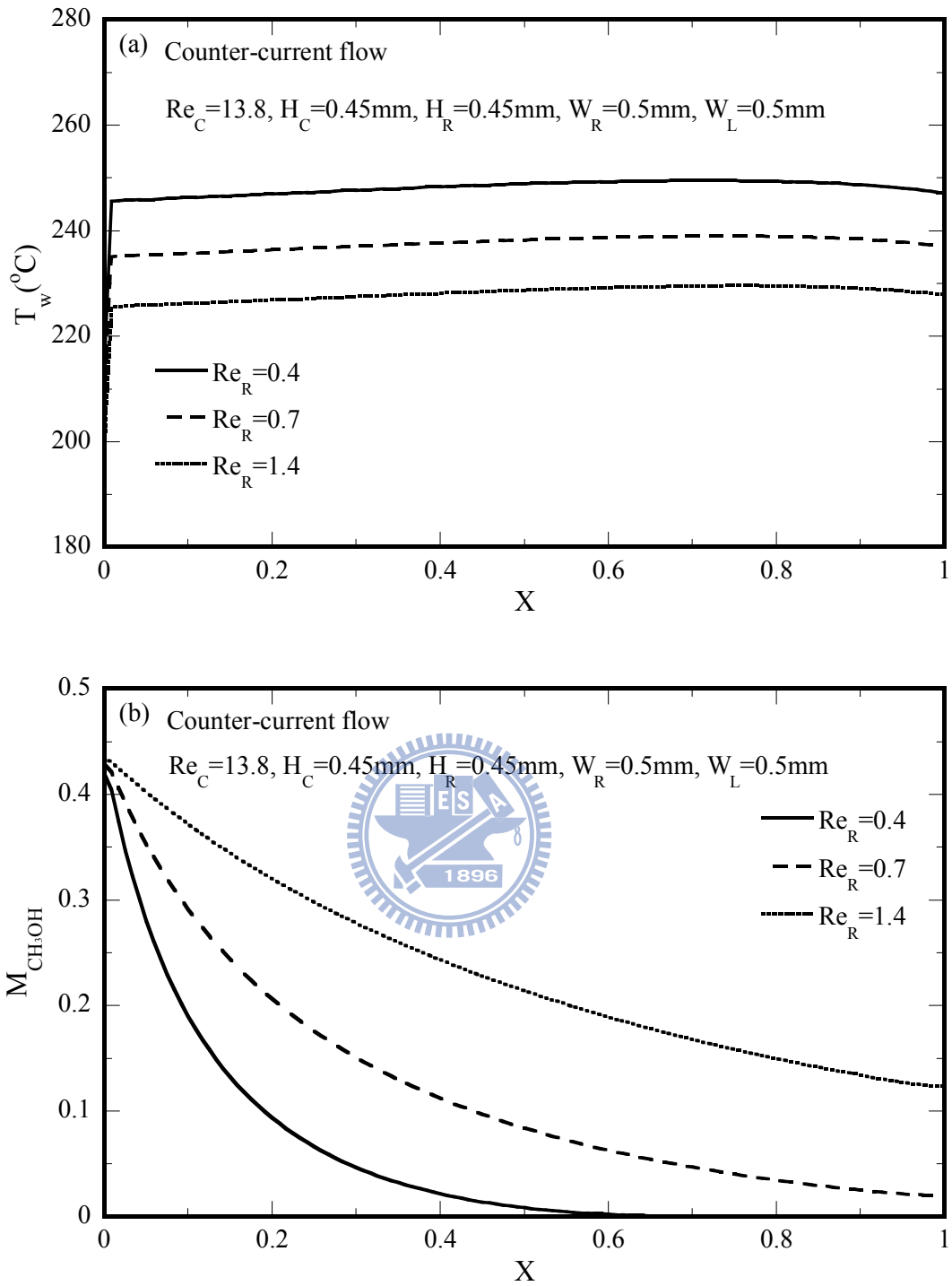


Fig. 4-41 Effects of the Reynolds number (Re) for the reformer on (a) the temperature distributions along the top centerline of the reforming channel ($Y=0.333$) and (b) the CH_3OH mole fraction distributions along the center line of the reforming channel ($Y=0.167$)

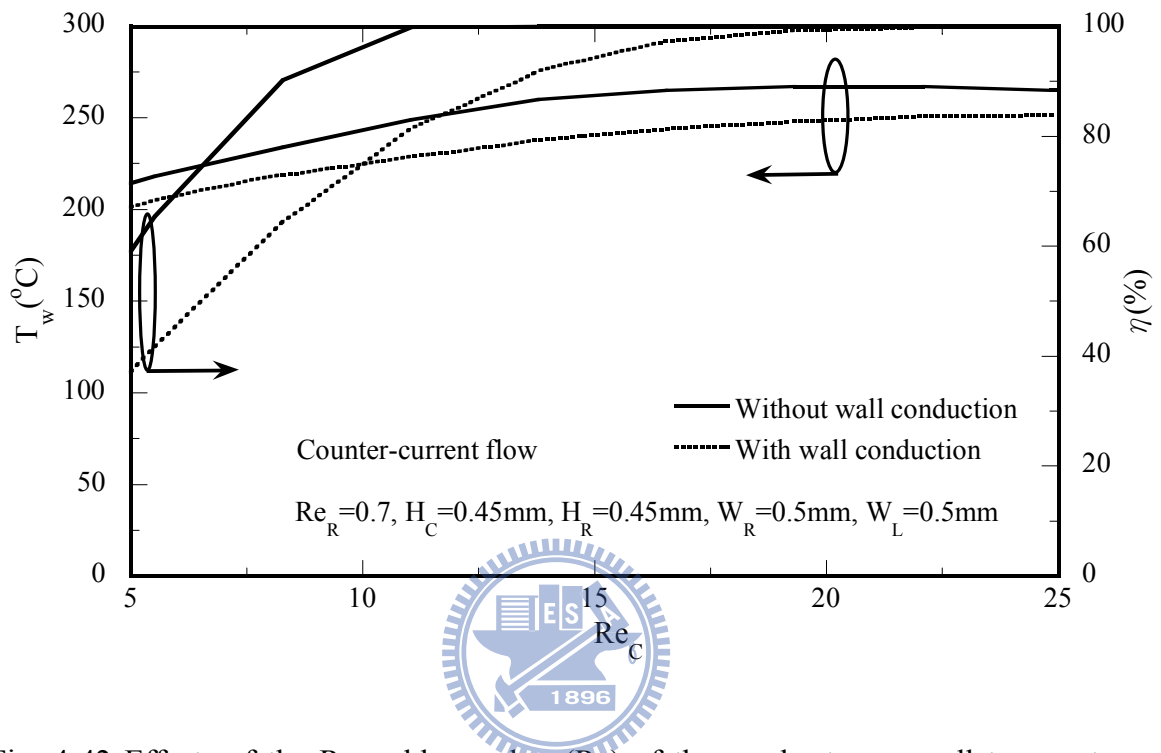


Fig. 4-42 Effects of the Reynolds number (Re) of the combustor on wall temperature and methanol conversion

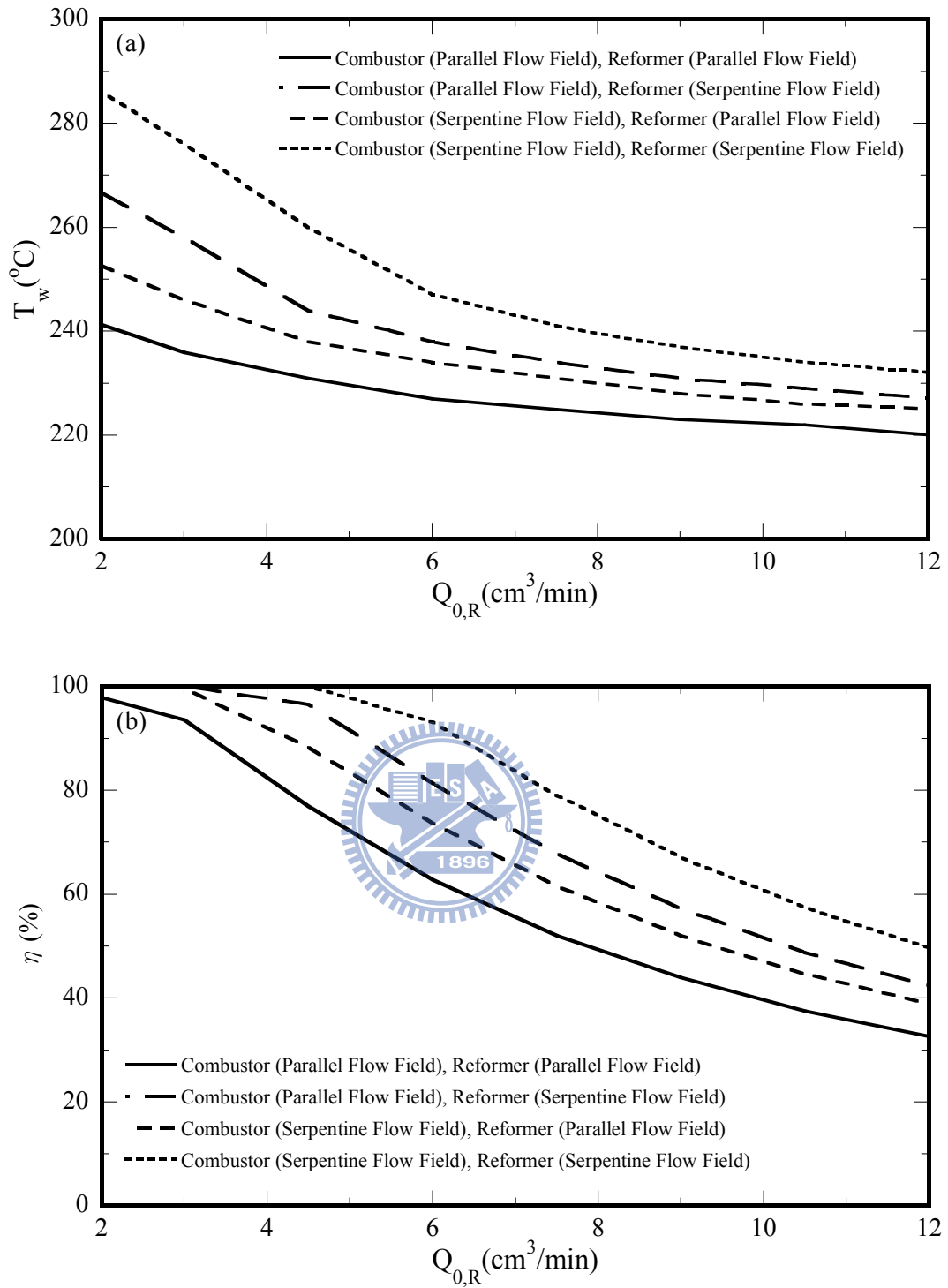


Fig. 4-43 Effects of the inlet flow rate ($Q_{0,R}$) of the reformer and various flow field designs on (a) wall temperature and (b) methanol conversion

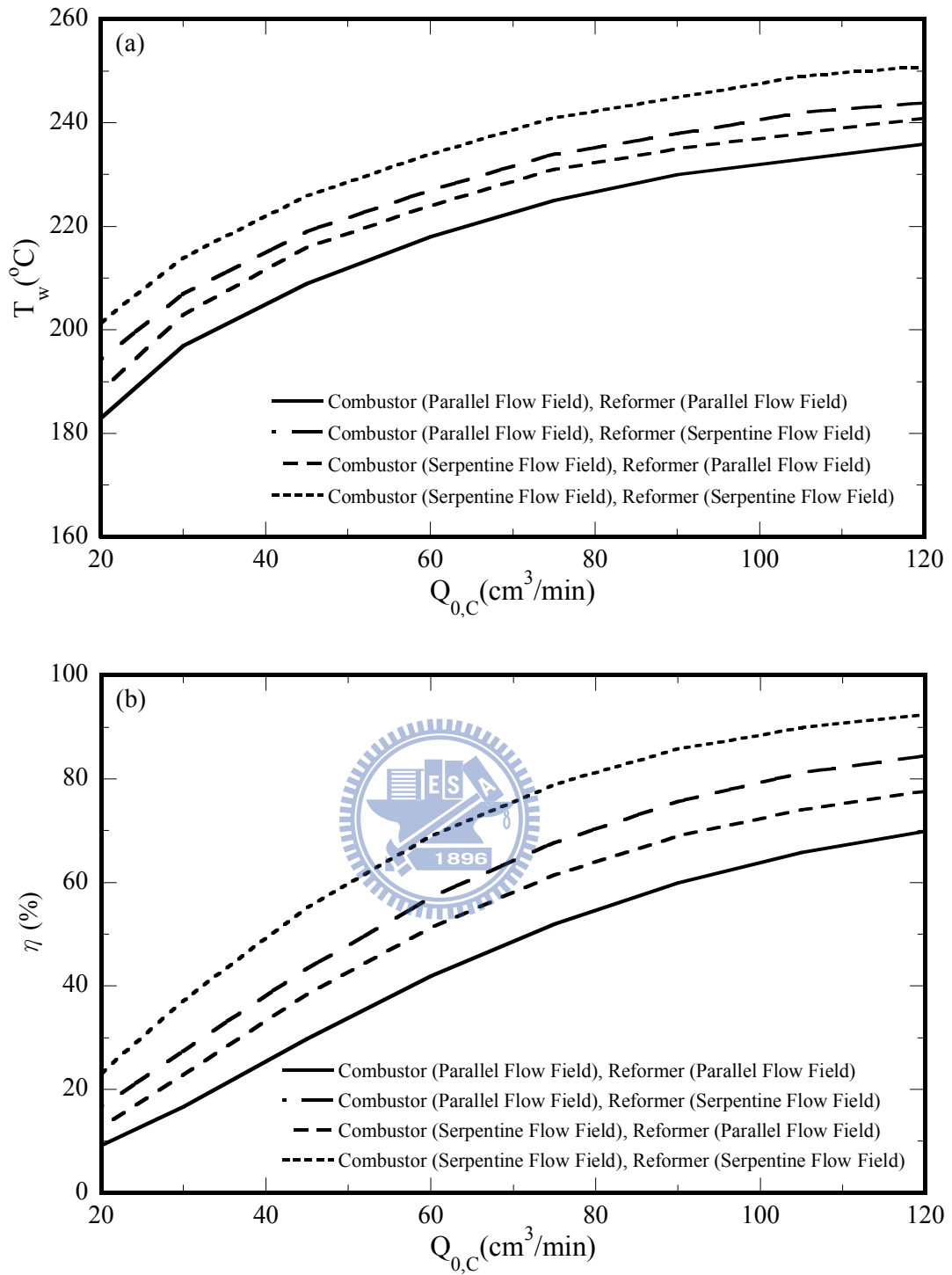


Fig. 4-44 Effects of inlet flow rate ($Q_{0,C}$) of the combustor and various flow field designs on

(a) wall temperature and (b) methanol conversion

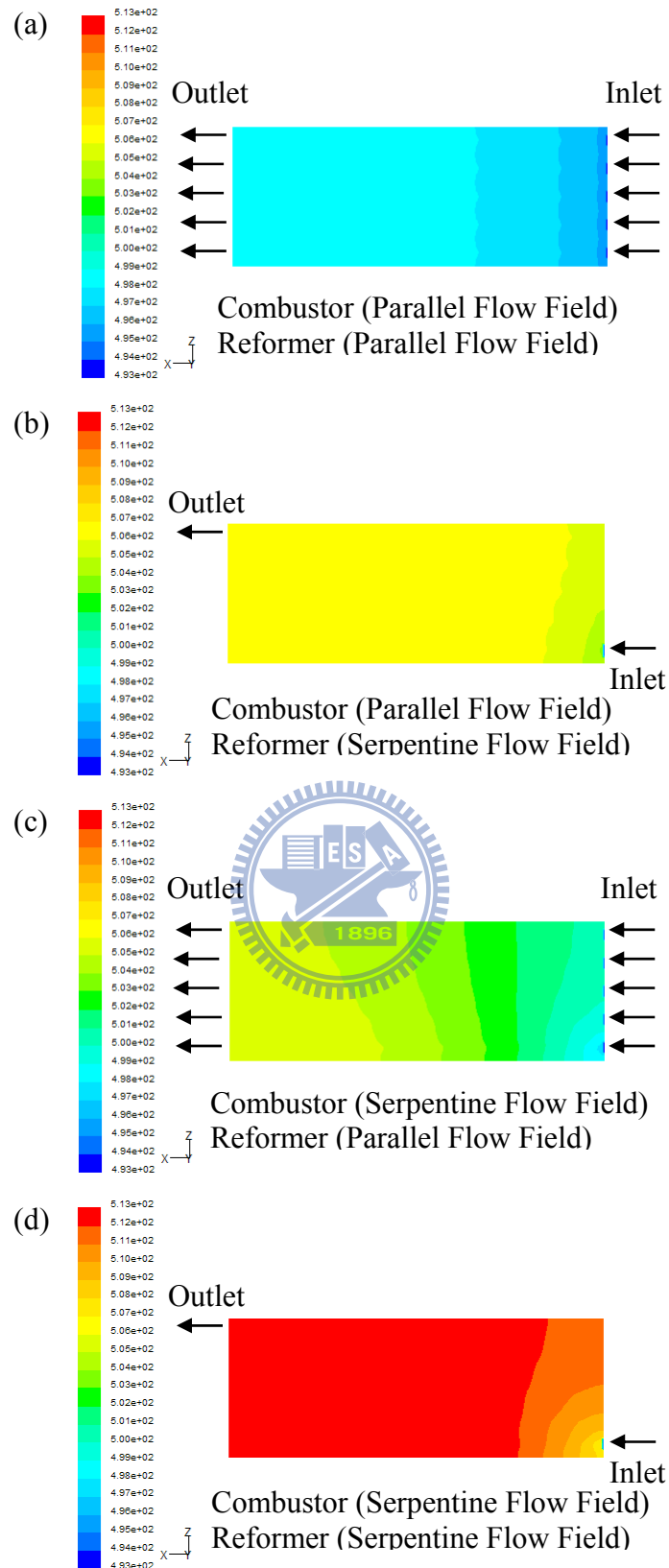


Fig. 4-45 The temperature distributions on the top cross-section of the reforming channel for reformer and combustor with various flow field designs

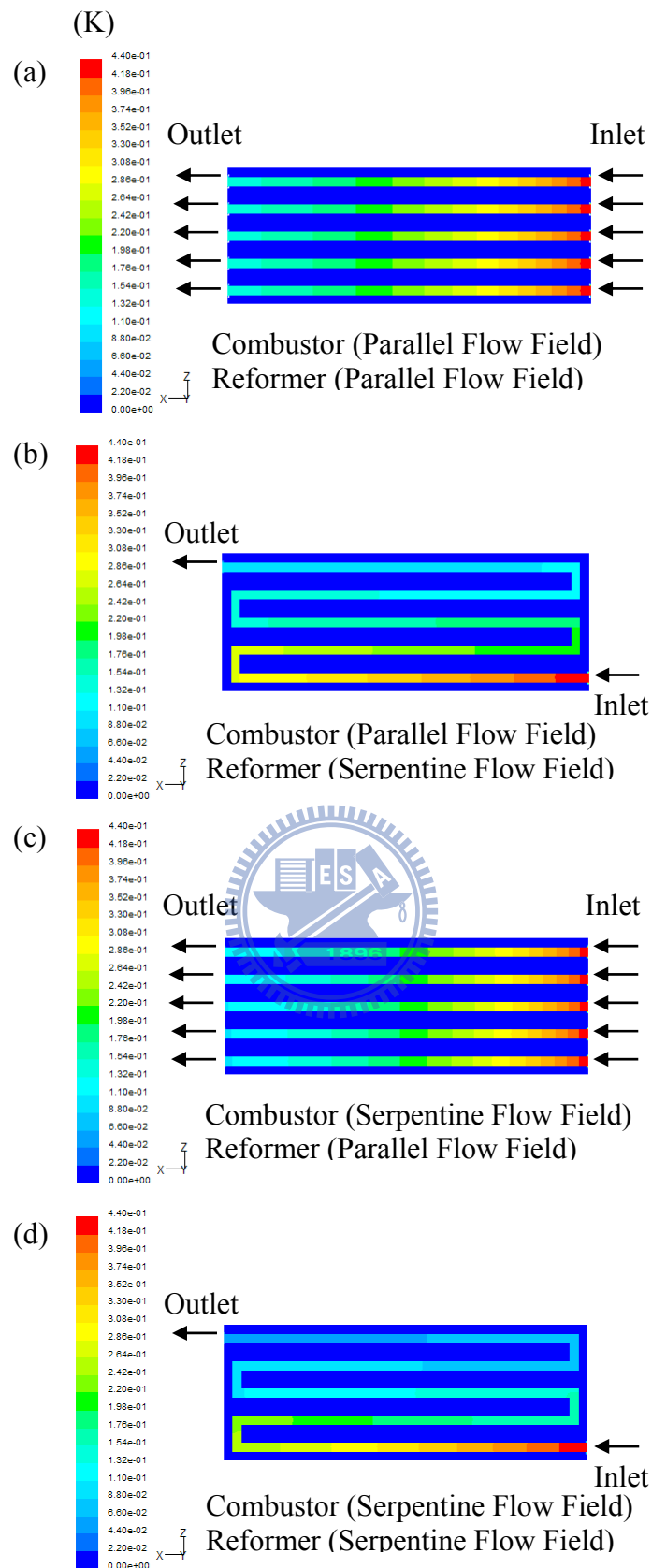


Fig. 4-46 The CH_3OH mole fraction distributions on the middle cross-section of the reforming channel for reformer and combustor with various flow field designs

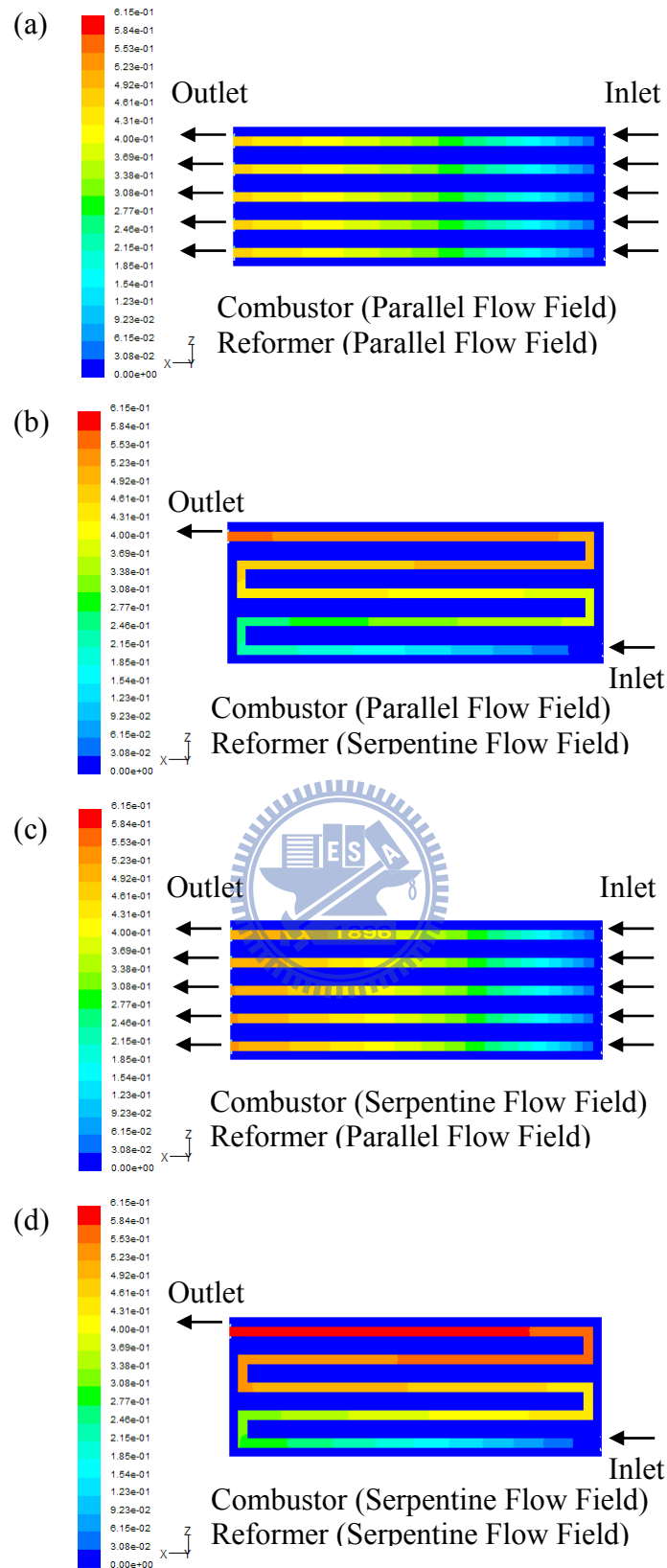


Fig. 4-47 The H_2 mole fraction distributions on the middle cross-section of the reforming channel for reformer and combustor with various flow field designs

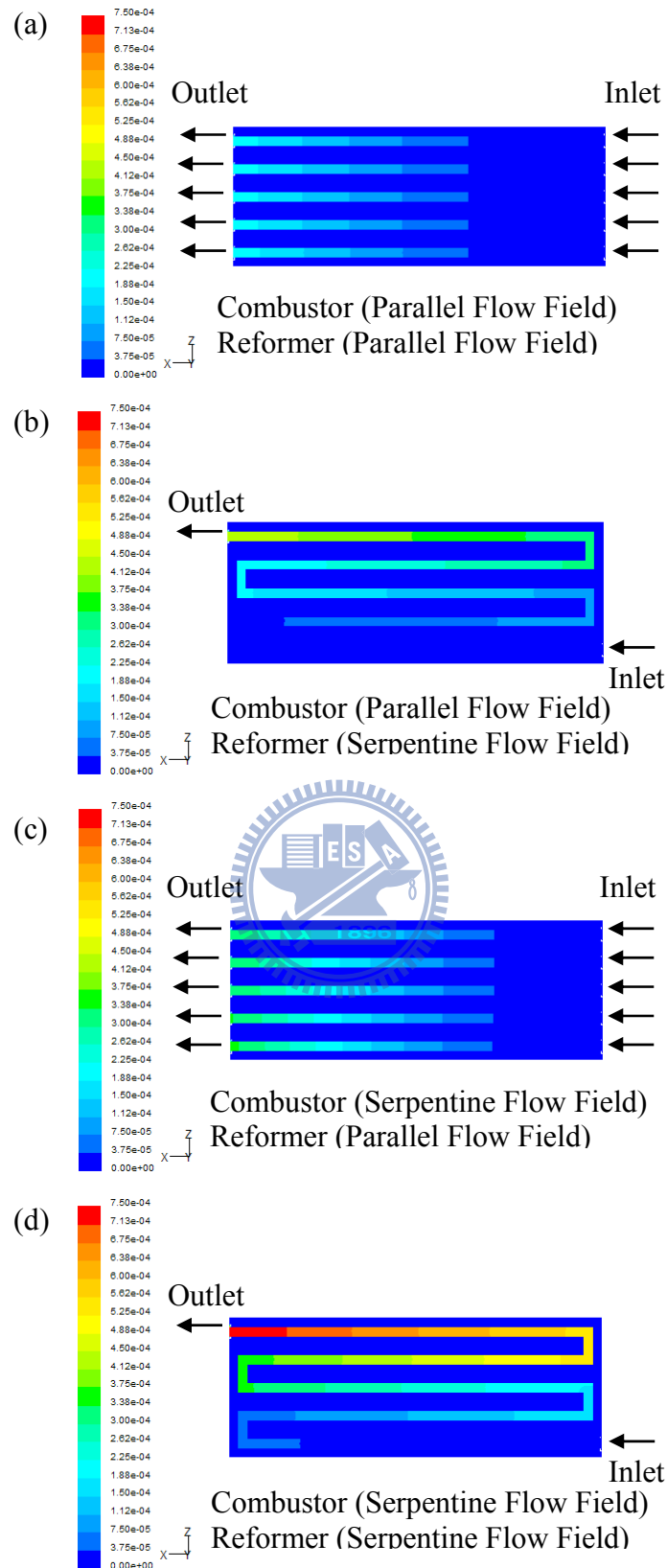


Fig. 4-48 The CO mole fraction distributions on the middle cross-section of the reforming channel for reformer and combustor with various flow field designs

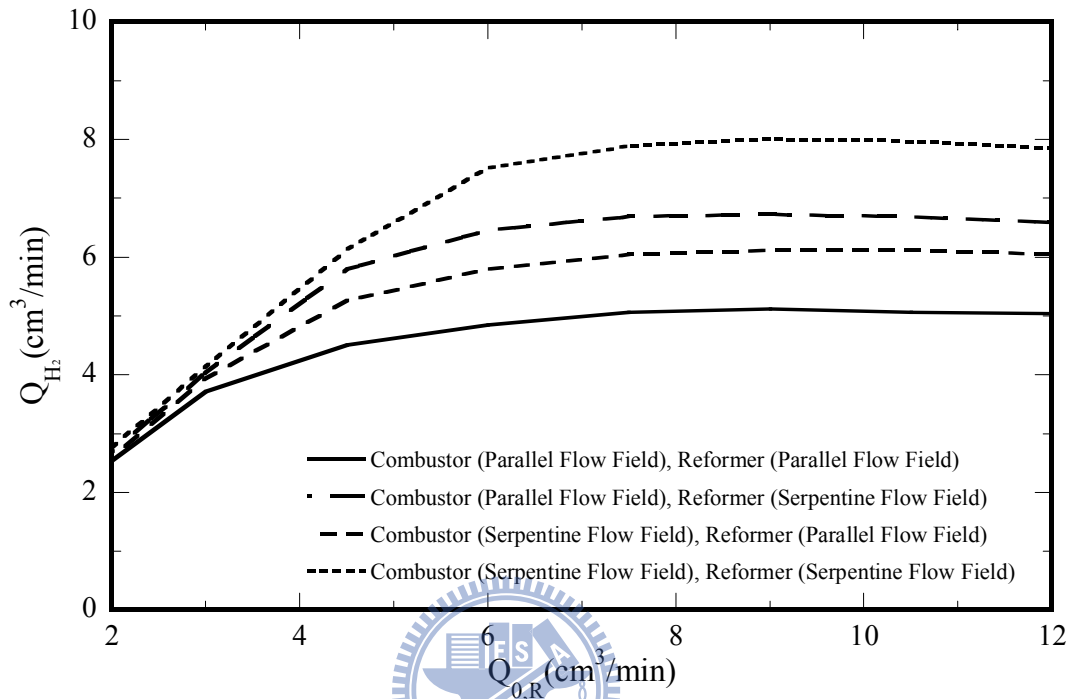


Fig. 4-49 Effects of the inlet flow rate ($Q_{0,R}$) of the reformer and various flow field designs on the H_2 production rate

CHAPTER 5

CONCLUSIONS AND RECOMMENDATION

5-1 Conclusions

This present study investigates heat and mass transport phenomena in the plate methanol steam micro-reformer (including methanol steam micro-reformer and methanol catalytic combustor). In this work, an attempt is made to examine the detailed fluid flow, heat and mass transfer coupled with chemical reactions in the plate methanol steam micro-reformer. This work can accurately predict methanol conversion and local transport phenomena in the channel of a plate steam methanol micro-reformer, thus giving the following conclusions:

Firstly, this study numerically investigated the effects of the geometric and thermo-fluid parameters on the heat and mass transfer and methanol conversion in a two-dimensional micro-reformer channel. The results show the effects of channel geometry and catalyst thickness have a significant impact on the methanol conversion and heat and mass transfer in the plate micro-reformer. The micro-reformer performance increases with increasing wall temperature due to increase in the chemical reaction rate. Smaller channel heights have much more uniform temperature distributions. Therefore, the methanol conversion of the micro-reformer is slightly enhanced with the smaller channel height at higher wall temperature. A reduced Reynolds number for the reactant gas in the channel would rise the reactant gas residence time, which in turn, increases the reaction time and improves the methanol conversion. The CO concentration decreases with increasing H_2O/CH_3OH molar ratio of the inlet fuel.

Secondly, a three-dimensional channel model was developed to investigate the geometric sizes (aspect ratios and channel size) and thermo-fluid parameters (Reynolds number and wall

temperature) on methanol conversion and local transport phenomena in the channel of a plate steam methanol micro-reformer. The predictions with and without wall conduction effects show that this has a significant impact on the thermal development and a negligible effect on the chemical reactions. A decrease in the aspect ratio can increase methanol consumption and the hydrogen mole fraction along the channels. This is because that a reduction in the aspect ratio also yields a much more uniform temperature distribution, whilst also increasing the steam reforming reaction rate and methanol conversion. The better methanol conversion and the H₂ production rate are noted for the smaller aspect ratio. Smaller channels have much more uniform temperature distributions, which in turn, result in a decrease in the thermal entrance lengths. Therefore, fuel utilization efficiency is improved for a small channel. For the same hydraulic diameter, a reduced Re increases the reactant gas residence time, which in turn increases the reaction time and significantly increases methanol conversion.

Thirdly, a three-dimensional heat and mass transfer of micro-reformer with the serpentine flow field numerical model is developed to examine the effects of various values of wall temperature, fuel ratio and Reynolds number on the plate methanol steam micro-reformer performance and local transport phenomena. The prediction shows that the methanol conversion increases with an increase in wall temperature T_w . The methanol conversion for $T_w = 260\text{ }^\circ\text{C}$ could be improved by 53% relative to that of $T_w = 200\text{ }^\circ\text{C}$. A reduced Reynolds number for the reactant gas in the channel would raise the reactant gas residence time and yield more uniform temperature distributions, which in turn increases the reaction time and improves the methanol conversion efficiency. The CO concentration would be reduced from 0.27% to 0.21% at $T_w = 230\text{ }^\circ\text{C}$ as the H₂O/CH₃OH molar ratio value is increased from 1.0 to 1.6. By comparing the predicted results with top or bottom heated condition, it indicates that the methanol conversion for the condition with the top heated plate could be improved by 4.4%.

Fourthly, this study extends the previous research to be a three-dimensional channel numerical model of a micro-reformer with combustor. With an appropriate design of the flow configurations in the reactor, the thermal management of a micro-reformer with combustor can be achieved efficiently. To reach this end, various flow configurations for co- and counter-current flow have been proposed. In addition, the effects of the Reynolds number and various geometric parameters have also been investigated by using numerical simulations of the detailed gas transport phenomena and micro-reformer performance. The deviations between the predictions with and without consideration of the wall conduction effects reveal the influences of the wall conduction on the transport phenomena and the performance of the micro-reformer. The present results provide evidence for the significance of a wall conduction effect and imply that it is necessary to include this effect in the modeling and analysis. The application of the flow configuration design in a plate methanol steam micro-reformer with methanol catalytic combustor leads to improved thermal management and micro-reformer performance. The effects can be enhanced with a counter-current flow configuration in a plate methanol steam micro-reformer with methanol catalytic combustor. With a higher Reynolds number on the combustor side, the wall temperature is increased and the methanol conversion can thus be enhanced. Meanwhile, a reduced Reynolds number for the reactant gas on the micro-reformer side will raise the reactant gas residence time, which in turn increases the methanol conversion and improves the temperature distributions. The effects of channel geometry have a significant impact on the methanol conversion and heat and mass transfer in the plate methanol micro-reformer with methanol catalytic combustor.

Finally, the three-dimensional numerical models of a methanol steam micro-reformer with a methanol catalytic combustion chamber have been developed in this analysis. The flow fields including the parallel flow field and the serpentine flow field are under investigation. The temperature, methanol mole fraction, hydrogen mole fraction and CO mole fraction for

the various flow fields have been studied in detail. The results show that a higher temperature distribution is note for the plate methanol steam micro-reformer with the serpentine flow field and the methanol catalytic combustor with the serpentine flow field. The plate methanol steam micro-reformer with the serpentine flow field and the methanol catalytic combustor with the serpentine flow field have a better methanol conversion than any other flow field designs in this study.

5-2 Recommendations

The research above has demonstrated that the appropriate geometric parameters and thermo-fluid parameters are crucial for achieving higher methanol conversion for a plate methanol steam reformer. Proper thermal management is required to keep higher methanol conversion and better fuel utilization efficiency. Hence, the investigations and findings presented in previous results provide essential knowledge base for future study. This model is useful and can be reduce the design time of a plate methanol steam micro-reformer, and sufficiently improved thermal management.

The investigations and findings in previous research offer an essential knowledge base for the subsequent study. There are many research works that can be done in the future. Firstly, to confirm the analytical model, one may conduct further experiments in the future. Secondly, the catalysts have very significant effects on the performance of micro-reformer. The catalysts may be different in density, porosity and permeability which play a very complex role in the micro-reformer. However, the purpose of this study is to focus the geometric effects on the performance of micro-reformer. Therefore, the parametric effects of catalyst layer are simplified in this work. The parametric effects of catalyst layer are very important. It is an excellent topic for the future study. Finally, future research could be conducted on the

transient mathematical model. It may be beneficial to examine further transient behaviors of the plate methanol steam micro-reformer with methanol catalytic combustor.



REFERENCE

- [1] A. Kundu, J.H. Jang, J.H. Gil, C.R. Jung, H.R. Lee, S.H. Kim, B. Ku and Y.S. Oh, 2007, "Micro-fuel cells-Current development and applications," *J. Power Sources*, Vol.170, pp.67-78.
- [2] M. Ball and M. Wietschel, 2009, "The future of hydrogen - opportunities and challenges," *Int. J. Hydrogen Energy*, Vol.34, pp.615-627.
- [3] J.D. Holladay, Y. Wang and E. Jones, 2004, "Review of developments in portable hydrogen production using microreactor technology," *Chem. Rev.*, Vol.104, pp.4767-4790.
- [4] J.D. Holladay, J. Hu, D.L. King and Y. Wang, 2009, "An overview of hydrogen production technologies," *Catal. Today*, Vol.139, pp.244-260.
- [5] G. Kolb, V. Hessel, V. Cominos, C. Hofmann, H. Lowe, G. Nikolaidis, R. Zapf, A. Ziogas, E.R. Delsman, M.H.J.M. De Croon, J.C. Schouten, O. De La Iglesia, R. Mallada and J. Santamaria, 2007, "Selective oxidations in micro-structured catalytic reactors-for gas-phase reactions and specifically for fuel processing for fuel cells," *Catal. Today*, Vol.20, pp.2-20.
- [6] T. Terazaki, M. Nomura, K. Takeyama, O. Nakamura and T. Yamamoto, 2005, "Development of multi-layered microreactor with methanol reformer for small PEMFC," *J. Power Sources*, Vol.145, pp.691-696.
- [7] T. Kim, 2009, "Micro methanol reformer combined with a catalytic combustor for a PEM fuel cell," *Int. J. Hydrogen Energy*, Vol.34, pp.6790-6798.
- [8] J.D. Holladay, E.O. Jones, M. Phelps and J. Hu, 2002, "Microfuel processor for use in a

- miniature power supply,” J. Power Sources, Vol.108, pp.21-27
- [9] J.D. Holladay, E.O. Jones, R.A. Dagle, G.G. Xia, C. Cao and Y. Wang, 2004, “High efficiency and low carbon monoxide micro-scale methanol processors,” J. Power Sources 131, pp.69-72.
- [10] M.T. Lee, R. Greif, C.P. Grigoropoulos, H.G. Park and F.K. Hsu, 2007, “Transport in packed-bed and wall-coated steam-methanol reformer,” J. Power Sources, Vol.166, pp.194-201.
- [11] G. Kolb and V. Hessel, 2004, “Micro-structured reactors for gas phase reactions,” Chem. Eng. J., Vol.98, pp.1-38.
- [12] D. J. Seo, W. L. Yoon, Y. G. Yoon, S. H. Park, G. G. Park and C. S. Kim, 2004, “Development of a micro fuel processor for PEMFCs,” Electrochim. Acta, Vol.50, pp. 719-723.
- [13] O. J. Kwon, S. M. Hwang, J. G. Ahn and J. J. Kim, 2006, “Silicon-based miniaturized-reformer for portable fuel cell applications,” J. Power Sources, Vol.156, pp.253-259.
- [14] J.W. Ha, J.H. Jang, J.H. Gil and S.H. Kim, 2008, “The fabrication and performance of a poly(dimethylsiloxane) (PDMS)-based microreformer for application to electronics,” Int. J. Hydrogen Energy, Vol.33, pp.2059-2063.
- [15] M.S. Lim, M.R. Kim, J. Noh and S.I. Woo, 2005, “A plate-type reactor coated with zirconia-sol and catalyst mixture for methanol steam-reforming,” J. Power Sources, Vol.140, pp.66-71.
- [16] G.G. Park, D.J. Seo, S.H. Park, Y.G. Yoon, C.S. Kim and W.L. Yoon, 2004, “Development of microchannel methanol steam reformer,” Chem. Eng. J., Vol.101, pp.87-92.

- [17] H. Jeong, K. I. Kim, T. H. Kim, C. H. Ko, H. C. Park and I. K. Song, 2006, "Hydrogen production by steam reforming of methanol in a micro-channel reactor coated with Cu/ZnO/ZrO₂/Al₂O₃ catalyst," J. Power Sources, Vol.159, pp.1296-1299.
- [18] A. Kundu, J. E. Ahn, S. S. Park, Y. G. Shul and H. S. Han, 2008, "Process intensification by micro-channel reactor for steam reforming of methanol," Chem. Eng. J., Vol.135, pp.113-119.
- [19] O.J. Kwon, D.H. Yoon and J.J. Kim, 2008, "Silicon-based miniaturized reformer with methanol catalytic burner," Chem. Eng. J., Vol.140, pp.466-472.
- [20] D.E. Park, T Kim, S. Kwon, C.K. Kim and E. Yoon, 2007, "Micromachined methanol steam reforming system as a hydrogen supplier for portable proton exchange membrane fuel cells," Sens. Actuators, A, Vol.135, pp.58-66.
- [21] K. Yoshida, S. Tanaka, H. Hiraki and M. Esashi, 2006, "A micro fuel reformer integrated with a combustor and a microchannel evaporator," J. Micromech. Microeng., Vol.16, pp.191-197.
- [22] G.G. Park, S.D. Yim, Y.G. Yoon, C.S. Kim, D.J. Seo and K. Eguchi, 2005, "Hydrogen production with integrated microchannel fuel processor using methanol for portable fuel cell systems," Catal. Today, Vol.110, pp.108-113.
- [23] G. G. Park, S. D. Yim, Y. G. Yoon, W. Y. Lee, C. S. Kim, D. J. Seo and K. Eguchi, 2005, "Hydrogen production with integrated microchannel fuel processor for portable fuel cell systems," J. Power Sources, Vol.145, pp.702-706.
- [24] J.Y. Won, H.K. Jun, M.K. Jeon and S.I. Woo, 2006, "Performance of microchannel reactor combined with combustor for methanol steam reforming," Catal. Today, Vol.111, pp. 158-163.
- [25] J. M. Sohn, Y. C. Byun, J. Y. Cho, J. Choe and K. H. Song, 2007, "Development of the

- integrated methanol fuel processor using micro-channel patterned devices and its performance for steam reforming of methanol,” *Int. J. Hydrogen Energy*, Vol.32, pp. 5103-5108.
- [26] O.J. Kwon, S.M. Hwang, J.H. Chae, M.S. Kang and J.J. Kim, 2007, “Performance of a miniaturized silicon reformer-PrOx-fuel cell system,” *J. Power Sources*, Vol.165, pp.342-346.
- [27] T. Kim and S. Kwon, 2009, “MEMS fuel cell system integrated with a methanol reformer for a portable power source,” *Sens. Actuators, A*, Vol.154, pp.204-211.
- [28] M. Hishida, Y. Nagano and M.S. Montesclaros, 1982, “Combined forced and free convection in the entrance region of an isothermally heated horizontal pipe,” *J. Heat Transfer*, Vol.104, pp.153–159.
- [29] J.T. Liu, X.F. Peng and W.M. Yan, 2007, “Numerical study of fluid flow and heat transfer in microchannel cooling passages,” *Int. J. Heat Mass Transfer*, Vol.50, pp.1855-1864.
- [30] H.C. Chiu, J.H. Jang and W.M. Yan, 2007, “Mixed convection heat transfer in horizontal rectangular ducts with radiation effects,” *Int. J. Heat Mass Transfer*, Vol.50, pp.2874-2882.
- [31] H.C. Chiu and W.M. Yan, 2008, “Mixed Convection Heat Transfer in Inclined Rectangular Ducts with Radiation Effects,” *Int. J. Heat Mass Transfer*, Vol.51, pp.1085-1094.
- [32] D.J. Nelson and B.D. Wood, 1986, “Combined heat and mass transfer natural convection between vertical parallel plates with uniform flux boundary conditions,” *Heat Mass Transfer*, Vol.4, pp.1587–1592.
- [33] D.J. Nelson and B.D. Wood, 1989, “Combined heat and mass transfer natural convection between vertical parallel plates,” *Int. J. Heat Mass Transfer*, Vol.32, pp.1779–1787.

- [34] K.Z. Lee, H.L. Tsai and W.M. Yan, 1997, "Mixed convection heat and mass transfer in parallel rectangular ducts," *Int. J. Heat Mass Transfer*, Vol.40, pp.1621–1631.
- [35] N. Boukadida and S.B. Nasrallah, 2001, "Mass and heat transfer during evaporation in laminar flow inside a rectangular channel-validity of heat and mass transfer analogy," *Int. J. Therm. Sci.*, Vol.40, pp.67–81
- [36] M.J. Stutz, N. Hotz and D. Poulidakos, 2006, "Optimization of methane reforming in a microreactor-effects of catalyst loading and geometry," *Chem. Eng. Sci.*, Vol.61, pp.4027- 4040.
- [37] J. Yuan, F. Ren and B. Sunden, 2007, "Analysis of chemical-reaction-coupled mass and heat transport phenomena in a methane reformer duct for PEMFCs," *Int. J. Heat Mass Transfer*, Vol.50, pp.687-701.
- [38] J.C. Amphlett, K.A.M. Creber, J.M. Davis, R.F. Mann, B.A. Peppley and D.M. Stokes, 1994, "Hydrogen production by steam reforming of methanol for polymer electrolyte fuel cells," *Int. J. Hydrogen Energy*, Vol.19, pp.131-137.
- [39] B.A. Peppley, J.C. Amphlett, L.M. Kearns and R.F. Mann, 1999, "Methanol steam reforming on $\text{CuZnOAl}_2\text{O}_3$: Part 1 the reaction network," *Appl. Catal. A*, Vol.179, pp. 21-29.
- [40] B.A. Peppley, J.C. Amphlett, L.M. Kearns and R.F. Mann, 1999, "Methanol steam reforming on $\text{CuZnOAl}_2\text{O}_3$ catalysts. Part 2. A comprehensive kinetic model," *Appl. Catal. A*, Vol.179, pp.31-49.
- [41] A. Mastalir , B. Frank, A. Szizybalski, H. Soerijanto, A. Deshpande, M. Niederberger, R. Schomäcker, R. Schlögl and T. Ressler, 2005, "H₂ production by steam reforming of methanol over $\text{CuZnOAl}_2\text{O}_3$ catalysts transient deactivation kinetics modeling," *J. Catal.*, Vol.230, pp.464-475

- [42] J. K. Lee, J. B. Ko and D. H. Kim, 2004, "Methanol steam reforming over $\text{CuZnOAl}_2\text{O}_3$: catalyst kinetics and effectiveness factor," *Appl. Catal. A*, Vol.278, pp.25-35.
- [43] Y. Kawamura, N. Ogura, T. Yamamoto and A. Igarashi, 2006, "A miniaturized methanol reformer with Si-based microreactor for a small PEMFC," *Chem. Eng. Sci.*, Vol.61, pp. 1092-1101.
- [44] T. Kim and S. Kwon, 2006, "Design, fabrication and testing of a catalytic microreactor for hydrogen production," *J. Micromech. Microeng.*, Vol.16, pp.1760-1768.
- [45] A.V. Pattekar and M.V. Kothare, 2005, "A radial microfluidic fuel processor," *J. Power Sources*, Vol.147, pp.116-127.
- [46] A.T. Stamps and E.P. Gatzke, 2006, "Dynamic modeling of a methanol reformer—PEMFC stack system for analysis and design," *J. Power Sources*, Vol.161, pp.356-370.
- [47] H.C. Yoon, J. Otero and P.A. Erickson, 2007, "Reactor design limitations for the steam reforming of methanol," *Appl. Catal., B*, Vol.75, pp.269-76.
- [48] J.S. Suh, M.T. Lee, R. Greif and C.P. Grigoropoulos, 2007, "A study of steam methanol reforming in a microreactor," *J. Power Sources*, Vol.173, pp.458-466.
- [49] J.S. Suh, M.T. Lee, R. Greif and C.P. Grigoropoulos, 2009, "Transport phenomena in a steam-methanol reforming microreactor with internal heating," *Int. J. Hydrogen Energy*, Vol.34, pp.314-22.
- [50] A. Karim, J. Bravo and A. Datye, 2005, "Nonisothermality in packed bed reactors for steam reforming of methanol," *Appl. Catal., A*, Vol.282, pp.101-109.
- [51] A. Karim, J. Bravo, D. Gorm, T. Conant and A. Datye, 2005, "Comparison of wall-coated and packed-bed reactors for steam reforming of methanol," *Catal. Today*,

Vol.110, pp.86-91.

- [52] A.V. Pattekar and M.V. Kothare, 2004, "A Microreactor for hydrogen production in micro fuel cell applications," *J. Microelectromech. Syst.*, Vol.13, pp.7-18.
- [53] C. Cao, Y. Wang, J.D. Holladay, E.O. Jones, D.R. Palo, 2005, "Design of micro-scale fuel processors assisted by numerical modeling," *AIChE J.*, Vol.51, pp.982-988.
- [54] H.G. Park, J.A Malen, W.T. Piggott III, J.D. Morse, R. Greif and C.P. Grigoropoulos, 2006, "Methanol steam reformer on a silicon wafer," *J. Microelectromech. Syst.*, Vol.15, pp. 976-985.
- [55] C. Cao, G. Xia, J. Holladay, E. Jones and Y. Wang, 2004, "Kinetic studies of methanol steam reforming over Pd/ZnO catalyst using a microchannel reactor," *Appl. Catal., A*, Vol.262, pp.19-29.
- [56] C.Y. Hsueh, H.S. Chu and W.M. Yan, 2009, "Numerical study on micro-reformer performance and local transport phenomena of the plate methanol steam micro-reformer," *J. Power Sources*, Vol.187, pp.535-543.
- [57] F. Chen, M.H. Chang, C.Y. Kuo, C.Y. Hsueh and W.M. Yan, 2009, "Analysis of a plate-type microreformer for methanol steam reforming reaction," *Energy Fuels*, Vol.23, pp.5092-5098
- [58] M. Zafir and A. Gavriilidis, 2003, "Catalytic combustion assisted methane steam reforming in a catalytic plate reactor," *Chem. Eng. Sci.*, Vol.58, pp.3947-3960.
- [59] J.R. Lattner and M.P. Harold, 2007, "Autothermal reforming of methanol : experiments and modeling," *Catal. Today*, Vol.120, pp.78-89
- [60] T.L. Reitz., S. Ahmed, M. Krumpelt, R. Kumar and H.H. Kung, 2000, "Characterization of CuO/ZnO under oxidizing conditions for the oxidative methanol reforming reaction," *J.*

Mol. Catal. A: Chem., Vol.162, pp.275-285.

- [61] S.R. Deshmukh and D.G. Vlachos, 2005, "Effect of flow configuration on the operation of coupled combustor reformer microdevices for hydrogen production," Chem. Eng. Sci., Vol.60, pp.5718-28.
- [62] S.R. Deshmukh and D.G. Vlachos, 2005, "CFD simulations of coupled, countercurrent combustor/reformer microdevices for hydrogen production," Ind. Eng. Chem. Res., Vol.44, pp.4982-92.
- [63] G. Arzamendi, P.M. Dieguez, M. Montes, M.A. Centeno, J.A. Odriozola and L.M. Gandia, 2009, "Integration of methanol steam reforming and combustion in a microchannel reactor for H₂ production: A CFD simulation study," Catal. Today, Vol.143, pp.25-31.
- [64] G. Arzamendi, P.M. Dieguez, M. Montes, J.A. Odriozola, E.F. Sousa-Aguiar and L.M. Gandia, 2009, "Methane steam reforming in a microchannel reactor for GTL intensification: A computational fluid dynamics simulation study," Chem. Eng. Sci., Vol.154, pp.168-173.
- [65] N. Liu, Z. Yuan, C. Wang, L. Pan, S. Wang, S. Li, D. Li and S. Wang, 2008, "A plate-type reactor coated with zirconia-sol and catalyst mixture for methanol steam-reforming," Chem. Eng. J., Vol.139, pp.56-62.
- [66] L. Pan and S. Wang, 2005, "Modeling of a compact plate-fin reformer for methanol steam reforming in fuel cell systems," Chem. Eng. J., Vol.108, pp.51-58.
- [67] A. Varesano, I. Guaglio, G. Saracco and P.L. Maffettone, 2005, "Dynamics of a methanol reformer for automotive applications," Ind. Eng. Chem. Res., Vol.44, pp.759-768.
- [68] W.M. Yan, C.H. Yang, C.Y. Soong, F. Chen and M.C. Mei, 2006, "Experimental studies

- on optimal operating conditions for different flow field designs of PEM fuel cells,” *J. Power Sources*, Vol.160, pp.284-292.
- [69] W.M. Yan, H.Y. Li, P.C. Chiu and X.D. Wang, 2008, “Effects of serpentine flow field with outlet channel contraction on cell performance of proton exchange membrane fuel cells,” *J. Power Sources*, Vol.178, pp.174-180.
- [70] J.H. Jang, W.M. Yan, H.Y. Li and W.C. Tsai, 2008, “Three-dimensional numerical study on cell performance and transport phenomena of PEM fuel cells with conventional flow fields,” *Int. J. Hydrogen Energy*, Vol.33, pp.156-164.
- [71] W.M. Yan, H.Y. Li and W.C. Tsai, 2006, “Three-dimensional analysis of PEM fuel cells with different flow channel designs,” *J. Electrochem. Soc.*, Vol.153, pp.1984-1991.
- [72] A. Kundu, J.H. Jang, H.R. Lee, S.H. Kim, J.H. Gil, C.R. Jung and Y.S. Oh, 2006, “MEMS-based micro-fuel processor for application in a cell phone,” *J. Power Sources*, Vol.162, pp.572-578.
- [73] O.L. Ding and S.H. Chan, 2008, “Autothermal reforming of methane gas—Modelling and experimental validation,” *Int. J. Hydrogen Energy*, Vol.33, pp.633-643.
- [74] A.P. Kagyrmnova, I.A. Zolotarskii, E.I. Smirnov and N.V. Vernikovskaya, 2007, “Optimum dimensions of shaped steam reforming catalysts,” *Chem. Eng. J.*, Vol.134, pp.228-234.
- [75] D.D. Davieau and P.A. Erickson, 2007, “The effect of geometry on reactor performance in the steam-reformation process,” *Int. J. Hydrogen Energy*, Vol.32, pp.1192-1200.
- [76] S. Ergun, 1952, “Fluid flow through packed columns,” *Chem. Eng. Prog.*, Vol.48, pp. 89-94.
- [77] F.M. White, 1991, “Viscous fluid flow,” 2nd ed., McGraw-Hill, New York.

- [78] N. Hotz, M.T. Lee, C. P. Grigoropoulos, S. M. Senn, and D. Poulidakos, 2006, “Exergetic analysis of fuel cell micropowerplants fed by methanol,” *Int. J. Heat Mass Transfer*, Vol.49, pp.2397-2411.
- [79] H. Purnama, T. Ressler, R.E. Jentoft, H. Soerijanto, R. Schlogl and R. Schomacker, 2004, “CO formation/selectivity for steam reforming of methanol with a commercial CuO/ZnO/Al₂O₃ catalyst,” *Appl. Catal., A*, Vol.259, pp.89-94.
- [80] J. Agrell, H. Birgersson and M. Boutonnet, 2002, “Steam reforming of methanol over a Cu/ZnO/Al₂O₃ catalyst : a kinetic analysis and strategies for suppression of CO formation,” *J. Power Sources*, Vol.106, pp.249-257.
- [81] J. Pasel, B. Emonts, R. Peters and D. Stolten, 2001, “A structured test reactor for the evaporation of methanol on the basis of a catalytic combustion,” *Catal. Today*, Vol.69, pp.193-200

